White adipose tissue characterization and lipid profiling in obesity

Norma Dahdah,

UNIVERSITAT DE BARCELONA

DOCTORAL PROGRAMME IN BIOMEDICINE

WHITE ADIPOSE TISSUE CHARACTERIZATION AND LIPID PROFILING IN OBESITY

PhD Student

Norma Dahdah

Supervisors

Pablo M. García-Rovés González (tutor)

María del Mar Malagón Poyato

Department of Physiological Sciences

Faculty of Medicine and Health Sciences, Campus Bellvitge

Universitat de Barcelona

July 2022

Abstract

Obesity has become exceedingly pervasive, a resultant of amplified food availability and reshaped human behavior stimulated by urbanization. It poses as a major challenge for human metabolic physiology testing the limitations of metabolic plasticity; an adaptive capacity against internal or environmental stressors. A stressor persisting and turning into a chronic situation, diminishes the ability to adapt, thus debilitating metabolic plasticity. In the face of the various strategies for combatting obesity, it has become increasingly crucial to further advance the understanding of obesity-associated metabolic adaptations at a systemic and a tissue-specific level.

Committed towards this purpose, the LiMa (Lifestyle Matters) project aimed at an integrative multidisciplinary approach addressing phenotypical and functional transitions induced by obesity and weight loss. A combined nutritional and exercise intervention was implemented on a mouse model of diet-induced obesity in order to evaluate metabolic plasticity and interpret the crosstalk among tissues and its manifestation systemically. An assessment of several parameters, systemically and in major tissues dictating metabolic responses, revealed an impressive capacity to overcome the impairment induced by obesity. However, a lack of plasticity emphasized by a deteriorating mitochondrial function in epididymal white adipose tissue (eWAT) was evident in our study.

The aim of this doctoral thesis is to gain further insight on metabolic plasticity of formerly obese mice by adding on to the description of the phenotypes of the experimental groups and by focusing on different depots of white adipose tissue and their stromal vascular fraction. A lipidomic study identified lipid profiles as tissue-specific, and reported lipidomes of liver and skeletal muscle reflective of energy balance contrary to eWAT lipidome, which was reflective of the content of the administered diet. With the attention shifted towards adipose tissue, eWAT seemed to be more susceptible than the other adipose tissue depot investigated – subcutaneous white adipose tissue (sWAT) – to damage initiated by high-fat feeding. This vulnerability was highlighted by an intense inflammatory profile, as indicated by the M1 proinflammatory phenotype of infiltrating macrophages in eWAT and the

presence of crown-like structures surrounding adipocytes, together with worsening of mitochondrial function of adipose-derived stem cells in eWAT. Moreover, other macrophage subtypes seem to participate in eWAT expansion and remodeling, including M2a macrophages induced by HFD, which are involved in endocytic processes, as well as M2b macrophages, controlling the intensity of inflammatory reactions, and M2c macrophages, involved in the phagocytosis of apoptotic adipocytes. eWAT remodeling also involved significant changes in the composition and appearance of the extracellular matrix, with HFD increasing the expression of both collagens and proteoglycans involved in fibrosis, such as COL1, COL3 or COL6, and lumican and versican, respectively. Notably, intervention studies aimed at reducing body weight (exercise and decreased feeding) reverted, though only partially, the matrisome of eWAT while the macrophage population recovered the original, lean phenotype upon weight loss.

Hence, data from previous LiMa studies combined with data from this doctoral thesis illustrate visceral white adipose tissue as the most affected tissue in the progression of obesity. In addition, the deterioration in its mitochondrial function despite improvements in tissue morphology hints at mitochondrial health as a key determinator of the state of metabolic plasticity.

Abbreviations

A2R	A2 adenosine receptor
AMPK	AMP-activated protein kinase
AAs	Amino acids
ACC	Acetyl-CoA carboxylase
Acetyl-CoA	Acetyl-Coenzyme A
ACS	Acyl-CoA synthetase
ADAMs	A disintegrin and metalloproteinases
ADAMTS	ADAMs with a thrombospondin type 1 motif
AdipoR1	Adiponectin receptor protein 1
ADP	Adenosine diphosphate
ADSCs	Adipose-derived stem cells
AEE	Activity-induced energy expenditure
Aps	Adipocyte progenitors
ARA-EPA	Arachidonic and eicosapentaenoic acids
ASP	Acylation stimulating protein
ATGL	Adipocyte triglyceride lipase
ATMs	Adipose tissue macrophages
ATP	Adenosine-triphosphate
BAT	Brown adipose tissue
BDNF	Brain-derived neurotrophic factor
BMAT	Bone marrow adipose tissue
BMMSCs	Bone marrow mesenchymal stem cells
BMP	Bone morphogenetic protein
BW	Body weight
C/EBP	CCAAT/enhancer binding protein
CACT	Carnitine acylcarnitine translocase
cAMP	cyclic Adenosine monophosphate
CCK	Cholecystokinin
CCRs	CC chemokine receptors
CD105	Cluster of differentiation 105
CE	Esterified cholesterol

CER	Ceramides
CETF	Electron transferring flavoprotein complex
Chi3l3	Chitinase 3-like-3
Chol	Cholesterol
ChoP	Phosphocholine
ChREBP	Carbohydrate response element binding protein
CI	Complex I
CIII	Complex III
CIV	Complex IV
CLS	Crown-like structures
CNS	Central nervous system
COL6	Collagen 6
CoQ	Coenzyme Q
CPT	Carnitine palmitoyltransferase
CR	Calorie restriction
CRP	C-reactive protein
CV	Complex V
CVDs	Cardiovascular diseases
DAG	Diacylglycerol
DHA	Docosahexaenoic acid
DIT	Diet-induced thermogenesis
DKK	Dickkof
DMEM	Dulbecco's modified eagle medium
DNL	De novo lipogenesis
dWAT	Dermal white adipose tissue
ECM	Extracellular matrix
EE	Energy expenditure
EECs	Enteroendocrine cells
EI	Energy intake
Elovl	Fatty acyl-CoA elongase
ER	Endoplasmic reticulum
ETS	Electron transport system
FABPpm	Fatty acid-binding protein plasma membrane
FACS	Fluorescence-activated cell sorting

FAK	Focal adhesion kinase
FAS	Fatty acid synthase
FAT	Fatty acid translocase
FATPs	Fatty acid transporter proteins
FC	Free cholesterol
FCCP	Carbonyl cyanide-4 (trifluoromethoxy) phenylhydrazone
FeS	Iron-sulfur
FFA	Free fatty acids
FFM	Fat-free mass
FGF-2	Fibroblast growth factor
FGF21	Fibroblast growth factor 21
FMN	Flavin mononucleotide
G3P	Glycerol-3-phosphate
G6P	Glucose-6-phosphate
GAP	Glyceraldehyde-3-phosphate
GDH	Glutamate dehydrogenase
GH	Growth hormone
GI	Gastro-intestinal
GLP-1	Glucagon-like peptide-1
GLUT4	Glucose transporter 4
GPAT	Glycerol-3-phosphate acyltransferase
1H-NMR	Proton based nuclear magnetic resonance
H&E	Hematoxylin and Eosin
HA	Hyaluronic acid
HFD	High-fat diet
HGF	Hepatocyte growth factor
HIF-1α	Hypoxia-inducible factor 1α
HLA-DR	Human Leukocyte Antigen- DR
HNF4A	Hepatocyte nuclear factor 4-α
HSL	Hormone-sensitive lipase
iBAT	Interscapular BAT
IGF-1	Insulin-like growth factor 1
IGTT	Intraperitoneal glucose tolerance test
IL-6	Interleukin 6

ILC2	Type II innate lymphoid cells (ILC2)
ILCs	Innate lymphoid cells
ILK	Integrin-linked kinase
IMCL	Intramyocellular lipids
IMM	Inner mitochondrial membrane
IntD	Intervention diet
IRS-2	Insulin receptor substrate 2
ISCT	International Society for Cellular Therapy
iWAT	Inguinal WAT
JNK	c-Jun N-terminal kinase
LCFAs	Long-chain FAs
LD	Lipid droplets
LDH	Lactate dehydrogenase
LEPRs	Leptin receptors
LI	Lifestyle intervention
LIF	Leukemia inhibitory factor
Lox	Lysyl oxidase
LPL	Lipoprotein lipase
LPS	Lipopolysaccharides
MAG	Monoacylglycerol
MFe	Iron-rich macrophages
MGL	Monoacylglycerol lipase
MHC-II	Class II major histocompatibility complex
Mme	Metabolically activated macrophage
MMPs	Matrix metalloproteins
Mox	Antioxidant macrophage
Mrc2	Mannose receptor C type 2
MSCs	Mesenchymal stem cells
mtDNA	Mitochondrial DNA
MUFAs	Mono-unsaturated FAs
n3.D-E-L	Omega3-docosahexaenoic acid-EPA-Linolenic
NAD+	Nicotinamide adenine dinucleotide
NADH	Nicotinamide adenine dinucleotide
NADPH	Nicotinamide adenine dinucleotide phosphate

NAFLD	Non-alcoholic fatty liver disease
NASH	Non-alcoholic steatohepatitis
NCD	Non-communicable diseases
NEFA	Non-esterified fatty acids
NF-κB	Nuclear factor-κB
NMR	Nuclear magnetic resonance
NP	Natriuretic peptides
OCR	Oxygen consumption rate
OXPHOS	Oxidative phosphorylation
P/S	Penicillin-Streptomycin
PBS	Phosphate-buffered saline
PDH	Pyruvate dehydrogenase
PE	Phosphatidylethanolamine
PEP	Phosphoenolpyruvate
PEPCK	PEP carboxylase
PGs	Proteoglycans
Pi	Inorganic phosphate
PI3K	Phosphatidylinositol-3-kinase
PKA	Protein kinase A
PKCε	Protein kinase C-ε
PPARα	Peroxisome proliferator-activated receptor α
PPARγ	Peroxisome proliferator-activated receptor γ
PPP	Pentose phosphate pathway
PRRs	Pattern recognition receptors
PUFA	Poly-unsaturated FAs
PYY	Peptide YY
QH2	Ubiquinol
RBP4	Retinol-binding protein 4
REE	Resting energy expenditure
RNAseq	RNA sequencing
ROS	Reactive oxygen species
ROX	Residual oxygen consumption
RT	Room temperature
SCD	Stearoyl-CoA desaturases

SCFAs	Short-chain fatty acids
SGLTs	Sodium glucose cotransporters
SLRPs	Small leucine rich proteoglycans
SM	Sphingomyelin
sn-GPC	sn-glycerophosphocholine
SNS	Sympathetic nervous system
SREBP1c	Sterol response element binding protein 1c
STAT	Signal transducer and activator of transcription 3
StdD	Standard chow diet
STRA6	Stimulated by retinoic acid 6
SVF	Stromal vascular fraction
sWAT	Subcutaneous white adipose tissue
T2DM	Type 2 diabetes mellitus
TAG	Triacylglycerol *or* triglyceride
TCA	Tricarboxylic acid
TEE	Total energy expenditure
TGFα	Transforming growth factor alpha
TH2	T helper 2
TIMPs	Tissue inhibitors of metalloproteinases
TLR-4	Toll-like receptor 4
TNFs	Tumor necrosis factors
Tpt1	Translationally controlled tumor protein 1
Treg	T regulatory
TSH	Thyroid-stimulating hormone
TZDs	Thiazolidinediones
UDP-glucose	Uridine diphosphate glucose
UFA	Unsaturated fatty acids
VEGF	Vascular endothelial growth factor
vLDL	Very low-density lipoproteins
vWAT	Visceral white adipose tissue
WAT	White adipose tissue
WHO	World health organization
WISP2	Wnt1-inducible-signalling pathway protein 2
ZNF423	Zinc-finger protein 423

Table of contents

List of figures

List of tables

INTRODUCTION

1.1 Adipose tissue

Adipose tissue previously recognized solely for its energy storage capacity, is now considered a complex endocrine organ contributing to systemic (whole body) metabolism and energy balance. The traditional view of the function of adipose tissue is that of a long-term fuel reservoir which, during nutritional deprivation, can mobilize and release its content of triglycerides into fatty acids to be oxidized by other organs. In 1994, a critical discovery, that of leptin, lead to shifting the interest in adipose tissue from just a passive site for energy storage to an endocrine organ (1). Leptin is a hormone produced mainly by adipocytes and acts both centrally - having receptors in the hypothalamus - and peripherally affecting multiple organs (1,2). This finding paved the way for the identification of a large number of factors with hormonal properties emphasizing on the role of adipose tissue in physiological homeostasis and metabolic regulations (2).

1.1.1 Adipose tissue: form and structure

Adipose mass or fat mass can range from 5 to 60% of total body weight (3). This fat mass and its distribution is affected by sex (4), race (5) and age (3). Adipose tissue is categorized on the basis of its anatomic location and major cell type constituent. In mammals, two main types of adipose tissue exist: white adipose tissue and brown adipose tissue representing, respectively, more than 95% and between 1 to 2% of the adipose mass of (1). A third type of adipose tissue, beige or brite adipose tissue, has been also identified (6). The remaining adipose mass is attributed to several small adipose depots that are closely associated with other anatomic structures performing diverse organ-specific functions (2,7). Some examples of these depots are dermal adipose tissue (2,7), facial adipose tissue (7), mammary adipose tissue (8,9), bone marrow adipose tissue (10,11), etc…

Morphological and functional heterogeneity among adipose depots has been observed and explored. The 3 most discussed adipose tissue types – white, brown and beige - are differentiated primarily by the type of adipocytes – fat cells – they

consist of. While adipocytes are the major components of the different types of adipose tissue; other cell types which form the stromal vascular fraction (SVF) of the tissue can vary between types of tissues and depots, affecting the morphology and function of the tissue.

White adipose tissue (WAT):

The primary function of WAT is to regulate energy homeostasis through the storage of excess energy as triglycerides (TAG) (12). The white yellowish color of WAT is due to its major cell type component, the white adipocytes. These polygonal cells characterized by unilocular large lipid droplets (LD) and low mitochondrial density. The LD occupies about 95% of the volume of the cell forcing the nucleus and all other organelles to the periphery of the cell (3,12,13). Thus, a white adipocyte size ranges between approximately 20 to 200 μm depending of the volume of the LD (3).

Brown adipose tissue (BAT):

Unlike white adipocytes, brown adipocytes are multilocular, with multiple small LDs and high mitochondrial density (7). The main role of BAT is non-shivering thermogenesis, to dissipate energy in the form of heat through uncoupled mitochondrial respiration (2,7,14). Brown adipocytes are primarily found around interscapular, axillary, paravertebral and perirenal sites (12). In humans and other large mammals, it was thought that the main BAT depot- interscapular- is restricted to neonatal and early childhood periods and to adults who are chronically exposed to extreme cold (7,12). But this conception has changed when new technologies in imaging revealed active BAT in adult humans at several discrete anatomical sites, essentially in the upper trunk (15,16).

Beige or brite adipose tissue:

This tissue resides within WAT and in rodents it has been identified mainly in inguinal WAT. It consists of adipose cells that, upon cold exposure, adrenergic stimulation or local hyperthermia via heat stress factor 1 activation (17), are capable of transforming into brown-like adipocytes (2,7,12,14). These brite ("brown in white") adipocytes are morphologically similar to both white and brown adipocytes; they can have either one large unilocular LD or multiple smaller ones and their mitochondrial density is intermediate and prone to an increase upon stimulation (12).

Adipose tissue origins

Even though, both white and brown adipocytes are dependent of similar transcriptional factors for development, such as peroxisome proliferator-activated receptor γ (PPARγ) and many others, their origins differ (14). Most WAT formation begins *in utero* and its further development is stimulated after birth when adipocytes are needed for energy storage (18). It is assumed that most white adipocytes originate from mesenchymal progenitor cells of the mesoderm. But white adipocytes from different depots seem to have different origins. For example, neuroectoderm seems to be the origin of white adipocytes of the craniofacial region and hematopoietic cells acting through the myeloid lineage in bone marrow adipose tissue (14,18). When tracing the origins of brown adipocytes found in BAT depots, these cells were found to be of myogenic lineage expressing the transcription factor, Myf5 (14,18,19).

Adipose tissue distribution

The distribution of adipose tissue in humans and mice is quite similar. The different depots are distinguished by their distinct anatomical locations (1–5,7). WAT is distributed throughout the body but can be categorized into two main subpopulations, subcutaneous white adipose tissue (sWAT) and visceral white adipose tissue (vWAT). sWAT, as it suggests, is the WAT located under the skin in several body regions. Not only, it can also be found interspersed between skeletal muscles forming the intramuscular fat. The most common and most studied depots of sWAT in humans are the abdominal, femoral and gluteal (7,12) and in mice the inguinal WAT (iWAT) found anterior to the upper site of the hind limbs. vWAT surrounds many organs intra-abdominally providing protective padding. vWAT is differentiated according to the organ it envelops; omental WAT surrounds the stomach and the spleen, mesenteric WAT forms a web that supports the intestines, perirenal WAT covers the kidneys, gonadal WAT is attached to uterus and ovaries in females and the epididymis and testis in males, etc… (12).

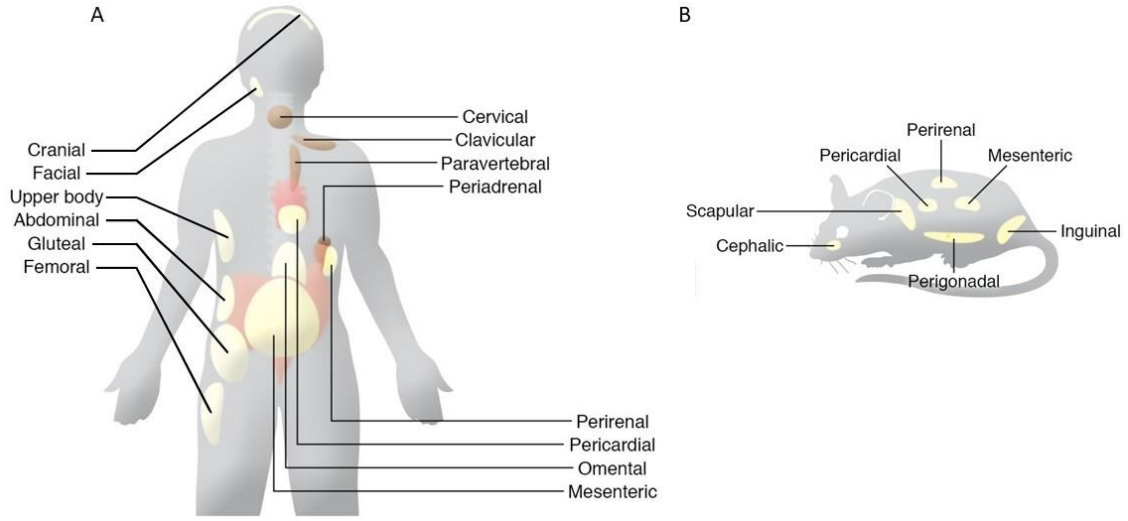

Figure 1: Adipose tissue distribution in (A) humans and (B) mice (adapted from (2)).

Other discrete and small WAT depots with distinct origins and functions have been detected (2,7). Dermal adipose tissue (dWAT) scattered within dermal layers closely to hair follicles is involved in hair development, pathogen resistance and skin wound healing (2,7). Two types of bone marrow adipose tissue (BMAT) can be distinguished, the constitutive and the regulated. The constitutive or yellow BMAT develops in the distal skeletal bones such as distal tibia or tail vertebrae in mice. While the regulated or red BMAT is dispersed in the spine and proximal skeletal limb bones. BMAT is important in the regulation of bone metabolism and osteoblastic activity (10). It was also found to be crucial for the secretion of circulating adiponectin- a hormone essential in regulation of glucose levels and in fatty acid breakdown- during caloric restriction (10,11). As for mammary adipose tissue, the governing type of adipocytes is known as pink adipocytes because of their unique function and morphology. Pink adipocytes have an apical surface with microvilli and they have the ability to secrete milk as well as store large amounts of lipids in the mammary glands. These cells arise in females from subcutaneous WAT during pregnancy and lactation periods (20). Another type of adipocytes present in sWAT, specially iWAT, is the brite adipocytes or the inducible brown adipocytes (12). These cells are distinct from classical brown adipocytes which form BAT depots. Brown fat is mainly distributed around cervical-interscapular, paravertebral and perirenal regions (3). In humans, interscapular BAT (iBAT) is found in the thorax region, chest and abdomen as well.

1.1.2 Stromal vascular fraction

In addition to all previously mentioned, the heterogeneity of the adipose tissue extends to its stromal vascular fraction (SVF). Adipocytes are the primary constituents of this tissue, but a multitude of other cell types in the SVF contribute to its physiology and function including vascular cells, stem cells, endothelial cells, preadipocytes and a variety of immune cells.

Stem cells to adipose derived stem cells

First recognized in the 1950s while experimenting on the bone marrow, stem cells are unspecialized cells with clonogenic potential giving them the ability to self-replicate or differentiate into multiple cell lineages. Stem cells are at the center of the development and regeneration of tissues and organs (21,22). Stem cells exist in early embryonic stages and in adult organisms. With each step, developmental potency is decreased; a pluripotent SC can differentiate into more cell types than a unipotent SC. Multipotent SCs like mesenchymal stem cells give rise to specialized cells of the tissue they are isolated from. Precursor cells or adult stem cells are imbedded within a certain tissue and are activated to replace specialized cells for tissue regeneration and repair (21–23). Mesenchymal stem cells, hematopoietic, epithelial, neural, hepatic and pancreatic stem cells are all examples of progenitor cells (23).

Mesenchymal stem cells (MSCs) are a heterogenous population of adherent fibroblast-like cells with the ability to grow rapidly or differentiate into bone, cartilage and fat cells (24). In the field of regenerative therapies for the past few years, these cells have become a huge interest due to their availability and versatility (21,24). The most studied MSCs are the ones extracted from the umbilical cord and peripheral blood considering the non-invasive procedures performed to acquire these cells. MSCs have been isolated and explored from many other adult and fetal tissue or fluids including some that require a more invasive approach such as bone marrow, muscle, cartilage, tendons, synovial fluid and amniotic fluid (21,25,26).

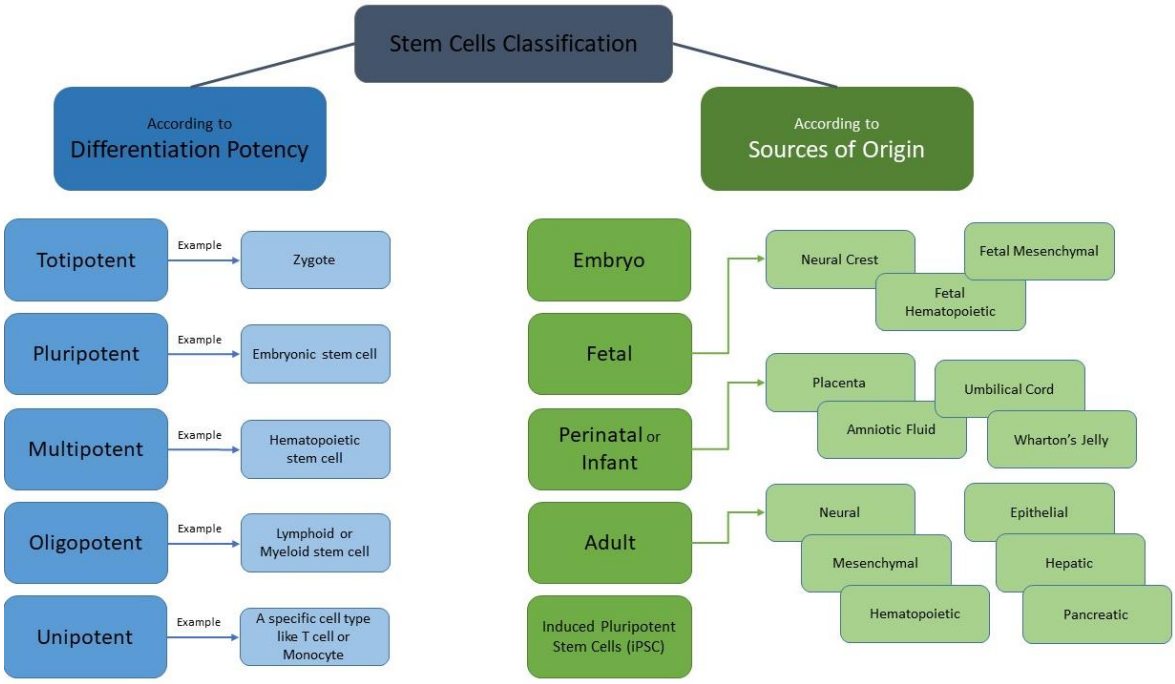

Figure 2: Stem cells classification. It can be according to the stem cells differentiation potency or sources of energy.

A direct correlation exists between the availability of MSCs in a specific tissue and its blood vessel density (26). A key characteristic of MSCs is the expression of mitogenic proteins that induce cell proliferation and angiogenesis (26). MSCs secrete growth factors and chemokines activating cell multiplication such as transforming growth factor alpha (TGFα), insulin-like growth factor (IGF-1), hepatocyte growth factor (HGF), and basic fibroblast growth factor (FGF-2) (26). Vascular endothelial growth factor (VEGF), IGF-1, and angiopoietin-1 amongst others are produced and released to recruit endothelial lineage cells and stimulate vascularization (27). MSCs also have anti-inflammatory and anti-apoptotic properties (24,28–31). They secrete immunomodulatory cytokines such as TGF-β1, HGF, nitrous oxide, interleukin 6 (IL-6), IL-10 and thus suppress the proliferation and function of several pro-inflammatory immune cells like T cells, macrophages and dendritic cells (24,28,29). Also, some of the cytokines produced by MSCs like VEGF, TGF-β1 and HGF have the capacity to reverse apoptosis of endothelial cells (30,31). For the identification of MSCs, the International Society for Cellular Therapy (ISCT) has limited the criteria to the following 3 minimum. MSCs have to be plastic adherent in standard culture conditions, and they ought to show a differentiation

potential towards adipocytes, osteoblasts and chondrocytes under corresponding stimulation. They also have to express non-specific markers – cluster of differentiation 105 (CD105), CD90 and CD73 – and lack the expression of class II major histocompatibility complex (MHC-II) molecules, mainly Human Leukocyte Antigen- DR (HLA-DR), and non-specific markers – CD34, CD45, CD11b or CD14, CD79α or CD19 (32).

Due to the appeal of regenerative medicine worldwide, research on MSCs has been focused on adipose-derived stem cells (ADSCs) since they seem to be advantageous in comparison to other MSCs. ADSCs are abundant, they can be harvested in large quantities by a minimally invasive procedure and they rapidly grow and proliferate (21,32). In comparison to other MSCs and specifically to bone marrow mesenchymal stem cells (BMMSCs), ADSCs show higher autocrine activity through growth factors and immunomodulators (32,33) and more delayed signs of senescence (32,34). ADSCs from younger donors display a higher proliferation rate compared to ADSCs from older individuals but their differentiation capacity remain the same between both age groups (34). A negative impact on their functionality has been shown to occur in long term expansion cultures and in response to cryopreservation (35). The scientific consensus agrees on a low expression in the SVF population of the following markers – CD13, CD29, CD44, CD73, CD90, CD105 and CD106 –that becomes increasingly pronounced with cultured ADSCs (36).

Immune cells

Within WAT, immune cells are deemed crucial in tissue physiology and function. The profile of immune cells present in each WAT depot contributes to its morphology and regulatory adaptations and defines its involvement in metabolic processes, both in health and pathology (37–41). Immune cells in WAT can be classified as innate or adaptive immune cells. Innate immune cells include neutrophils, eosinophils, different subtypes of macrophages, natural killer cells and innate lymphoid cells (ILC) while adaptive immune cells encompass various subtypes of T and B lymphocytes. The abundance of the different immune cell types and their function varies between depots and between healthy and dysfunctional WAT.

The most abundant immune cell type in WAT is adipose tissue macrophages (ATMs) accounting for 50% of WAT immune cells and 15% of SVF (37–39). Both in health and pathology, ATMs content in vWAT is more pronounced than in sWAT (37). In a steady state, ATMs are the resident macrophages already found in WAT and they have several functions contributing to the physiology of the tissue. They are involved in many processes such as scavenging, regulating angiogenesis and remodeling of the extracellular matrix (ECM) (39). One of their important roles as scavenger cells is to help in the turnover of adipocytes. Occasionally, ATMs form crown-like structures (CLS) around dying adipocytes but are unable to engulf them entirely due to differences in size. Thus, ATMs form extracellular acidic compartments that allows, through lysosomal enzymes, the liberation of free fatty acids (FFA) from the dying adipocytes into the macrophages for further processing (42). In a healthy state, the predominant ATM population is M2 macrophages that express genes like interleukin-10 (*IL-10*), mannose receptor C type 2 (*Mrc2*) and chitinase 3-like-3 (*Chi3l3*, *Ym1*) and that are characterized by surface markers CD206 mainly in mice and CD163 in humans. M2 macrophages recognized for driving immune regulation and tissue remodeling can be divided into 4 different subtypes: M2a, M2b, M2c and M2d. Each M2 phenotype has distinctive markers and specialized function (detailed in section 1.3). On the other hand, in obesity, proinflammatory M1 macrophages predominate (detailed in section 1.3). Most ATMs in animals and humans are characterized by surface markers F4/80 and/or CD68 (39,40).

Tregs form around 10% of the SVF and they exhibit high CC chemokine receptors (CCRs) expression which makes them important for chemotaxis (40,41). Eosinophils in lean adipose tissue, accounting for 4-5% of SVF, are the major producers of IL-4. Type II innate lymphoid cells (ILC2) allows the accumulation of eosinophils and M2 macrophages in murine WAT through the secretion of IL-5 and IL-13 (43). ILC2 play also a role in the regulation of thermogenesis and browning in mice WAT by producing methionine-enkephalin peptides (44). As for neutrophils, their role in lean WAT is not well defined so far. Innate immune cells such as Th2 cells secrete cytokines like IL-4, IL-13, IL-5 and the alarmin IL-33 to mediate anti-inflammatory responses (41).

In all, an array of pro- and anti-inflammatory cytokines is actively released by immune cells contributing to the maintenance of WAT tissue homeostasis in a healthy state (37–41). In lean subjects, anti-inflammatory cytokines like IL-10 and transforming growth factor beta (TGF-β) are secreted by M2 macrophages and T regulatory (Treg) inhibiting WAT dysfunction through suppression of inflammation and enhancement of insulin sensitivity (37,39).

Extracellular matrix

The extracellular matrix (ECM) is a three-dimensional non-cellular network composed of a variety of multidomain macromolecules. It is found in all tissues but its composition and function are unique to every tissue. ECM functions range from physical support for tissue integrity and elasticity to reservoir of growth factors by sequestering and releasing them. ECM is a highly dynamic structure in constant remodeling to match cellular processes such as proliferation, differentiation, adhesion, migration, apoptosis, etc… (45–47). Dysregulations in ECM dynamics are linked to pathological conditions and can contribute to further disease progression. Fibrosis and osteoarthritis are examples where in fibrosis there is abnormal ECM deposition and stiffness and in osteoarthritis excessive ECM degradation (45).

Adipose tissue is categorized as loose connective tissue and its resident adipocytes and stromal cells, especially fibroblasts, maintain the ECM by secreting ECM components (46,47). Due to the role of the adipose tissue as energy storage tissue, the requirement for increased triglycerides storage leads to the enlargement in size (hypertrophy) and/or number (hyperplasia) of its main cellular components – the adipocytes. For a healthy tissue expansion, the adjustment of the other cellular components and the ECM is necessary. ECM molecules rely on two different ways to interact with residing cells; either they bind directly to cellular receptors, or they adopt the proteolytic release of biologically active peptides. Hyaluronic acid (HA) is one of the former molecules. HA is a non-sulfated glycosaminoglycan found in various molecular weights and its direct binding to cellular receptors regulates several signaling pathways involved in cell migration, inflammation, angiogenesis, and ECM remodeling. Whereas collagen VI, a major component of AT ECM, acts via the release of a peptide cleaved at the C5 domain of its α3 subunit leading to the

induction of collagen deposition, macrophage infiltration and endothelial cell migration (47).

In mammals, the ECM comprises around 300 proteins forming the core matrisome. The major components of this matrisome include collagens, proteoglycans and glycoproteins (45–47). The adipose tissue ECM is mainly formed of collagens (I, II, II and IV), fibronectin and a small amount of laminin with collagens being the major component and contributing considerably to the non-cell mass of AT (48,49). Mostly adipocytes but also pre-adipocytes, SCs and endothelial cells contribute to the production of collagens. Collagen I, a fibrillar type collagen, is the most abundant of collagens and the key structural component of the ECM (50). Collagen fibrils exist as homo- and hetero-trimers of collagen α-chains and they provide mechanical rigidity to the tissue and bind to specific cell receptors. The most common collagen cell receptors are the integrins which are a family of heterodimeric transmembrane receptors formed by α- and β- subunits and play an important role in cell adhesion to ECM proteins and cell-cell adhesions. Integrins are activated by intracellular adaptor proteins such as talins and kindlins and require the presence of focal adhesion kinase (FAK) and integrin-linked kinase (ILK) for downstream signaling (48,50). Collagen IV is responsible for the thick membrane of ECM surrounding each adipocyte referred to as basal lamina. Adipose tissue also contains COL6, which helps maintain ECM stability (51). Interestingly, studies in ob/ob mice deficient for COL6, which seems to be somewhat specific to AT, exhibit less inflammation in the AT and maintain insulin sensitivity under a high-fat diet (HFD) (52). Collagen XVIII was identified as a component of basement membranes that supports cells during differentiation from pre-adipocytes to mature adipocytes. A lack of collagen XVIII in mice caused a reduction in adiposity and induced ectopic lipid accumulation in liver (53).

Other major, non-fibrillar constituents of the ECM are the proteoglycans (PGs), which enable the formation of a hydrated gel that provides viscoelasticity to the tissues, participate in cell-ECM interactions and growth factor and cytokine signalling, and regulate cell proliferation, migration, angiogenesis and inflammation (54). The largest subfamily of PGs, the small leucine rich proteoglycans (SLRPs), such as decorin, biglycan or lumican, organize ECM structure by regulating collagen

fibril assembly (54). The ECM also contains elastin and its regulators (fibrillins, fibulins, etc), the components of basal membranes, laminins, the fibril-forming protein, fibronectin, that acts as a bridging molecule in matrix organization and cell–matrix interactions, and nonstructural matrix glycoproteins as thrombospondins, tenascins, or osteopontin (55).

In the process of the maintenance of adipose tissue homeostasis, ECM degradation through breakdown by proteases is a common occurrence. The most widely discussed enzymes involved in ECM degradation are matrix metalloproteins (MMPs), a disintegrin and metalloproteinases (ADAMs), and ADAMs with a thrombospondin type 1 motif (ADAMTS) (45,48). MMPs are a family of zinc-containing endopeptidases that can be produced as soluble or cell membrane-anchored proteinases. They have a wide substrate range which means, collectively, MMPs can degrade all ECM proteins. For example, MMP2 and MMP9 are secreted by endothelial cells, fibroblasts and macrophages and they degrade collagen IV thus participating in vasculature remodeling, angiogenesis and inflammatory responses. Also, MMP3 and MMP10 have affinities for fibronectin, laminin, gelatins I, III, IV and V, collagen fibers and proteoglycans, among others (45,48). As for the ADAMs, they are known as 'sheddases'. By cleaving transmembrane protein ectodomains that are adjacent to the cell membrane, ADAMs release back to the ECM the complete ectodomains of cytokines, growth factors, receptors and adhesion molecules. Out of many ADAMTS identified, some are counted as proteoglycanolytic, others are deemed important in the processing of pro-collagens I, II and III and in the deposition of normal collagen fibrils onto the ECM, and many others have no recognized function yet. Meprins, another family of ECM proteases, are capable of the cleavage of collagen IV and fibronectin and the cleavage of pro-collagen I helping in the generation of mature collagen molecules (45,48). The proteolysis of the ECM is controlled further in order to avoid excessive tissue degradation. Tissue inhibitors of metalloproteinases (TIMPs) suppress the activity of MMPs, ADAMs and ADAMTS but not that of meprins. The overall proteolytic activity is determined by the MMP/TIMP ratios and each TIMP shows preferential MMP-binding specificity (45,48).

1.1.3 Adipose tissue functions and dynamics

Adipogenesis

In certain conditions, when the balance between energy expenditure and caloric intake is leaning towards energy excess, adipose tissue expansion is stimulated. AT increase in size by promoting hypertrophy and/or hyperplasia. Hypertrophy is the enlargement of already existing adipocytes (further discussed in chapter 3) whereas hyperplasia is the emergence of new adipocytes from differentiation of resident precursors – preadipocytes. Through hyperplasia, the number of adipocytes or the adiposity of the tissue is increased which is the process known as adipogenesis.

Adipogenesis can be divided into two main consecutive events: the commitment of pluripotent stem cells to becoming preadipocytes and then the differentiation of preadipocytes into fully mature adipocytes (14,56,57). Pluripotent MSCs from AT are capable of committing to different lineages that lead to white pre-adipocytes, myogenic precursors, osteoblast progenitors or condensing mesenchymal stem cells that become chondrocytes. The commitment of pluripotent MSCs into the adipogenic lineage is determined by a network of extracellular signaling factors that often promote one pathway while inhibiting another (14,56,57). The most crucial signaling pathways in this case are that of bone morphogenetic protein (BMP), Wnt and hedgehog signaling. BMP2 and BMP4 bind to their receptors BMPr1 and BMPr2 inducing phosphorylation thus the activation of BMPr1 kinase. Then, phosphorylated SMAD-1, -5 and -8 form a complex with SMAD-4 transcriptional factor. Activated SMAD-4 is translocated to the nucleus where it induces the transcription of PPARγ considered as the master regulator of adipogenesis (56,57). Amongst the many proteins upregulated by BMP signaling, the expression of 3 cytoskeleton-associated proteins – lysyl oxidase (Lox), translationally controlled tumor protein 1 (Tpt1) and αB crystallin - was increased by more than 10-fold by both BMP2 and BMP4. When Lox was knockdown, commitment of MSCs into adipogenic lineage was completely inhibited while it was partially blocked with the knockdown of Tpt1 and αB crystallin. For the commitment of pluripotent SCs, a drastic change in cell shape should take place and the absence of these cytoskeleton-

associated proteins results in a failing adipogenic commitment (57). Wnts are a family of autocrine and paracrine ligands which require the mediation of low-density lipoprotein-related protein 5/6 coreceptor. Canonical Wnt signaling leads to the stabilization of β- catenin which, in pre-adipocytes, inhibits the activation of PPARγ and another master regulator of adipogenic gene transcription, co- activator CCAAT/enhancer binding protein (C/EBP). Whereas the β-catenin-dependent signaling blocks the adipogenic lineage, it promotes both myogenic and osteogenic lineages. Hedgehog signaling results in the redirection of adipose precursors towards an osteogenic commitment. The hedgehog family of ligands suppresses adipogenesis through inhibition of the BMP signaling pathway (56,57). The second step towards the formation of new mature insulin sensitive adipocytes lies in the differentiation of already committed pre-adipocytes. In order for the mature adipocyte phenotype to be fully achieved, a functional synergy between PPARγ2 and C/EBPα is necessary. These 2 isoforms of PPARγ and C/EBP coordinately transactive a large number of genes expressed in mature adipocytes like insulin receptors encoding genes, adipose-specific gene *AP2* and adiponectin encoding gene *APM1*. A natural physiological ligand for PPARγ have not yet been identified but members of the synthetic thiazolidinediones (TZDs) family have been used as potent PPARγ ligands. Whereas a vital downstream effect of PPARγ is the activation of C/EBPα, both PPARγ2 and C/EBPα genes have C/EBP regulatory elements. Other regulators of adipogenesis are microRNAs that are found to promote adipogenesis or negatively regulate it (58,59). For example, mammalian homologs miR-8 induce adipogenesis through inhibition of Wnt signaling (59). But for most of the identified microRNAs, the mechanisms behind their effect have not been fully understood yet (57). Once all these regulatory processes align and adipogenesis induction is maximized, pre-adipocytes exit the mitotic clonal expansion phase and start losing their fibroblastic identity to acquire the morphological and metabolic features of adipocytes. This entitles the coordinated expression of proteins that include insulin receptors, enzymes of fatty acid and triacylglycerol biosynthesis, insulin-responsive glucose transporter 4 (GLUT4), secreted hormones like leptin and adiponectin, and many others (57).

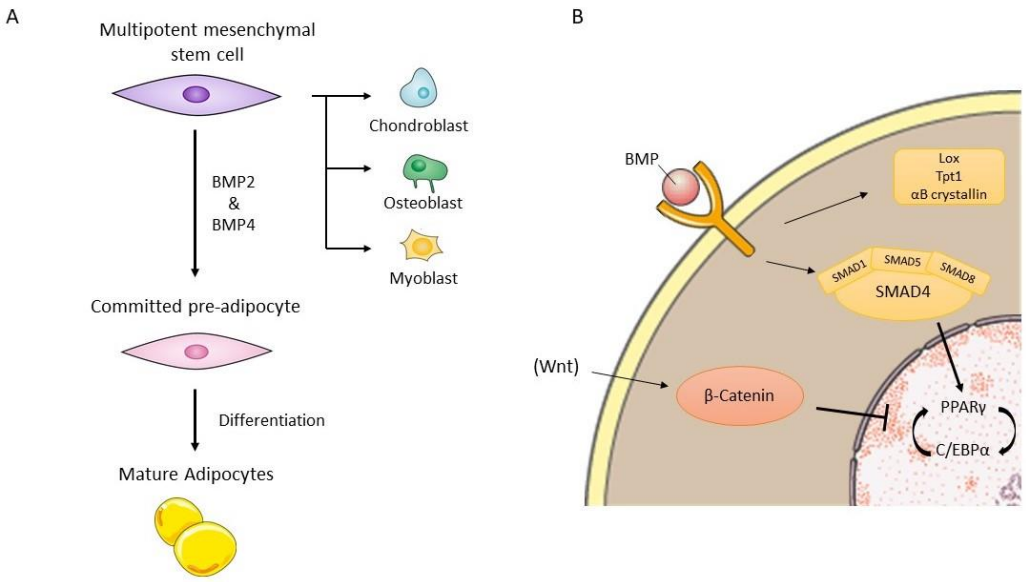

Figure 3: Adipogenesis. A: Multipotent fibroblast-like mesenchymal stem cells are adipocytes precursors but also that of chondroblast, osteoblasts and myoblasts. From MSC to mature adipocytes, 2 steps are involved; the commitment into pre-adipocytes and differentiation to adipocytes. B: The commitment into pre-adipocytes, BMP binding to its receptor induces a pathway leading to the functional synergy between PPARγ2 and C/EBPα – a requirement to achieve fully mature adipocytes.

Adipose tissue as a secretory organ

Adipose tissue, an endocrine organ, is responsible for the production of an array of cell-signaling molecules identified as "adipokines". Adipocytes are not the sole actors in the generation of the complete adipose secretome; precursor cells, fibroblasts and immune cells among others are major contributors. Within the AT, adipokines regulate adipogenesis, invasion of immune cells and the function and metabolism of adipocytes. And by targeting other organs like liver, muscle and brain, adipokines are involved in the regulation of food appetite and satiety, fat distribution, insulin sensitivity, glucose homeostasis, inflammation, etc… (2,60–64). The human adipokines pool comprises potentially at least 600 secretory proteins (61). Currently, out of all adipokines, only leptin and adiponectin are accepted as adipose tissue-derived hormones. But this does not exclude the role of various factors secreted by adipocytes in paracrine signaling (60,61).

Leptin, the first adipokine to be identified, is secreted primarily by adipocytes and its essential role lies in the suppression of appetite and the promotion of energy expenditure. Circulating leptin levels are in a positive correlation with body fat. Low

circulating leptin levels can reflect depleted lipid stores in AT and elevated energy demand. Leptin exerts its effect through the binding to leptin receptors (LEPRs) which is a type I cytokine receptor expressed in multiple cell types. In the hypothalamus, leptin suppresses appetite by inducing synthesis of anorexigenic peptides and blocking that of orexigenic peptides (65). By binding to LEPRs found in other peripheral tissues, leptin plays a regulatory role in bone, immune responses and angiogenesis. Leptin is also considered an important modulator of β-cell mass and survival (66).

The other adipose-secreted hormone is adiponectin, an adipokine exclusively produced by adipocytes and characterized by insulin sensitizing, anti-inflammatory and antiapoptotic systemic properties (2,60–64). The subcutaneous WAT is the depot mostly responsible for the circulating levels of adiponectin. The role of adiponectin in systemic insulin sensitization was demonstrated when adiponectin-deficient mice developed insulin resistance and when adiponectin-overexpressing obese mice preserved insulin sensitivity (67,68). Adiponectin activity is initiated by its binding to receptors adiponectin receptor protein 1 (AdipoR1) and AdipoR2. Adiponectin binds to AdipoR1 in muscle activating the AMP-activated protein kinase (AMPK) pathway whereas it binds to both AdipoR1 and AdipoR2 in liver suppressing hepatic glucose output through AMPK and/or increased ceramidase activity (2,60). Adiponectin effects extend to β-cells preventing their apoptosis and supporting their regeneration by inducing expression of β-cells transcriptional factor hepatocyte nuclear factor 4-α (HNF4A) (60,64). In addition, adiponectin displays anti-inflammatory and anti-fibrotic roles in other organs mediated by action on macrophages and fibrogenic cells (60).

Moreover, some adipokines are secreted by other cell types along with adipocytes (60–64). Examples of those are fibroblast growth factor 21 (FGF21) and retinol-binding protein 4 (RBP4) which are both secreted by hepatocytes. During fasting conditions, liver-secreted FGF21 stimulates the hypothalamus-pituitary-adrenal axis leading to increased hepatic gluconeogenesis and fatty acid oxidation. Whereas FGF21 secreted by AT induces the development of thermogenic beige adipocytes in WAT- a process known as browning. In the case of obesity and insulin resistance, increased plasma levels of RBP4 have been identified in several studies. And this

increase correlated with over-expression of *RBP4* in visceral AT. RBP4 directly stimulates insulin resistance in skeletal muscle and adipocytes through its receptor – stimulated by retinoic acid 6 (STRA6). Also, RBP4 generates systemic insulin resistance via the activation, in macrophages, of the toll-like receptor 4 (TLR4)-dependent signaling pathway inducing an inflammatory state specifically in AT (69). Interleukin-6 (IL-6) is secreted by many cell types besides adipocytes like immune cells. It can act as a pro-inflammatory cytokine at times and as anti-inflammatory at others, depending on the cell type that produces it, the receiving end and the context of systemic metabolic state at the time (2,60). Omentin is produced by stromal vascular cells of multiple tissues and is considered an insulin-sensitizing adipokine. Initially identified in vWAT, visceral adipose tissue-derived serpin – vaspin – is a serine protease inhibitor acting as an insulin sensitizer (2,60).

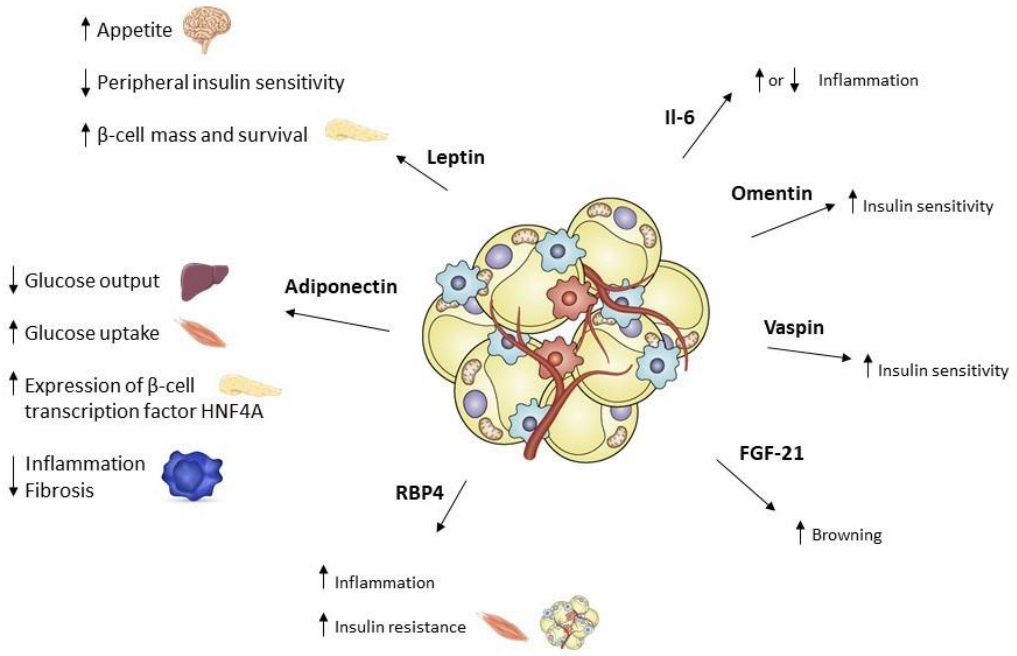

Figure 4: Adipose tissue as a secretory organ. Adipocytes and cells from the stromal vascular fraction of WAT produce and secrete adipokines that exert effects on WAT itself and other tissues like liver, skeletal muscle and hypothalamus. The action of these adipokines allows control over glucose and lipid metabolism.

A multitude of other adipokines have been identified but for most, more investigations around their activity and the mechanism through which they achieve it are imperative. However, the role of these adipokines, thus that of the adipose tissue, in the dynamics of metabolic homeostasis is undeniable.

Lipid and glucose metabolism

The function that defines adipose tissue most of all is the sustainment of energy homeostasis by regulating systemic glucose and lipid levels. A multitude of internal and external factors, like nutritional status and environmental temperature, generate a response from peripheral tissues to maintain energy homeostasis. The main processes adopted in response to the altering factors are lipogenesis, lipolysis, glycolysis and glyceroneogenesis. Under normal conditions, stimulated by endocrine and non-endocrine signals, the highly dynamic adipose tissue adapts to meet physiological needs (70–76).

During energy surplus, adipocytes store the excess of energy as triglycerides – triayclglycerols (TAG) – in the process of lipogenesis. Glucose is considered the first stimulator of the lipogenic pathway by triggering the synthesis and secretion of insulin from the pancreas. Insulin action is the most critical for lipogenesis since it induces two major aspects of this pathway. On one hand, insulin binds to its receptors on the surface of adipose cells activating the Akt pathway leading to the mobilization of the GLUT4 transporter thus allowing the uptake of glucose by the cell. And glucose in adipocytes undergoes glycolysis yielding acetyl-Coenzyme A (acetyl-CoA), the substrate for de novo synthesis of lipids like TAG and yielding glycerol-3-phosphate (G3P), important for another step in lipogenesis. On the other hand, insulin induces the activity of lipoprotein lipase (LPL) which is the key enzyme hydrolyzing circulating TAG that are bound to chylomicrons and very low-density lipoproteins (VLDL). After hydrolysis, the entry of the non-esterified fatty acids (NEFA) to cells is eased but still requires the facilitation of specific transporters like CD36, also known as fatty acid translocase (FAT), fatty acid transporter proteins (FATPs) and fatty acid-binding protein plasma membrane (FABPpm). It is important to mention that insulin also stimulates the translocation of these fatty acid transporters to cell membranes which makes insulin the predominant stimulus on the lipogenesis process. Once FFA are inside adipocytes a sequence of reactions leads to the synthesis of TAG. First, NEFAs are converted by acyl-CoA synthetase (ACS) to acetyl-CoAs where both pathways – the pathway initiating with circulating TAG and the de novo lipogenesis (DNL) initiating with glycolysis – converge. Next, G3P is acylated by glycerol-3-phosphate acyltransferase (GPAT) to produce

lysophosphatidic acid (LPA). Then, LPA becomes phosphatidic acid (PA) which is dephosphorylated to form diacylglycerols (DAG). The final step in TAG synthesis is dependent of the conversion of DAG to TAG by diacylglycerol acyltransferase (DGAT) (72,73,75,76). The sources for G3P, a limiting substrate for lipogenesis, are more than that provided by glucose through glycolysis; glyceroneogenesis is a different source from non-carbohydrate substrates like pyruvate, amino acids or lactate. In addition, lipogenesis is regulated by several factors. For example, acylation stimulating protein (ASP) increases TAG synthesis through stimulation of DGAT activity whereas growth hormone (GH) suppress the lipogenic pathway through the regulation of insulin sensitivity (72). De novo lipogenesis is regulated by sterol response element binding protein 1c (SREBP1c) and carbohydrate response element binding protein (ChREBP) that are transcriptional factors for two key enzymes in the DNL in adipocytes; fatty acid synthase (FAS) and acetyl-CoA carboxylase (ACC) (72,75,76).

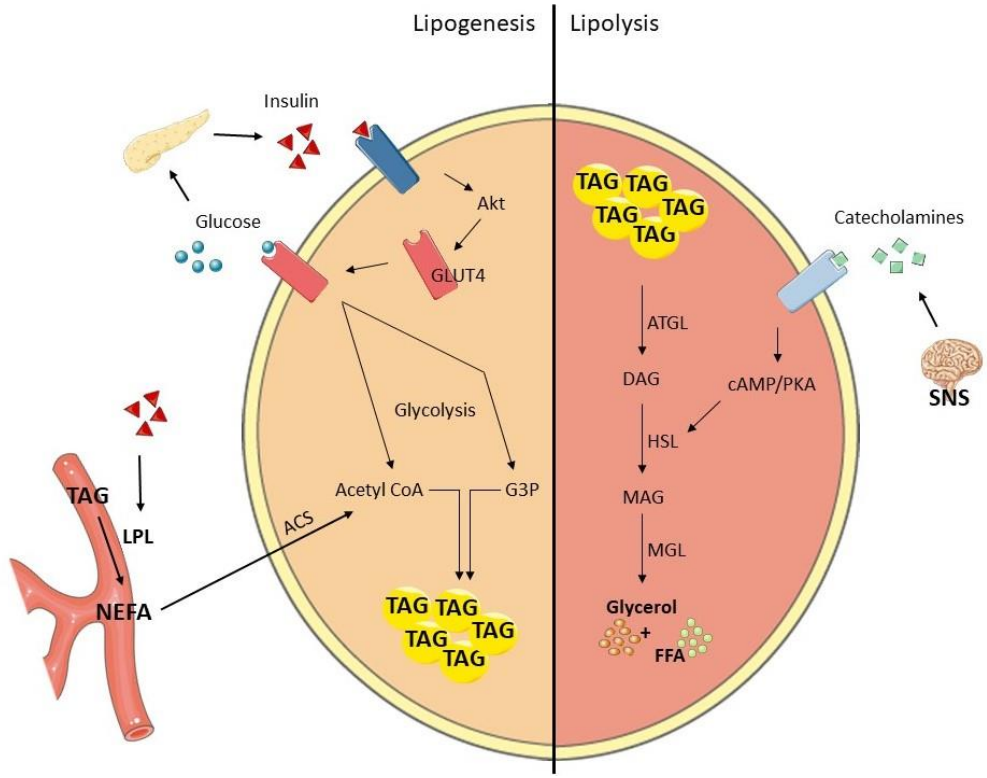

Figure 5: Lipogenesis and lipolysis in AT. Stimulated by energy excess, lipogenesis leads to the formation of TAG-containing lipid droplets in adipocytes. Lipolysis is induced by energy demand and causes the release of glycerol and FFA from adipocytes.

In opposite conditions, during periods of energy demand like fasting or exercising, lipolysis is stimulated. Lipolysis is the catabolic process leading to the release of FFA and glycerol from TAG stored in lipid droplets (LD) of adipocytes. The liberated molecules from WAT enter the bloodstream to fulfill the energy need and supply other peripheral tissues such as liver and muscle. In a state of high energy requirement, decreased levels of circulating insulin with increased levels of glucagon suppress lipogenesis and induce the lipolytic pathway. Glucagon and other factors such as catecholamines, natriuretic peptides (NP), growth hormone and thyroid-stimulating hormone (TSH) are stimulators of lipolysis. Glucagon and catecholamines induce cyclic adenosine monophosphate (cAMP)-dependent protein kinase A (PKA) activity by increasing cAMP production and activation of PKA. In the case of catecholamines, that include adrenaline and noradrenaline and are released by the sympathetic nervous system (SNS), this action is exerted through the binding to membrane-bound β-adrenergic receptors found on adipocytes. In a simplified manner, lipolysis is the lipase-based breakdown process of TAG, DAG and monoacylglycerols (MAG) into individual fatty acids. TAG is hydrolyzed into DAG by the adipocyte triglyceride lipase (ATGL). Once PKA is activated, it phosphorylates hormone-sensitive lipase (HSL) and allows its translocation to the lipid droplet through the phosphorylation of lipid droplet-associated proteins like perilipin 1. HSL is necessary for the conversion of DAG into monoglycerides and monoacylglycerol lipase (MGL) further hydrolyzes MAG into fully liberated glycerol and free fatty acids. Lipolysis is also tightly linked to thermogenesis where fatty acids are needed for heat production through β-oxidation (72–75).

1.2 Energy and metabolism

Homeostasis has been a widely used term over the past few decades. It originates from the Greek words translated into “same” and “steady”. Homeostasis, in living systems, is a self-regulation process that maintains internal stability while adjusting to changing conditions to keep an optimal status for survival. It is a dynamic equilibrium that favors a steady state by resisting the forces that disrupt a relatively uniform internal environment. Homeostasis is achieved through regulatory responses known as feedback controls; negative feedback – counteracting the direction of change caused by the disturbance – and positive feedback – amplifying the effect of the disturbance thus moving the system away from its starting state. Homeostatic regulations imply the existence of a “preferable” steady state and an integration of functions and coordination between multiple systems to achieve that state. Human physiology is subjected to an array of intrinsic and external elements threatening its equilibrium. Here, we discuss some critical concepts in physiological homeostasis and the factors that influence it.

1.2.1 Energy balance

Energy balance is achieved through a complex physiological control system. The main components of energy balance are energy intake, energy expenditure and energy storage. Energy intake (EI) is derived from individual daily consumption of dietary nutrients whereas energy expenditure (EE), better identified as total energy expenditure (TEE), can be divided into different components: the resting energy expenditure (REE), diet-induced thermogenesis (DIT), activity-induced energy expenditure (AEE) and energy for body thermoregulation (77–79). REE is the energy necessary to support basic metabolic activities and diet-induced thermogenesis (DIT) is the energy required to process the ingested food and it can from 10 to 15% of TEE. AEE is the energy spent on physical activity and exercise making it the component of TEE with the highest variability based on the amount of exercise performed, the energy cost of the physical activity and the individual performing it. When EI and EE are equal, energy balance – generally considered

equivalent to body weight (BW) – is stable. BW changes have been attributed to an inequality between EI and EE over, a not fully understood, given period of time making energy balance a complex process subjected to physiological control (77–79). Metabolic adaptations that are independent of fat-free mass (FFM) or FFM composition but influence energy balance are known as adaptive thermogenesis (79). This adaptive thermogenesis limits the effect of changes in EI and/or EE and it is thought to be responsible for about 50% of the less-than expected weight loss in obese patients (80).

Adaptive thermogenesis has been associated to physiological alterations in response to weight loss, chronic overfeeding, refeeding after weight loss and maintaining weight loss. During calorie restriction and/or excessive exercise leading to weight loss, decreases in all the EE components, the resting and non-resting, are recorded (77,79). Adaptive thermogenesis varied between individuals in this case but was not influenced by the strategy employed for the achieved weight loss (79). Studies with controlled overfeeding have observed a lower-than expected increase in BW in correlation with the excess of EI. This was attributed to a rise in EE, more specifically the non-resting EE, due to obligatory costs such as gaining body protein and increased energy cost in physical activity. The composition of the dietary intake during overfeeding generates different adaptations in EE. Overfeeding based on macronutrients of carbohydrates and fat had no effect on EE while a hypercaloric protein-rich diet (25% of total dietary intake) increased EE. After starvation periods, the spontaneous response from recovering individuals is overeating. And because of the starvation-induced suppression of thermogenesis, documented as mass-independent, weight gain and expansion of fat mass occur rapidly. But with controlled caloric restriction-refeeding cycles, within two weeks, the previously decreased REE was reversed (81,82).

The modern way of life threatens energy homeostasis and favors positive energy balance. Industrialization and urbanization have allowed food to be more available, accessible and less costly encouraging increase in EI. In addition, a sedentary life is more common and even aided by all the advancements and facilitations for daily tasks which causes a significant decrease in EE.

Regulation of energy balance by gut-brain axis

The complex regulations promoting a homeostatic state of systemic energy are predominantly coordinated by the brain. Neural and chemical input from peripheral organs is constantly received by the central nervous system (CNS) and then integrated and processed for the generation of the appropriate responses to preserve energy homeostasis. The input can be divided into two types; long-term signals also known as tonic signals and short-term signals or episodic. Tonic signals like leptin and insulin are continuously secreted reflecting fat mass whereas episodic signals fluctuate depending on the state of ingestion. The first site in the body to interact with ingested nutrients is the gastro-intestinal (GI) tract. It is a highly innervated site responsible for the majority of episodic signals that reveal and communicate the caloric value of the dietary intake and its macronutrients composition (83). The gut-brain axis is a bi-directional signaling axis crucial for the maintenance of energy balance. The sensory information gathered in the GI tract is converted into neural, hormonal and immunological signals that communicate with the CNS. These signals were firstly identified as satiety signals with the role of suppressing EI but, more recently, have been demonstrated to impact EE as well. The most recognized episodic signals are cholecystokinin (CCK), glucagon-like peptide-1 (GLP-1) and peptide YY (PYY). Throughout the GI tract and at several sites, specialized cells that respond to pre-absorptive nutrients play a role in regulating energy balance by inducing responses from the CNS resulting in acute and chronic modification in EI and EE. These specialized cells are named enteroendocrine cells (EECs) and they occupy the intestinal lining, open to luminal contents, and express on their apical surfaces the chemosensory machinery. Starting with the stomach, EECs are X/A-like cells that produce ghrelin and chief cells that produce gastric leptin. I and K cells can be found in the proximal small intestine and they produce CCK and glucose-dependent insulinotropic hormone, respectively. And L cells that produce GLP-1/2 and PYY reside in the distal small intestine. Upon stimulation, the gut-derived peptides are released from EECs into the proximal circulatory vessels allowing them to act as endocrine messengers that target peripheral tissues. However, in a large part, gut-derived peptides have local paracrine activity through binding to receptors expressed in afferent neurons

innervating the GI tract lining (83). The role of these gut-derived peptides and the mechanism through which they exert their effect differ and are unique for each. Ghrelin is found in high concentration during fasting and is associated with the feeling of hunger thus promoting energy intake. During and just after a meal, ghrelin is inhibited to rise again gradually until the next meal. Ghrelin induces gastric emptying, inhibits insulin secretion by pancreatic β-cells and encourages glucagon secretion (84). CCK is the best-established satiation signal and controls meal-related glycemia directly by reducing hepatic glucose production and indirectly by sowing gastric emptying (83,84). GLP-1 inhibits food intake by stimulating satiation, it delays gastric emptying and it also acts on the pancreas suppressing glucagon secretion (84,85). PYY is best recognized as an anorectic peptide inhibiting food intake. It may contribute to delaying gastric emptying and inhibiting intestinal mobility (84,86).

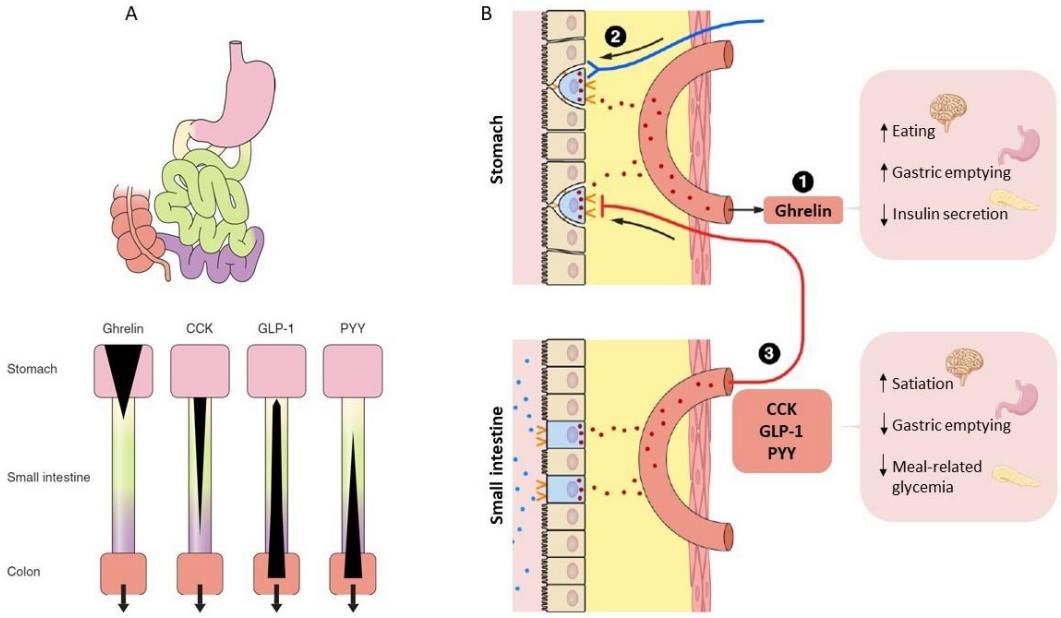

Figure 6: Enteroendocrine cells distribution, secretion and physiological role. A: Distribution of EECs secreting ghrelin, CCK, GLP-1 and PYY in the stomach (pink), duodenum (yellow), jejunum (green), ileum (violet) and proximal large intestine (dark pink). Black areas indicate the relative densities of expression of EECs producing the indicated hormones. B: Ghrelin is secreted from close-type EECs (blue cells in stomach lining) into gastric capillaries (1). The secretion of ghrelin is stimulated by neural controls (2) and inhibited by small-intestine nutrient sensing and the secretion of CCK, GLP-1 and PYY (3). These secretory controls are produced by open-type EECs. (adapted from (84))

Another important regulator of energy balance is gut microbiota, the collective microbial community residing in the GI tract. This community exists in a symbiotic

relationship with the host organism: nutrient-rich environment is provided for the survival of the microbiota and in exchange, the microbiota contributes to protective, structural and metabolic functions (78,83). These micro-organisms are involved in the digestive process, they extract energy from nutrients indigestible by humans. Gut microbiota supplies almost 10% of daily energy requirement via the production short-chain fatty acids (SCFA) – mainly butyrate, acetate and propionate – from indigestible carbohydrates that are the major sources of energy for many peripheral tissues like the intestines and the liver. In addition, SCFAs activate receptors on the surfaces of EECs and thus, induce the release of gut-derived peptides. Several studies with prebiotics revealed the effect of gut microbiota to influence the gut-brain axis by improving gut nutrient sensing mechanism and inducing EEC differentiation and subsequently increasing gut-derived peptides production (78,83). All that was mentioned means that energy intake is not only dependent on the caloric intake and nutritional composition but also on the inhabitants of the GI tract. A complexity in individual microbiota introduces further variations and errors in the prediction of EI and EE where the role of microbiota is not accounted for or considered difficult to control and measure. Hence, estimation of the contribution of nutrition on energy balance is extremely complex.

1.2.2 Energy metabolism and mitochondria

"*Rien ne se perd, rien ne se crée, tout se transforme*" is the famous saying by Antoine Laurent Lavoisier who is considered the father of modern chemistry. At a cellular level, this statement cannot be more true to describe energy metabolism. The sum of all chemical reactions occurring in a living cell enabling it to survive, multiply and reproduce is the definition of metabolism. These reactions can either harness energy or release it which creates the difference between the two metabolic pathways, anabolic and catabolic. Anabolism is the biosynthesis of macromolecules and biomolecular polymers via utilization of energy whereas catabolism is the breakdown of these complex macromolecules into simpler molecules and generating energy. In a simplistic manner, the ingested macronutrients – carbohydrates, lipids and proteins – fuel the organism when digested providing the

energy needed to perform whole-body functions. Animal tissues have five major sources of fuel: glucose, fatty acids, amino acids, ketones and lactate. When in excess, glucose and FAs are stored in polymers mainly glycogen and TAG, respectively. During starvation, these polymers are degraded and amino acids are liberated from proteins to sustain different tissues. Ketone bodies and lactate cannot be stored and are only transiently produced in the organism (87).

Glucose metabolism

Glucose is transported from the bloodstream into a cell via GLUTs – type and class depending on cell type – and sodium glucose cotransporters (SGLTs) by facilitated diffusion. In a critical rate-limiting step, glucose is phosphorylated with a phosphoryl group from adenosine-triphosphate (ATP) into glucose-6-phosphate (G6P) by the enzyme hexokinase or glucokinase. From that point on, the fate of G6P depends on physiological conditions and metabolic needs.

Glycolysis is the breakdown of a glucose molecule into pyruvate or lactate molecules in the cytosol that occurs in most living cells. The end product of the glycolytic pathway depends on whether the cells are in aerobic or anaerobic conditions. In the first phase of glycolysis – the investment phase – every glucose molecule yields two 3-carbon molecules glyceraldehyde-3-phosphate (GAP) utilizing 2 ATP. With the second phase – the payout phase – each GAP molecule, utilizing adenosine diphosphate (ADP), an oxidized forms of nicotinamide adenine dinucleotide (NAD^+) and inorganic phosphate (Pi) is further oxidized, phosphorylated and interconverted to yield a total of 2 pyruvate molecules, 4 ATP, 2 reduced forms of nicotinamide adenine dinucleotide (NADH) and $2H^+$ and 2 H_2O molecules. In the case of aerobic conditions, the produced NADH passes its electrons onto the electron transport system (ETS) where it is re-oxidized thus regenerating cytosolic NAD^+. The recycling of NAD^+ is crucial to allow the continuity in glycolysis. During anaerobic conditions, that same NADH via the activity of lactate dehydrogenase (LDH) reduces pyruvate to lactate regenerating NAD^+ (88–90).

Intermediates of glycolysis can also be generated from other pathways such as the pentose phosphate pathway (PPP) which occurs in the cytosol in parallel to glycolysis. In regard to metabolism of sugars, the PPP provides a pathway to

breakdown the consumed 5-carbon sugars and the less popular 4- and 7-carbon sugars. In its oxidative phase, the PPP allows the production of the important reducing agent for several cellular processes, nicotinamide adenine dinucleotide phosphate (NADPH). In its following phase, the non-oxidative, pentose sugars are synthesized which are precursors for nucleotide synthesis (87).

Gluconeogenesis is the anabolic process opposing glycolysis. Following glycogen depletion, gluconeogenesis is adopted by the liver and the kidneys to supply the bloodstream with glucose. It is not an exact reversal of the glycolytic pathway due to the irreversible reactions in the glycolytic pathway specially the highly energetically favorable formation of pyruvate from phosphoenolpyruvate (PEP). To move from pyruvate to PEP, first, pyruvate is converted in the mitochondria into oxaloacetate then malate to be transported out into the cytosol where, in the second step, it is converted back to oxaloacetate and finally to PEP through PEP carboxylase (PEPCK) (91).

Glucose is essentially stored in the form of glycogen mainly within the liver and muscles. Glycogen is a multibranched polysaccharide of glucose stored as granules in the cytosol. Its synthesis is known as glycogenesis and it requires uridine diphosphate glucose (UDP-glucose), an activated form of glucose. This activation allows glucose to be added to non-reducing end of glycogen for further expansion of the polymer. When in need, glycogen is degraded releasing glucose-1-phosphate which is converted to G6P. Within the liver, this breakdown allows the delivery of glucose into the bloodstream whereas within a muscle, the degradation of glycogen is in the purpose of supplying energy to that tissue (91).

Amino acids metabolism

Amino acids, the building blocks of proteins and nucleotide bases among other nitrogenous products, provide alternative carbon sources for metabolic processes. Amino acids (AAs) are categorized according to their sources; essential AAs can only be acquired via dietary intake, non-essential AAs can be synthesized by the organism and conditionally essential AAs are synthesized by body but additional amounts should be consumed to meet the need for utilization. The major

site for AA metabolism is the liver but other tissues like skeletal muscle, kidneys and adipose tissue mostly are also involved.

Amino acid transamination is the transfer of an α-amino group from an AA to a carrier molecule, usually an α-keto acid, yielding another AA and α-keto acid. This reaction is catalyzed by aminotransferases. Three very common α-keto acids are pyruvate, oxaloacetate and α-ketoglutarate. An AA transamination generating pyruvate is the reaction between L-alanine with α-ketoglutarate to give pyruvate and the new AA L-glutamate. Another pathway for the catabolism of AAs is oxidative deamination. It occurs mainly in liver and in the mitochondria of cells. Oxidative deamination generates α-keto acids and the toxic byproduct ammonia which is later neutralized in the urea cycle. Glutamate is the essential AA involved is this pathway and it is catalyzed by glutamate dehydrogenase (GDH) utilizing co-enzymes NAD^+ and $NADP^+$ to give α-ketoglutarate, ammonia and NADH (87,92).

Fatty acids metabolism

Among the many functions of lipids in the organism, in terms of metabolism, they are stored as TAGs in adipose tissue and provide a potential alternative source of energy to carbohydrates. TAGs have high energy value since their degradation provides more energy per gram than carbohydrates and proteins. Fatty acids provide 50 to 70% of the energy required by the heart, the most energy-demanding organ.

FAs are either consumed or synthesized de novo. In the liver, the main site for FA synthesis, excess glucose is converted into FAs. The hepatic lipogenic pathway begins with pyruvate, the product of glycolysis, being imported into the mitochondria where it is converted to citrate. Citrate is exported out of the mitochondria and catalyzed to yield acetyl -CoA. In the cytosol, acetyl-CoA is carboxylated by ACC to give malonyl-CoA that is the precursor, along with NADPH, of the enzyme fatty acid synthase (FAS) for palmitic acid synthesis. Palmitate is a 16-carbon FA that is further elongated in the endoplasmic reticulum (ER) by fatty acyl-CoA elongase (Elovl) to generate long-chain FAs (LCFAs). The enzymes stearoyl-CoA desaturases (SCD) cause the desaturation of these LCFAs yielding mono- and poly-unsaturated FAs (MUFA and PUFA, respectively). All 3 latest products – palmitic

acid, LCFA and UFA – are esterified with glycerol-3-phosphate from the glycolytic pathway to produce TAGs. They can also be esterified with cholesterol to generate cholesterol esters.

In the fasted state, FAs undergo fatty acid β-oxidation in the mitochondria providing energy supply and ketone bodies (91,93). In the first rate-limiting step of this process, previously activated FAs into acyl-CoAs in the cytosol require their translocation to the mitochondria. This translocation is mediated by the carnitine palmitoyltransferase system that includes carnitine palmitoyltransferase 1 and 2 (CPT1 and CPT2) and carnitine acylcarnitine translocase (CACT). CPT1 integrated in the outer-mitochondrial-membrane transesterifies acyl-CoA to acylcarnitine that is transported across the inner mitochondrial membrane via CACT. Then, CPT2 located on the inner-mitochondrial-membrane protein completes the cycle by reconverting the acylcarnitine into an acyl-CoA. Once inside the mitochondria, acyl-CoAs are degraded through a 4 steps enzymatic process releasing with each step two carbons in the form of acetyl-CoA. First, acyl-CoA dehydrogenase with FAD^+ oxidizes acyl-CoA to form trans-enoyl-CoA which is subsequently hydrated by enoyl-CoA hydratase to generate (3)-hydroxyacyl-CoA. Next, NAD-dependent dehydrogenation occurs producing (3)-ketoacyl-CoA and reduced electron carrier NADH. In the last reaction of fatty acid β-oxidation, a thiolase cleaves the 3-ketoacyl-CoA into an acetyl-CoA and a two-carbon chain–shortened acyl-CoA. Fatty acid β-oxidation can also occur in peroxisomes for FAs that the mitochondria are unable to utilize. Besides the acetyl-CoA and ketone bodies produced by the β-oxidation pathway, the reduced electron carrier $FADH_2$ and NADH are directly fed by the ETS. Mitochondrial β-oxidation is regulated by several transcriptional and posttranscriptional factors such as PPARα and malonyl-CoA, respectively. PPARα is the master regulator of this pathway promoting fatty acid β-oxidation by controlling gene expression of many fatty acid oxidation enzymes in the liver, skeletal muscle and heart (94). Whereas malonyl-CoA acts as an inhibitor of the CPT1 enzyme thus blocking the translocation of acyl-CoAs into the mitochondria.

Tricarboxylic acid (TCA) cycle or Krebs cycle

Under aerobic conditions, the end-product of glycolysis – pyruvate – is oxidized by pyruvate dehydrogenase (PDH) to form acetyl-CoA which is also the product of fatty acid β-oxidation. The main function of acetyl-CoA is to promote energy production in mitochondria by transferring its acetyl group to the TCA cycle.

The TCA cycle is the sum of 8 reactions starting with the irreversible citrate synthesis from acetyl-CoA and oxaloacetate which is the end-product of the last reaction in the cycle. The first, third and fifth reactions of the TCA cycle are the most crucial and controlled. The 6-carbon citrate synthesized in the first step is either transported to the cytosol for initiation of FA synthesis or is committed to the oxidative steps in the TCA cycle. Step 3, generating α-ketoglutarate, is highly regulated and the commitment to the TCA cycle is promoted by NAD^+ and ADP but suppressed by NADH and ATP. The synthesis of succinate in the fifth step is coupled to the phosphorylation of GDP to GTP yielding the only high energy phosphate in this cycle. The whole Krebs cycle is highly controlled and its intermediates provide the substrates for other reactions in different metabolic pathways, hence, the importance of anaplerosis and cataplerosis. Anaplerosis is the replenishing of the intermediates of the TCA cycle that have been extracted for biosynthesis. Whereas cataplerotic reactions ensure the exit of the intermediates from the TCA cycle avoiding over-supply. Examples of cataplerosis are the use of citrate in fatty acid synthesis and α-ketoglutarate for amino acid and purine nitrogenous base synthesis (95,96).

Electron transport system (ETS) within the mitochondrion

Mitochondria are the site of not only the TCA cycle but also, oxidative phosphorylation (OXPHOS), the process making the ETS. The major contribution of the ETS to energy production in the form of ATP, the primary carrier of energy in cells, deemed mitochondria as energy powerhouses. NADH and $FADH_2$, the products of the TCA cycle, are critical for the ETS since they provide the first electrons used at the beginning of the ETS reactions. The mitochondrial electron transport system comprises 4 transmembrane complexes embedded in the inner mitochondrial

membrane (IMM) that allow the flow of electrons along themselves to reach the final electron acceptor, oxygen. This makes aerobic conditions critical for the occurrence of OXPHOS also recognized as mitochondrial respiration (97,98). At the start of OXPHOS, the energy potential is highest and as electrons pass through the complexes, energy level drops releasing energy via each step. Energy released is used by the complexes to pump protons into the intermembrane space from the matrix. Due to the impermeability of the IMM to protons, an electrochemical gradient across the membrane develops which drives the synthesis of ATP via ATP synthase, the final transmembrane protein involved in the OXPHOS (99). There are several entry points into the ETS which converge at two different sites, the N-junction or the Q-junction. The NADH pool in the matrix represents the N-junction. Complex I (CI), also known as NADH-ubiquinone oxidoreductase, is the largest of complexes in the ETS. It seizes electrons from matrix NADH and transfers them to ubiquinone also called coenzyme Q (CoQ) leading to its reduction to ubiquinol (QH_2). Ubiquinone along with cytochrome c are the two electron carriers of the ETS participating in OXPHOS in addition to the complexes. In CI, the passage of electrons from NADH to ubiquinone comprises a series of reactions via co-factors like flavin mononucleotide (FMN) and iron-sulfur (FeS) clusters. The mechanism allowing proton translocation is not fully understood, hence the definitive number of protons moved through the membrane through complex I, and the link between electron transfer and proton pumping remain unclear. Another entry into the ETS converging at the Q-junction- CoQ- occurs via CII, succinate dehydrogenase, which is an enzyme involved in the Krebs cycle as well. Distinctively to CI, no protons are translocation through the IMM when electrons flow pass CII. In addition, electrons can be transferred to the Q-junction via the electron transferring flavoprotein complex (CETF) or other mitochondrial enzymes such as glycerophosphate dehydrogenase, dihydroorotate dehydrogenase, proline dehydrogenase, choline dehydrogenase and sulfide-ubiquinone oxidoreductase. CETF gets its electrons from $FADH_2$ produced during fatty acid β-oxidation. Complex III (CIII), a cytochrome bc_1 complex commonly referred to as CoQ-cytochrome c reductase, oxidizes ubiquinol and transfers one electron an oxidation at a time to cytochrome c, the second electron carrier of the ETS. The last complex of the electron transfer pathways is, cytochrome c oxidase, complex IV (CIV) through which electrons are passed from reduced

cytochrome c to the final electron acceptor O_2 leading to production of H_2O. Throughout the flow of electrons from CI to CIV, a total of 10 protons is translocated to the intermembrane space creating a protonmotive force that drives the re-entry of protons to the matrix. This re-entry happens in two ways; either through complex V or through proton leak facilitated by uncoupling proteins. The proton leak dissipates the membrane potential as heat at the expense of ATP production. On the other hand, the dissipation of membrane potential through complex V (CV) recognized as F_1F_0 ATP synthase, is coupled to the production of ATP. F_1F_0 ATP synthase consists of two domains: F_1 and F_0 where F_0 is located at the IMM and F_1 in the matrix. Protons first pass through F_0 which causes the conformational change in CV by transferring the stored energy created by the electrochemical gradient to F_1. The conformational change allows ADP to be phosphorylated to generate ATP. The final ATP yield of a glucose molecule going through glycolysis followed by the TCA and OXPHOS, is between 30-32 ATP (97,98).

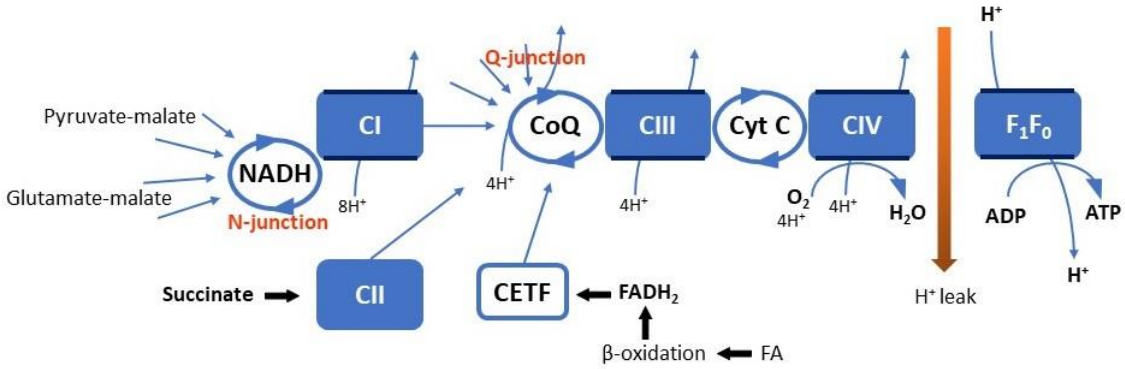

Figure 7: ETS and OXPHOS in mitochondria. The mitochondrial electron transfer system is fueled by diffusion and transport of substrates across the inner and outer mitochondrial membranes. There are two sites where electron transfer converges, the N-junction and the Q-junction. The unlabeled arrows into the Q-junction indicate the additional sources of electrons converging into the ETS. The resulting electrochemical gradient created in the intermembrane space, drives the phosphorylation of ADP to ATP via ATP-synthase and also induces proton leaks through the IMM (adapted from (99)).

Besides the role of each complex and co-factor in the ETS, it has been established that for optimal function of the oxidative phosphorylation, complexes interact and form supercomplexes. Complexes I to IV physically interact forming a variety of supramolecular structures – supercomplexes – dependent of assembly factors that affect their biogenesis and functional properties (100). It is important to mention that electrons which escape the ETS contribute to the generation of cellular reactive

oxygen species (ROS). Under physiological conditions, it is estimated that between 0.2 to 2% of electrons in the ETS leak out of it and interact with oxygen to form superoxide or hydrogen peroxide. Therefore, mitochondria are a main source for cellular ROS production. So far, 11 different sites along the ETS of the mammalian mitochondria have been identified as sites of superoxide and/or hydrogen peroxide production. CI and CIII are considered to be the most involved in this process. An increase in ROS production is tightly linked to hypoxia and a multitude of disorders (97,98).

The sum of all factors involved in the previously mentioned metabolic pathways and cellular processes make up the metabolome of adipose tissue. Any changes in lifestyle causing a shift in energy intake or energy output prompt modifications in the levels of certain metabolites provoking alterations to these processes. In the following chapter, obesity and its consequences on cellular pathways in white adipose tissue is outlined.

1.3 Adipose tissue revisited in obesity

1.3.1 Obesity

Maintaining a positive energy balance constantly for a significant period of time challenges the homeostatic controls and prevents stabilization of body weight and body fat mass. As defined by the world health organization (WHO), overweight and obesity are "abnormal or excessive fat accumulation that presents health risk". For the past years, overweight and obesity have reached epidemic proportions where the number of obese individuals has almost tripled since 1975. In the latest data released in 2016, it was stated that more than 1.9 billion adults were overweight which of, over 650 million were obese. These numbers mean that 39% of the adult world population was overweight and around 13% obese.

Obesity is a major risk factor for noncommunicable diseases (NCD) thus, it is linked to lowered life expectancy and premature disabilities. Due to the extent of its impact and the changes it drives, obesity has even been declared by various medical federations and associations as a chronic progressive disease instead of solely a risk factor for other diseases (101). Even though it is agreed upon that an energy imbalance leads to obesity, a full understanding of the causes behind obesity is still to be achieved. Obesity is complex since the same energy imbalance can have very different and unique ranges in the severity of the condition and its associated comorbidities. The rise in obesity has been paralleled with an eased access to food and a sedentary behavior. Nowadays, food is made more available and accessible; it has become less of a luxury for just a few with promotion of large portions at fair prices, encouragement for frequent snacking and consumption of products high in sugars, and the introduction of fast food along with the reduction in home-cooked meals. In addition, as a result of the recent work habits and advancement in technology, low energy expenditure is promoted; physical activity is decreased due to most occupations being computer-based, time-consuming jobs cause difficulties to keep healthy exercise routines, air conditioning use reduces energy expenditure required for body temperature maintenance, etc…(102–104).

1.3.2 Obesity in adipose tissue

A persistent positive energy balance imposes modifications to the structure and function of adipose tissue. The capacity of adipose tissue to adapt to the energy surplus and sustain it through expansion and alterations in metabolic pathways determines the metabolic health of obese individuals. The associated co-morbidities of obesity such as T2DM, non-alcoholic fatty liver disease (NAFLD), cardiovascular diseases (CVDs), and cancer are related to a low-grade chronic inflammatory state. Even though the trigger for this inflammatory state and the causal relationship between inflammation and obesity complications are not fully understood, the link between obesity and inflammation is undeniable; the degree of inflammation correlates directly with the severity of systemic insulin resistance (105–108).

Chronic inflammation starts with a trigger, usually a stressor, that induces an acute adaptive inflammatory response considered a protective response to restore physiological homeostasis. This response implies the suppression or overriding of incompatible homeostatic controls and when the stressor is continuous, these regulations persist and translate into a long-term maladaptive phase that prompts a change in homeostatic set points making the organism more vulnerable to chronic pathological states (108). The initial trigger in the case of obesity is a positive energy balance lead by overnutrition which particularly exerts its stressor effect on adipocytes. Adipocytes become hypertrophic, hypoxic, more prone to apoptosis and under mechanical stress from interactions with the ECM. Adipocytes, having a primary role in controlling energy homeostasis, are pushed to contain the energy surplus through the secretion of adipokines stimulating the recruitment of other cell types promoting healthy adipose tissue expansion. However, when this adaptive machinery is no longer a temporary adjustment, a restoration to the previous homeostatic state becomes more challenging and new set points for physiological cues are achieved such as weight, glucose blood levels, circulating lipid and hormone levels. These new set points are paralleled with reduced metabolic plasticity, insulin resistance, abnormal tissue remodeling and fibrosis (105).

With a focus on adipose tissue, the adaptive state turned into low-grade chronic inflammation is discussed in further detail. The purpose of the following section is

to emphasize on the role of the cross-talk between all cell types in adipose tissue producing an obesity-induced phenotype of WAT.

Adipocytes and adipogenesis in obesity

In adipose tissue, an increase in size and number of mature adipocytes is enforced in order to match the increased demand for lipid storage during caloric excess (109,110). It is thought that the number of adipocytes in WAT is tightly regulated and determined by adulthood which implies that the increase in size of adipocytes rather than the increase in number of adipocytes is the major and initial mechanism adopted by expanding WAT. The size of adipocytes positively correlates with glucose intolerance, insulin resistance, hyperinsulinemia, increased adipocyte death rate and inflammation of adipose tissue (111–114). Hypertrophic adipocytes show significant modifications in their cellular metabolism; their basal lipolysis levels are elevated leading to FFA leakage, and they express a lower lipogenesis-to-lipolysis ratio compared to smaller adipocytes (115,116). As a recovery mechanism to lipid-overloaded adipocytes, hyperplasia is induced and adipogenesis in WAT is stimulated in an attempt for metabolic repairs. Adipogenesis is highly dependent on the abundance of adipocyte progenitors (APs) in WAT. Among the differences between SAT and VAT is the larger number of APs in SAT compared to VAT which influences the capacity of these depots to expand. An increase in VAT mass in healthy lean subjects is predominantly attributed to hypertrophic adipocytes whereas in SAT, hyperplasia is a more common reoccurrence due to the increased progenitor number and/or activity (117,118). However, in diet-induced obese mice, a high-fat diet (HFD) initially stimulates hypertrophy in all depots but within two months of HFD, hyperplasia is seen in VAT while being very limited in SAT (119,120). In young animals, adipogenesis induced by HFD has been observed in both SAT and VAT whereas in adults, it was only observed in VAT. The reduced capacity of self-renewal of the tissue in SAT hence a failure in SAT plasticity is tightly linked to insulin resistance thus to metabolic derangements (121). In humans, similar findings were reported (122). Thus, even though characteristically SAT is more prone to cellular proliferation, at the onset of diet-induced obesity, adipogenesis may be restricted to VAT.

Impaired adipogenesis in obesity has been documented by numerous studies focusing on adipogenic genes, the commitment of AP to the adipogenic pathway and final adipogenic differentiation (109,110,123). Adipogenesis is a multistep process that includes firstly, the commitment of pluripotent stem cells to the adipocyte lineage followed by the terminal differentiation of preadipocytes into fully mature adipocytes. In hypertrophic adipose tissue, alterations to the pathways involved in the various steps of this process have been identified and associated with unhealthy adipose tissue expansion. In the commitment step of adipogenesis, BMP4 drives APs towards the adipogenic lineage by stimulating transcriptional activator zinc-finger protein 423 (ZNF423) and suppressing the activity of its inhibitor wnt1-inducible-signalling pathway protein 2 (WISP2). The canonical Wnt pathway, β-catenin dependent, maintain precursor cells as uncommitted and undifferentiated which is inhibited by the dickkof (DKK) family proteins. The DKK1 protein acts as an autocrine regulator during adipogenesis. In hypertrophic WAT, even though BMP4 is highly expressed and secreted by adipocytes, it is counteracted by increased levels of gremlin 1, a known inhibitor of BMP4. In addition, WISP2 expression is increased which stimulates the proliferation of MSCs and APs hence maintaining them lineage-uncommitted. Furthermore, in hypertrophic obesity, *DKK1* expression is decreased leading to a failure in the suppression of the canonical Wnt pathway (124–126). In the second step of adipogenesis, the adipocyte terminal differentiation is dependent on transcriptional factors PPARγ and C/EBPα. The promoters for the genes of these factors contain C/EBP regulatory elements and mainly require the expression of C/EBP-β as well as C/EBP-δ. Once induced, PPARγ and C/EBPα function synergically as pleiotropic transcriptional activators to further stimulate adipocyte differentiation. PPARγ and C/EBPα promote and maintain the expression of key adipogenic genes for adipocyte function and insulin responsiveness such as GLUT4, FABP4 and adiponectin (56,109,126). In human adipose tissue, PPARγΔ5 has been identified as a PPARγ isoform where a naturally-occurring splicing event leads to the skipping of exon 5. PPARγΔ5 acts as dominant-negative isoform by suppressing PPARγ activity thus affecting the differentiation potential of pre-adipocytes. In SAT, the expression of PPARγΔ5 was found to correlate positively with BMI of obese individuals which could contribute to the reduction of adipogenesis observed in SAT (127). In addition, various inflammatory molecules

act on cells of the adipose tissue disrupting adipogenesis. An example is TGF-β, considered an anti-adipogenic inflammatory molecule that is secreted by hypertrophic adipocytes and by immune cells infiltrating the adipose tissue. TGF-β acts by directly inhibiting PPARγ - C/EBPα complex. Other inflammatory factors can exert their effect indirectly through downstream signalling like tumor necrosis factors (TNF) inducing the expression of TGF-β (128).

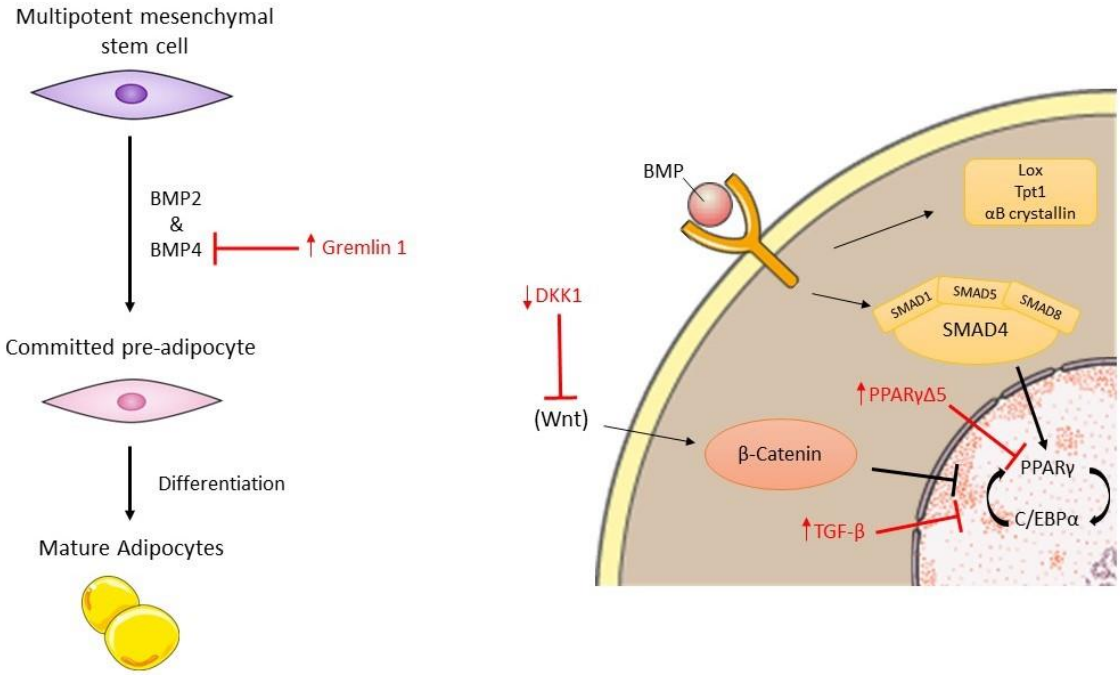

Figure 8: Impaired adipogeneis induced by obesity. In hypertrophic adipose tissue, some of the regulatory factors involved in adipogenesis have different levels of expression (marked in red). These alterations modify pathways involved in both, the commitment of progenitor cells into the adipogenic lineage and their differentiation into fully functional adipocytes.

An impaired adipogenesis profile, mainly caused by hypertrophic adipocytes, restricts WAT expansion and especially SAT to hypertrophy causing further derangements in cellular and metabolic processes. Therefore, the cellular population of WAT depots is altered and subsequently its function and metabolic processes.

Overnutrition as a trigger for inflammation in AT

Plasticity is a major characteristic of the adipose tissue and in cases of obesity, the limits of this plasticity are tested. An "expandability hypothesis" for adipose tissue has been the subject of many investigations. This hypothesis states

that absolute body mass is not the determinant of the demonstration of metabolic complications but instead it is the inability of WAT to further expand and appropriately accommodate for the energy surplus (123,129). A limited expandability results in adipose tissue dysfunction, insulin resistance and ectopic lipid deposition. In a simplistic manner, this hypothesis proposes that when a depot reaches the limit of its capacity to expand due to impaired hyperplasia and inadequate angiogenesis, adipocytes become overloaded and hypoxic. Subsequently, the function of those adipocytes and their cellular processes are modified generating a changed adipocyte secretome possibly inciting apoptosis. Consecutively, inflammation in the tissue is triggered promoting an array of detrimental alterations in WAT eventually inducing insulin resistance, mitochondrial dysfunction and ectopic lipid accumulation (123).

The precise mechanisms and cascade of triggers behind the obesity-associated inflammation are poorly understood but various obesity-associated alterations in adipose tissue favoring a pro-inflammatory profile have been identified (105,126) An increased intestinal permeability is linked to obesity contributing to elevated levels of gut-derived lipopolysaccharides that can activate pattern recognition receptors (PRRs) such as Toll-like receptor 4 (TLR-4) in adipocytes (130). Other stimulators of TLR-4 and TLR-2 are FFAs derived from dietary and endogenous lipids (131). Induced TLRs like TLR-4 and TLR-2 activate downstream inflammatory pathways via nuclear factor-κB (NF-κB). Intrinsic signals from adipose tissue caused by its expansion during a sustained positive energy balance participate in the inflammatory response. These signals include hypoxia, adipocyte cell death and mechanical stress from interactions between enlarged adipocytes and the ECM. The hypertrophic growth of adipocytes in not paralleled by a matching expansion rate of angiogenesis causing the formation of clusters of adipocytes distant from the vasculature. These clusters generate local hypoxic regions in adipose tissue influencing its function (132–135). The hypoxic regions of WAT have been found to correspond with regions displaying infiltration of macrophages (136). Furthermore, in obesity, levels of hypoxia-inducible factor 1α (HIF-1α) are increased in adipose tissue since the shortage of oxygen supply does not allow HIF-1α to be hydroxylated in proline residues and thus degraded, hence HIF-1α is stabilized (134). In a hypertrophic and hypoxic adipose tissue, apoptosis is induced. The secretome of

dead or dying adipocytes promotes the development of inflammation via recruitment and proliferation of pro-inflammatory macrophages. The adipose tissue resident classically activated macrophages proliferate forming crown-like structures around apoptotic adipocytes whereas non-resident pro-inflammatory macrophages are recruited from blood monocytes further increasing the number of ATMs (137,138).

Immune response in adipose tissue

Immune cells monitor and interact with other cell types of the adipose tissue, mainly adipocytes, to maintain homeostasis and the regulation of lipid handling and storage. In lean subjects, an overall type 2 or T helper 2 (T_H2) state governs the immune cells where master regulators like IL-33 drive the immune response. IL-33 stimulates the secretion of cytokines IL-5 and IL-13 by innate lymphoid cells (ILCs) activating eosinophils. IL-4 is secreted by eosinophils in WAT and it maintains macrophages in an M2-polarized state (43). The maturation of alternatively activated macrophages and to sustain an M2-phenotype require the activation of PPARγ and PPARδ that promote the expression of anti-inflammatory genes. M2 macrophages improve insulin sensitivity in the tissue via the secretion of many cytokines such as IL-10 and TGF-β, hence, preserving metabolic flexibility (139–141). Whereas in obese subjects, immune cells of the adipose tissue operate in an overall type 1 or T_H1 state where cells coordinate to preserve tissue function while adapting to the overnutrition-associated metabolic needs. In this T_H1 state, resident and recruited macrophages are inclined to adopt a pro-inflammatory phenotype. M1-polarized macrophages secrete pro-inflammatory cytokines such as TNF-α and IL-1β that influence further the recruitment and polarization of macrophages. Thus, the number of macrophages in WAT and the M1/M2 macrophages ratio are increased representing the hallmark of the adipose tissue inflammation accompanied with the development of insulin resistance and metabolic diseases (137). Macrophages cannot be categorized simply according to the two phenotypes, M1 and M2. Macrophages have various phenotypes and functions regulating and being regulated by the surrounding micro-environment. As mentioned previously, M2 macrophages are divided into 4 different subtypes: M2a, M2b, M2c and M2d.

M2a macrophages are known as wound-healing macrophages and they are induced by Il-4 and Il-13. They contribute to tissue repair by releasing pro-fibrotic factors like TGF-β, fibronectin and insulin-like growth factor (IGF). M2a macrophages express high levels of mannose receptor (CD206), CCL17 and decoy IL-1 receptor. Subtype M2b is a regulatory macrophage stimulated by exposure to immune complexes and TLR agonists or by IL-1R agonists. Il-10 is the primary marker for M2b and highly secreted by it. M2b are also recognized for a low level of secretion of Il-12 thus, high Il-10/Il-12 ratio is accepted as the major characteristic marker for M2b. Among the other marker for M2b are CCL1, CD86 and Il-6. M2c macrophages are induced by the activation of signal transducer and activator of transcription 3 (STAT3) via the binding of Il-10 to its receptor. These cells display strong anti-inflammatory and pro-fibrotic activities through the secretion of large amounts of Il-10 and TGF-β, respectively. M2d macrophages are known as tumor-associated macrophages and are stimulated by the binding of TLR ligands to A2 adenosine receptor (A2R) agonists or by Il-6. M2d cells are mainly characterized by high IL-10, TGF-β, and vascular endothelial growth factor (VEGF), and by low IL-12, TNF-α and IL-1β production (29,142). Moreover, ATMs are known scavengers of adipocyte debris and they are challenged when adipocytes are enlarged thus ATMs are unable to engulf the debris in a single step. Instead, macrophages aggregate in WAT forming crown-like structures (CLS) to envelope and ingest adipocyte debris at the site of adipocyte death. Several phenotypes of macrophages are found in the CLS structure. Some ATMs adopt a metabolically activated phenotype (Mme) allowing them to eliminate dead adipocytes through lysosomal exocytosis. Other ATMs, such as iron-rich macrophages (MFe) and antioxidant macrophage (Mox) are specific to the handling of iron and oxidative stress, respectively (143).

The evidence proving a direct association between inflammation of adipose tissue and insulin resistance is overwhelming (106–108,144). Insulin action can be blocked via various pathways either directly or indirectly. The key regulators from within the adipose tissue inducing insulin resistance are TNF-α and IL-1β. In obesity-induced inflammation, PRRs and their ability to sense the level of expression of endogenous ligands that are induced under obesogenic conditions play a key role in insulin resistance. In WAT, the TLR family is an example of PRRs that influence the development of inflammation linked to obesity. The knockout of TLR-4 and TLR-

2 in mice provided the mice protection from insulin resistance associated with diet-induced obesity (145,146). The downstream effect of many of the obesity-generated inflammatory signals converge into the activation of serine kinases that directly inhibit the activity of insulin. These kinases, such as c-Jun N-terminal kinase (JNK), act via serine/threonine phosphorylation of insulin receptor substrates thus, blocking insulin receptor downstream signalling (147). In addition, activated pathways involving JNK1 and NF-κB seem to be tightly related to the activation of the molecular pathways controlling the unfolded protein response stimulated by ER stress (148). Numerous pro-inflammatory pathways in WAT activated in obesity are found to be dissimilar from the inflammatory responses induced by different stimulus such as infection. A distinction between the pathways involved in acute inflammatory responses and the obesity-induced chronic low-grade should be acknowledged (149).

1.4 Reversing Obesity

Despite the ever-growing discoveries about obesity, the management of it still struggles. For a while now, it has been clear that obesity is due to changes in individual behavior and physiology drawn by powerful social and environmental factors. Creating programs by organizations and enforcing laws by many governments are actionable measures applied the past few years. Such programs are promoting healthy living through education, awareness, more affordable healthy food, better accessibility and lower costs for regular physical activity. Modifying dietary intake per quantity and quality as well as exercising are the strategies adopted to reach the goal of weight loss with no risks to one's health. These approaches hold their own challenges, and for most, they are difficult to maintain for long periods (102,150). To predict the long-term success of a weight loss plan, the rate of the initial weight loss is the best indicator. Hence, if the plan resulted in a less-than ideal outcome in the first 3-4 months, a different approach should be adopted. The consensus on the optimal course of treatment of obesity with minimal cost and risk of complications is a comprehensive intervention – a simultaneous implementation of behavioral training, nutritional modifications and increase in physical activity (151–153).

1.4.1 Calorie restriction

The first and obvious rule for weight loss is an energy deficit. In humans, a negative energy balance means a reduction of the daily energy requirements to meet an intake of 1200-1500 kcal/day for women and 1500-1800 kcal/day for men (152). Weight loss is more rapid at the initial stages of calorie restriction (CR) and then slows to reach a plateau. With very low-calorie diets, short-term weight loss is significantly greater than with low-calorie diets but both diets have similar long-term weight loss. In addition, weight loss is paralleled with a decrease in energy expenditure, all of which implicate the previously discussed metabolic adaptation (150). Diet-induced weight loss has been associated to multiple improvements in metabolic functions. A loss of 5% of baseline BW promotes insulin sensitivity in

liver, adipose tissue and skeletal muscle and it enhances β-cell function (154). A randomized controlled trial for the effects of CR on humans known as CALERIE revealed that a 10% reduction in BW induced by CR resulted in reduced total fat mass and fat free mass. CR was associated with improved biomarkers of longevity, decreased fasting levels of insulin, improved insulin sensitivity, reduced energy expenditure and core body temperature (155). CR has always been linked to anti-aging physiology based on the prediction that during periods of CR, there is an active increase in somatic maintenance in preparation for reproduction when resources are available. However, studies around the implications of CR once there was no limitations on rich-food availability, suggested a detrimental effect on reproduction and survival. Thus, CR-related longevity is not through increased investment in somatic maintenance rather than a forced evasion from the intrinsically harmful costs of calorie-rich diets (156).

1.4.2 Nutritional composition modifications

Besides a restriction in caloric intake, weight loss can be shaped by genetic variations as well as the response to different nutritional compositions of food intake. For decades, a reduction in fat-intake was emphasized on the fact that fat has a high-energy content – 9 kcal/g – compared to the low-energy content of carbohydrates and proteins – 4 kcal/g. However, meta-analysis of various trials comparing low-fat diets to other weight-loss diets showed no significant difference. Another meta-analysis comparing isocaloric low-fat/high-carbohydrates diets to low-carbohydrates/high-fat diets while keeping protein consumption constant, showed no changes in weight loss based on the type of diet (150). In fact, numerous reviews of evidence regarding the effect of nutritional modifications in dietary intake implied no significant differences in long-term weight loss between the diets (150–152). Nonetheless, alterations in the diet composition might matter when the target is not solely weight loss, but the alleviation of the pathologies related to it. For example, for type II diabetic patients, low-carbohydrates diets are favored (154). Hence, low-energy diets are encouraged with a consideration of the patient's

medical status and the practicality of the dietary plan proposed since adherence to the plan was the most effective factor for weight loss (150).

Apart from the beforementioned studies, there is enough evidence about the consequence of the ingestion of specific compounds like saturated and unsaturated FAs and complex or simple carbohydrates. Glucose consumption increases postprandial glucose levels in patients with metabolic syndrome while chronic fructose consumption raises substantially lipogenesis compared to a eucaloric consumption in glucose. Complex carbohydrates such soluble fibers have been shown to decrease blood cholesterol levels (157). Similarly to carbohydrates, lipid compounds are numerous and their interaction with cellular processes is unique and specific to each family or species. Fatty acids are major components of various complex lipids like triglycerides and phospholipids. The negative consequences of the intake of saturated FAs, such as palmitate, have been shown by several studies over the years. Major evidences have found SFA to increase total and LDL cholesterol, raise blood coagulation, promote insulin resistance and induce inflammation via increased expression of C-reactive protein (CRP) and Il-6 (158,159). When SFAs are replaced with monounsaturated FAs, a significant decrease in the risk of developing an impairment in glucose metabolism and in the risk for coronary heart disease (160). The benefits of polyunsaturated FAs have been investigated and reported repeatedly. ω-3 PUFAs are involved in a wide range of biological processes such as signal transduction, gene expression, and lipid mediators which suggest an important role in inducing anti-inflammatory regulations, modulating a number of metabolic pathways and preventing from cardiovascular diseases (159).

1.4.3 Exercise

The benefits physical activity exerts on health and weight loss have been well established and documented over the years. Increasing physical activity – thus increasing energy expenditure – is a major factor if the management of obesity by lifestyle interventions. By most guidelines, for adult overweight and obese patients, the starting assignment is a with 150 minutes per week of aerobic exercise such as

brisk walking. Even though the benefits of physical activity are undeniable, there is a vagueness around the perfect formula of exercise programs for an optimal personal result. With the wide range of types of exercise, duration of daily workout and the overall commitment period, the measurement of the effect of physical activity on physiological parameters is challenging (150,152,161–163). A meta-analysis of studies that investigated different training programs in adults, adolescents and/or children revealed improvements in anthropometric characteristics, physical performances and physiological capacities. Some of the anthropometric characteristics are BW, BMI and body fat percentage, while physical performance is assessed by endurance, sprint and strength, and physiological capacities are determined by the measurement of oxygen uptake, heart rate, maximal force, power output, and lactate threshold among others. Both aerobic and anaerobic exercises induced an enhancement in body composition of obese individuals. However, comparing all studies reinforced the view of aerobic training as the favorable form of exercise for achieving the best outcome in all age groups regarding weight loss, BMI and body fat percentage reduction and increases in muscle mass or free-fat mass. Nonetheless, these improvements were mostly observed after at least 12 weeks of trainings. Whereas during less than 12 weeks of anaerobic exercising such as high-intensity training, decreases in BW, fat mass and various risk indicators for metabolic and cardiovascular diseases were observed. When resistance training alone was implemented, the main change is a significant increase in muscle mass or fat-free mass which positively correlates with increased insulin sensitivity hence improved metabolic health (162). The assumption that with increased physical activity comes a proportional increase in total energy expenditure thus a corresponding reduction in weight was proved wrong by numerous studies. A somewhat linear correlation between physical activity and weight loss in sedentary subjects was suggested with low-intensity exercise. However, the expected effect of increased physical activity on EE seems to diminish as the body adapts to the higher intensity of training. In addition, it seems that the EE predicted to be induced by exercise is lower than expected when trainings are for longer periods, implying again an adaptive response. Even though the effect of physical activity on weight loss is limited and, in that regard, dietary modifications have proven to be more effective, the impact of physical activity on health is

indisputable. Exercising protects the organism from chronic diseases, improves overall cardiac function, induces anti-inflammatory responses, increases systemic insulin sensitivity, not to mention ameliorates psychological health via reduction of anxiety and risk of depression (163). The term “myokines” was introduced referring to the cytokines and other peptides produced and released by muscle fibers exerting autocrine, paracrine or endocrine effects. More than 650 myokines are identified and they are involved in the regulation of several processes in many tissues. In skeletal muscles, myokines regulate muscle mass. Myostanin acts in an autocrine manner inhibiting muscle hypertrophy. In contrast, Il-6 and leukemia inhibitory factor (LIF) stimulate myogenesis. Il-6 also acts on muscles by increasing basal glucose uptake and glucose transporter GLUT4 translocation. In addition to the myokines acting in an autocrine or paracrine manner, brain-derived neurotrophic factor (BDNF) induces lipid oxidation via AMPK activation. In the brain, a crucial effect of myokines on metabolism is via Il-6 suppressing appetite. Exercise-induced Il-6 regulates many metabolic processes such as stimulating lipolysis, reducing visceral fat mass, increasing hepatic glucose production, and, with myokines irisin and meteorin-like, promoting browning of WAT. During exercise, the interaction between myokines and all tissues modulates many metabolic processes affecting systemic glucose and lipid metabolism mainly (164).

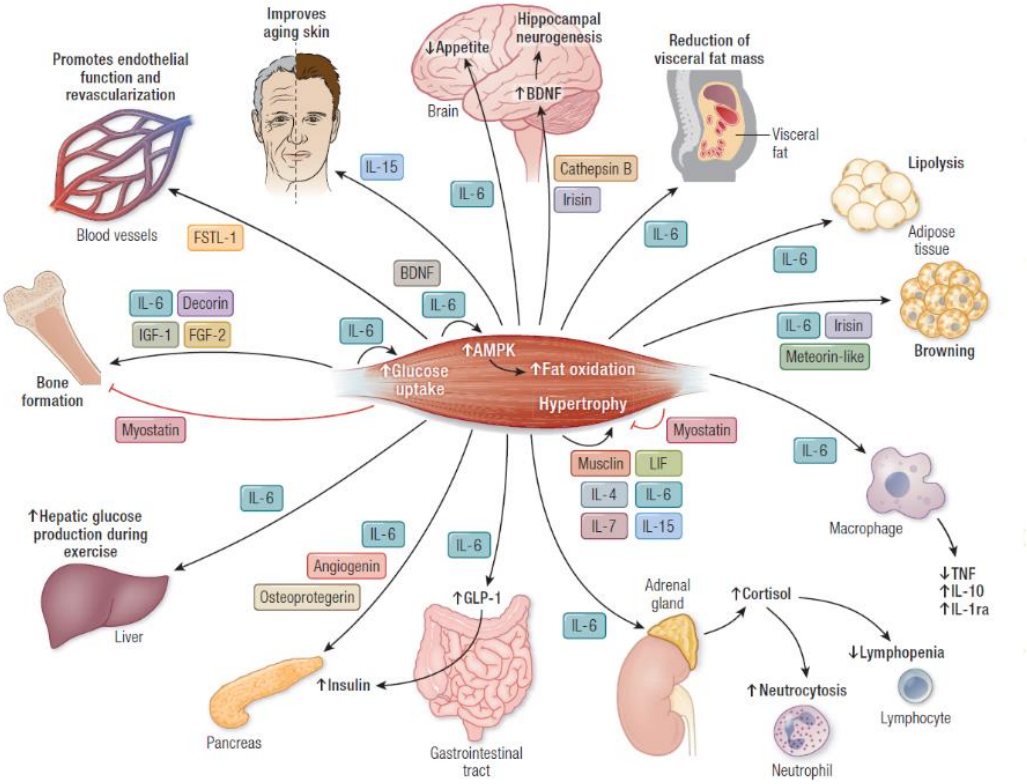

Figure 9: Myokines and organ cross-talk. During exercise, various myokines are secreted affecting the function of skeletal muscles themselves and organs such as brain, adipose tissue, liver and pancreas among others (adapted from (164)).

1.5 Insulin-sensitive tissues and lipidomics

Energy imbalance incites adaptive mechanisms and homeostatic controls to recenter the balance and maintain body weight and composition. However, when the imbalance endures, it generates a sequence of events and alterations resulting in changes in appearance and physiology. The duration required to initiate these changes is still unspecified and differs between individuals. At the center of the modifications triggered by energy imbalance, are insulin-sensitive tissues.

1.5.1 Ectopic fat accumulation

A dysfunctional WAT overloaded by a positive energy balance is incapable of containing all of the caloric excess while promote lipogenesis over lipolysis via insulin action. When WAT reaches its limitation on the storage of triglycerides, the excess of circulating lipids is deposited in non-adipose tissue organs. Ectopic fat accumulation is a main concern for insulin-sensitive tissues like liver, skeletal muscle and heart where it can induce local and systemic insulin resistance along with dysregulations in mitochondrial function. Lipotoxicity is the event where lipid accumulation in insulin-sensitive tissues stimulate metabolic alterations in processes involved in fatty acids utilization and intracellular signalling (109,126,165,166).

The liver is a key organ in lipid metabolism. Lipid homeostasis in liver is maintained via multiple hepatic metabolic pathways. The level of liver lipids is determined by several processes: hepatic uptake of FAs, their esterification into TAGs stored in lipid droplets, their excretion in lipoproteins such as very-low-density lipoprotein (VLDL) and β-oxidation in liver mitochondria (167). An imbalance in one or more of these processes influences the interplay between them and promotes abnormal hepatic lipid accumulation (168). Hepatic steatosis or non-alcoholic fatty liver disease (NAFLD), affecting around 30% of adult population in industrialized countries, has been identified as the most common chronic liver disorder worldwide. NAFLD can further progress into non-alcoholic steatohepatitis (NASH)

characterized by mild inflammation, hepatocyte ballooning, necrosis and different stages of fibrosis. A dramatic increase in NAFLD driven by the global obesity epidemic is observed and expected to intensify further (169,170). Hepatic steatosis has been linked to impaired insulin action in liver and other tissues in non-diabetic obese as well as lean subjects (171–175). The increased presence of lipids in liver in the form of lipid droplets containing TAGs does not cause harm per se but when lipid metabolic pathways are out of equilibrium toxic lipid intermediates such DAGs and ceramides (CER) are synthesized (176). DAGs induce insulin resistance through the activation of hepatic protein kinase C-ε (PKCε) causing a reduction in insulin-stimulated phosphorylation of insulin receptor substrate 2 (IRS-2) and Akt2 thus limiting the action of insulin on glycogen synthesis and gluconeogenesis (177,178). The role of CER has not been fully clarified but an association has been made between an increase in de novo synthesis of CER triggered by a diet rich in saturated FAs and hepatic insulin resistance (179,180).

Skeletal muscle contributing to around 40% of total body mass is another key regulator of systemic carbohydrate and lipid metabolism. Lipids are stored in the muscle as intramyocellular lipids (IMCL). When excess FAs uptake is not paralleled by an increased utilization of lipids via oxidation, IMCL accumulate in skeletal muscles. The total content of IMCL in a muscle was initially the indicator for insulin resistance but more recent studies showed it was particular lipid intermediates blocking insulin signalling to be the better indicators (181–184). Numerous investigations demonstrated an suppression of insulin-stimulated glucose uptake in skeletal muscle due to increased levels of FAs by showing reduced glucose uptake via GLUT4, reduced IRS-1 tyrosine phosphorylation and reduced activity of phosphatidylinositol-3-kinase (PI3K) (181,182). It is to be noted that high IMCL content in skeletal muscle is not always a feature of ectopic fat accumulation. Defined as “the athlete’s paradox”, several studies have reported in insulin-sensitive endurance trained athletes an elevated content of IMCL, similar to that found in obese individuals. When exercise was introduced for non-trained subjects, the increase in IMCL content was accompanied by an overall improvement in metabolic profile. A shift towards a more oxidative fiber type composition, an increased oxidative enzyme activity and an enhanced substrate delivery and storage capacity in muscle were observed (185).

1.5.2 Lipids and lipidomics

The interplay between lipid accumulation, lipid intermediates and mitochondrial function requires an understanding of lipids, their classification, their different distribution in tissues and their function.

Lipids are a family of biological substances found across all living cells as hydrophobic or amphipathic macromolecules. In abundance, they come second only to proteins. They are diverse with unique physical and chemical properties allowing their classification based on features such as the length of fatty acyl chain and degrees of saturation (186,187). Their most recent classification divides them into 8 different categories: fatty acyls, glycerolipids, glycerophospholipids, sphingolipids, sterol lipids, prenol lipids, saccharolipids and polyketides (188).

Lipid Category	Abbreviation	Structure / Example
Fatty Acyls	FA	Saturated Fatty Acids (SFA), Polyunsaturated FA (PUFA)…
Glycerolipids	GL	TAG, DAG…
Glycerophospholipids	GP	Phospholipids (PL), Plasmalogen…
Sphingolipids	SP	Sphingomyelin (SM), ceramides…
Sterol lipids	ST	Cholesterols
Prenol lipids	PR	Vitamin A, Coenzyme Q…
Saccharolipids	SL	Sugar backbone
Polyketides	PK	Acetyl or propionyl subunits

Table 1: Lipids classification.

Fatty acids are important in cellular lipid metabolism. They are further subdivided based on carbon-carbon double bonds; saturated FAs lack them, monounsaturated FAs have one while polyunsaturated FAs have several. All FAs contain an aliphatic chain of methylene groups which can vary in length affecting their hydrophobicity. Glycerolipids are complex group of lipids formed by the attachment of long-chain acyl and alkyl groups to a glycerol backbone. Glycerolipids are found as tri-, di- and monoacylglycerols with one, two or three fatty acid molecules, respectively. They

are essential for energy storage and intracellular signaling, Glycerophospholipids are crucial for the structure and function of cellular membranes. They are their primary building blocks of the lipid bilayer and thus, define the permeability of cell membranes.

Phospholipids are diacylglycerols with various alcohol phosphates in phosphodiester linkage to the free hydroxyl. The major phospholipids are phosphatidylcholine, phosphatidylethanolamine, phosphatidylserine, phosphatidylinositol, phosphatidylglycerol, and cardiolipin. Other lipids important on the structure of cell membranes are sphingolipids. They are composed of a sphingoid base backbone to which a fatty acid may be attached through an amide bond and a head group at the primary hydroxyl. The most recognized sphingolipids are ceramides and sphingomyelin that are involved in the coordination of cellular responses to extracellular stimuli and to stress in cellular processes such as differentiation, apoptosis and cell senescence.

Sterol lipids, mostly known for cholesterols, are also crucial for the structure and function of cell membranes. Structurally, sterol lipids typically have a sterol nucleus composed of 4 tightly fused carbon rings and a hydroxyl group attached to the first ring. Prenol lipids are synthesized from the 5-carbon precursors isopentenyl diphosphate and dimethylallyl diphosphate and have a range of functions. Carotenoids like Vitamins A and E, and ubiquinones are examples of prenols. Saccharolipids are complex lipid compounds where FAs are attached to a sugar backbone. Based on the different combinations of sugars and FAs, saccharolipids have a variety of structures and functions. Acylated glucosamine precursors of the lipid A component of the lipopolysaccharides (LPS) is the most recognized saccharolipid.

According to the main structure database of lipids, LIPID MAPS, as of June 2022, 47599 unique lipid structures have been identified (https://www.lipidmaps.org/databases/lmsd/overview). Lipids have evolved to perform numerous essential functions. Lipids are energy storehouses, they serve as major structural components like in cellular membranes and membranes of intracellular organelles. In addition, they act as signalling and regulatory molecules and interact with other molecules altering their function. Lipids also form

transporting molecules crucial for cellular processes (186,187). In mammals, lipids can be either consumed from exogenous sources or synthesized de novo and they are modified by various enzymes and other metabolites creating a unique lipid profile or "lipidome" (189). This implies that a lipid profile is modified depending on space and time. A lipidome varies between membranes withing the same cell, between cells of the same tissue and between organs. Moreover, the lipid profile of a certain biological unit fluctuates according to time. For example, it can be affected in a period of one day by the circadian rhythm or within a lifecycle like the effect of aging. Pathological conditions can also impact a lipidome such as genetic disorders associated to lipid metabolism and other conditions influencing lipid homeostasis like cancers, CVDs and diabetes (190). Due to all the factors that can provoke changes to it, a lipidome can be described as a dynamic and flexible system generating challenges for its analysis. Lipidomics, the study of lipid profiles, has advanced in past few years however, there is still a gap in lipid profiling of numerous tissues at different physiological states (189).

1.6 Visceral adipose tissue metabolic dysfunction. The LiMa project.

The complexity of obesity and the wide spectrum of comorbidities associated to it contributes to the challenges in addressing the biology underlying obesity. The pathological perturbations generated by obesity have systemic and tissue-specific manifestations, especially on metabolism. Biological systems have the ability to adapt their metabolic phenotype stimulated by environmental stressors – a phenomenon recognized as metabolic plasticity. Thus, an adequate assessment of the biology underlying obesity and its associated metabolic impairments requires multidisciplinary and integrative experimental approaches to capture interorgan communication and the resilience of tissues and the organism in face of different environmental stressors. And that was the starting point of the LiMa (Lifestyle Matters) project leading to a whole-body and tissue-specific phenotypic, functional, proteomic, metabolomic and transcriptomic approach to systematically assess metabolic plasticity in diet-induced obese mice after a combined nutritional and exercise intervention (191).

1.6.1 Phenotype of the LiMa experimental groups

Induced by HFD, an obesity-associated insulin-resistant phenotype was created (*Pat* group) which was challenged by a weight-loss strategy based on nutritional modifications and the introduction of physical activity (*Int* group). An additional maintenance period promoting the stabilization of a healthy physiological status through a less intense intervention was introduced (*LTint* group).

Several phenotypic parameters were measured for the different experimental groups such as body weight, fat volume, weights of few tissues and their triglycerides content, heat production and activity records via indirect calorimetry. HFD promoted an insulin-resistant phenotype highlighted by overweight, increased fat mass, hyperglycemia, hyperinsulinemia and glucose intolerance among others

(191). In Figure 10, the evolution of food intake and body weight were illustrated. The *Int* group demonstrated an intense weight loss following the intervention that was sustained with the second phase of intervention (*LTint* mice). In addition, glucose tolerance and insulin sensitivity were improved with the *Int* and *LTint* mice (Figure 11).

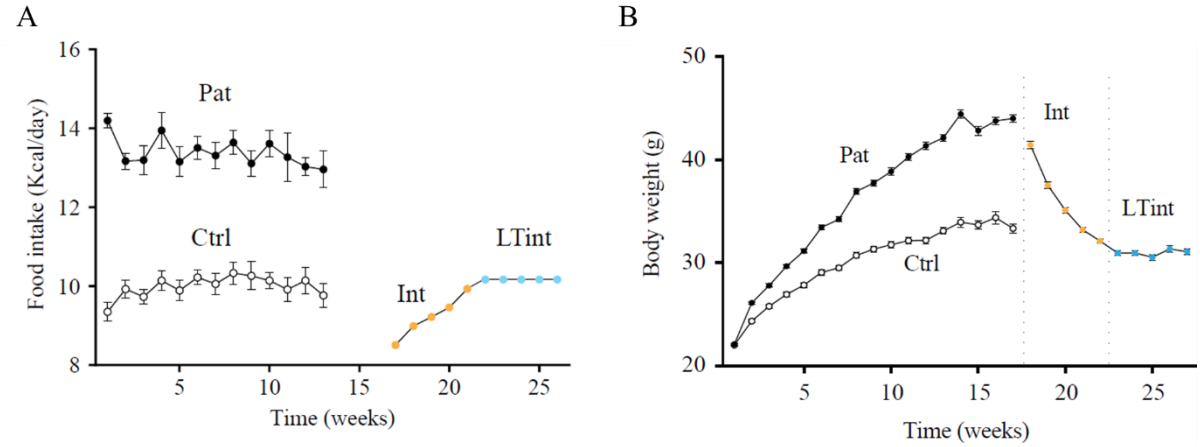

Figure 10: Evolution of food intake and body weight. Food intake (A) and body weight (B) records in the four experimental groups throughout the entire protocol. Food intake was recorded by cages and expressed as the averaged caloric intake/day. (Pau Gama Pérez. I used to be fat. Obesity-induced determinants on white adipose tissue plasticity [dissertation]. Barcelona (Spain): Universitat de Barcelona; 2021).

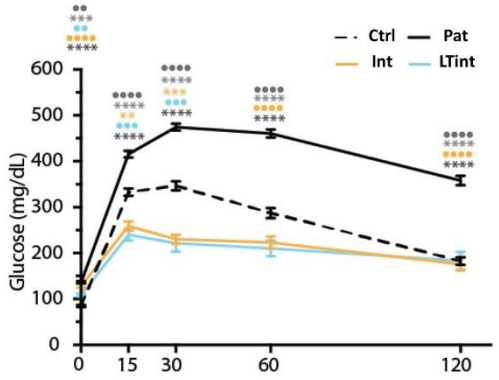

Figure 11: Intraperitoneal glucose tolerance test performed after 16h of fasting. Ctrl n=82; Pat n=168; Int n=32; LTint n=19. Mean±SEM, One-way ANOVA; ****p<0.0001. (191)

1.6.2 Visceral adipose tissue metabolic dysfunction

Although most obesity and overnutrition-related pathological features were successfully improved when healthier nutritional and activity programs were imposed (191), a profound metabolic dysfunction in visceral white adipose tissue

was reported through several assays after both sequential therapeutic interventions.

Mitochondrial function of visceral white adipose tissue (eWAT) was assessed via high-resolution respirometry of whole-tissue homogenate (Figure 12) revealing an impairment in mitochondrial respiration induced by HFD and never improved after the interventions.

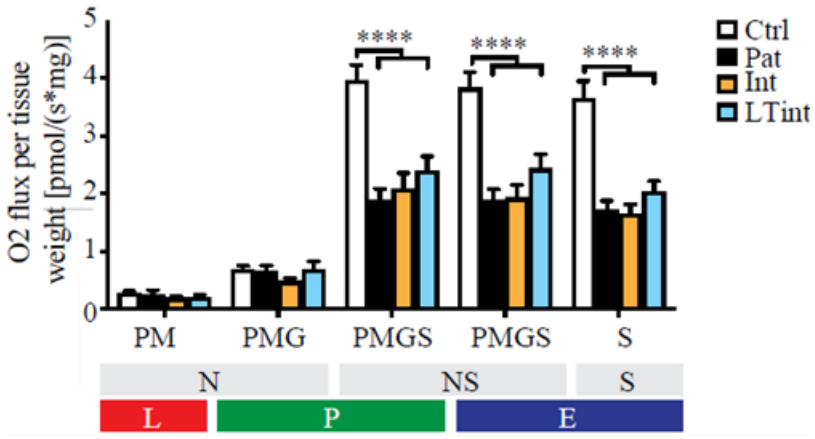

Figure 12: High-resolution respirometry in eWAT homogenates. Oxygen consumption rates at different mitochondrial respiratory states (L; leak, P; OXPHOS, E; maximal electron-transfer system) were assessed by the addition of saturating substrates (P; pyruvate, M; malate, G; glutamate, S; succinate) for the activation of convergent electron transfer pathways (N; NADH-derives, S; succinate-derived).
Mean±SEM, One-way ANOVA; ****p<0.0001. (191)

Considering the remodeled tissue morphology of eWAT after the maintenance phase of intervention (191), defects in mitochondrial function could be attributed to a potential metabolic plasticity breakdown. Following this lead and for a more comprehensive understanding of the eWAT metabolic profile, expression of genes of interest was evaluated (Figure 13). The cluster of genes that showed a downregulation in expression induced by HFD with no significant changes after interventions was mainly associated to mitochondria particularly, its inner membrane, the respiratory chain and ribosomal machinery. A gradual downregulation in the expression of genes linked to other organelles like the Golgi apparatus and endoplasmic reticulum was observed in eWAT of *Int* and *LTint* mice. This set of data confirmed a progressive tissue deterioration at the transcriptional level.

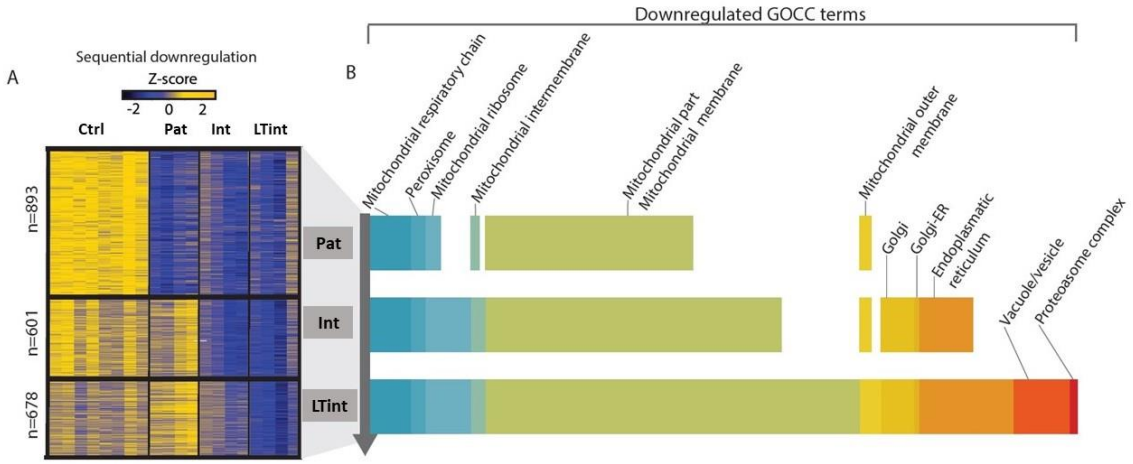

Figure 13: Metabolic plasticity breakdown in eWAT. A: Z-score for RNA-seq clusters of transcripts sequentially downregulated across the different experimental groups (Ctrl n=8, HFD n=4, Int n=4, Int2 n=4). B: Cumulative number of genes belonging to different enriched GOCC terms for each cluster in A. The same GOCC terms are indicated from Pat-cluster to LTint-cluster (y-axis), with increasing size (x-axis) denoting incremental number of genes for that specific term (191).

1.6.3 Metabolic dysfunction unique to eWAT

For further evaluation of mitochondrial perturbations in eWAT and to assess whether mitochondrial defects are unique to eWAT, mtDNA copy number was examined in eWAT and other tissues. A substantial reduction in mtDNA copy number induced by HFD was revealed in eWAT without a recovery after the interventions (Figure 14) which emphasized on mitochondrial derangements as a key component in eWAT metabolic deterioration.

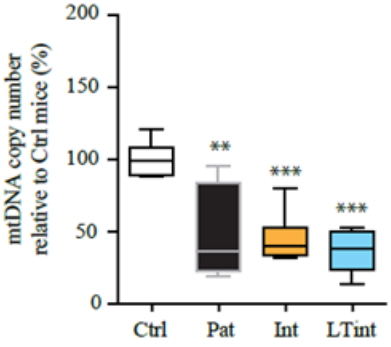

Figure 14: Comparative mtDNA copy number among the experimental groups (191)**.** One-way ANOVA, Post-hoc Tuckey; *indicates significance in respect to Ctrl.

The decrease and further reduction in mtDNA copy number was not observed in any of the other insulin-sensitive tissues tested such as the other white adipose

tissue depot, subcutaneous WAT (sWAT), the liver and the skeletal muscle gastrocnemius (Figure 15).

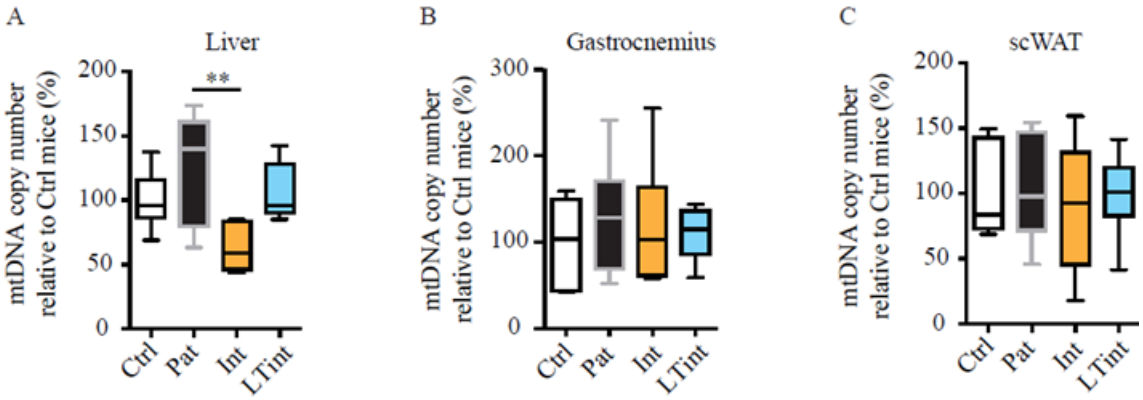

Figure 15: Mitochondrial DNA (mtDNA) copy number in different metabolic tissues; liver (A), gastrocnemius (B) and subcutaneous adipose tissue (C). Values are normalized to control mice. Mean±SEM, One-way ANOVA, Post-hoc Tuckey; **p<0.01. (191)

The distinctive mitochondrial profile of eWAT in comparison to sWAT was interesting in our findings. And the differences in functionality of depots were further reinforced by results of high-resolution respirometry. Mitochondrial respiration of whole-tissue WAT homogenates was assessed in *Ctrl*, *Pat* and *LTint* groups revealing an impairment in eWAT after the interventions which was absent in sWAT depot (Figure 16).

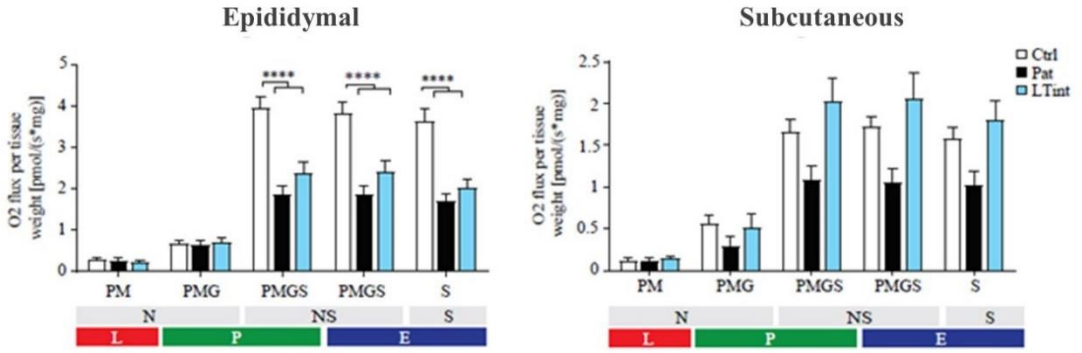

Figure 16: High-resolution respirometry in eWAT and sWAT homogenates. Oxygen consumption rates at different mitochondrial respiratory states (L; leak, P; OXPHOS, E; maximal electron-transfer system) were assessed by the addition of saturating substrates (P; pyruvate, M; malate, G; glutamate, S; succinate) for the activation of convergent electron transfer pathways (N; NADH-derives, S; succinate-derived).
Mean±SEM, One-way ANOVA; ****p<0.0001. (Pau Gama Pérez. I used to be fat. Obesity-induced determinants on white adipose tissue plasticity [dissertation]. Barcelona (Spain): Universitat de Barcelona; 2021).

AIMS

This doctoral thesis is established on the LiMa project that has been ongoing in our lab. The objective of the LiMa project over the years has been to address the metabolic basis of diet-induced obesity followed by weight loss by adapting a systemic, multidisciplinary and integral study. At the initial stages of this project, various tissues crucial for whole body glucose homeostasis were investigated. Pancreas, oxidative and glycolytic skeletal muscle, liver, hypothalamus, brown adipose tissue and several depots of white adipose tissue were the main insulin-sensitive tissues evaluated. The focus of our study was to determine whether the metabolic alterations stimulated by a maintained positive energy balance via HFD could be counter affected upon a lifestyle intervention promoting weight loss and a healthier phenotype (Methods section 3.1).

The intervention was designed in two phases; an extension after the first phase of intervention was required considering tissues such as pancreas and eWAT showed a lack of phenotypic plasticity. The second phase of intervention seemed to further enhance the phenotype and allow the recovery of some previously impaired parameters (Antecedents and LiMa paper).

Concentering the data from the LiMa project until this point, the attention was shifted mainly towards white adipose tissue. The aim of this PhD thesis is to identify whether the metabolic modifications exhibited in the pathological state could be positively altered with an intervention in the lifestyle, or whether a degree of dysfunction and deterioration – specifically in WAT – limits its plasticity, thus maintaining a "metabolic memory" associated to the pathological state.

The specific objectives of this PhD thesis are:

I. To describe the phenotypes of the experimental groups through the assessment of body weight, some tissue weights, glucose tolerance and the lipid profile of several insulin-sensitive tissues.

The knowledge that WAT depots have distinct origins and behavioral functions which is strengthened by previous results shown in Antecedents, generates an interest around a depot-specific focus. Hence, a common purpose was to draw a comparative between eWAT and sWAT in the following objectives. With the consideration of the various cell types and connective tissue structuring and dictating the function of white adipose tissues, this doctoral thesis aims:

II. To examine the morphology of WAT depots and its remodeling induced by HFD and the interventions.

III. To assess the metabolic function of adipose-derived stem cells in the context of obesity and subsequent weight loss strategy.

IV. To characterize the inflammatory response in WAT induced by HFD and the interventions based on transcriptomic studies identifying markers of macrophages phenotypes and ECM components.

MATERIALS & METHODS

3.1 Animals

Male C57BL/6JOlaHSD mice were purchased at 5 weeks old from Envigo (Indiana, IN, USA). Animals were housed at the Animal facilities (CCiT, University of Barcelona, campus Bellvitge) on a 12h light/12h dark cycle and under controlled temperature and humidity room conditions. For a period of 7 days, they were acclimatized in quarantine and then, they were split into 3-mice cages at the beginning of the experimental protocol. All animal procedures were approved by the local ethics committee, Comitè Ètic d'Experimentció Animal at the University of Barcelona, and the Departament d'Agricultura, Ramaderia, Pesca, Alimentació I Medi Natural at the Generalitat de Catalunya; complying with the current Spanish and European legislation.

3.1.1 Animal experimental design

The experimental design for the animals is represented in Figure 17 showing the different animal experimental groups, their diets and physical activity protocols.

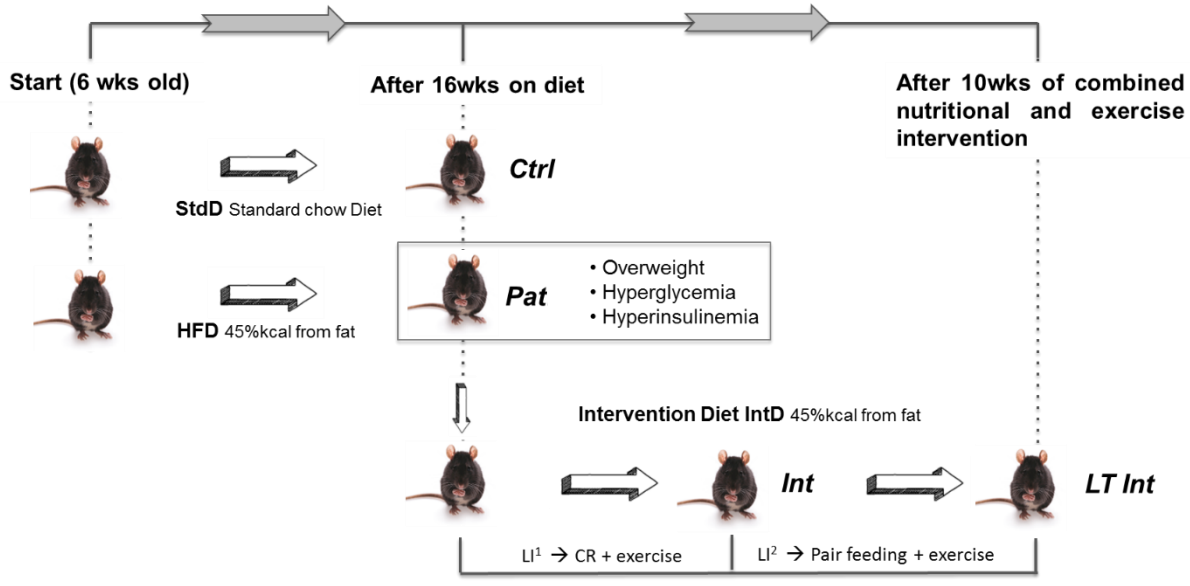

Figure 17: Experimental design. LI[1]; first phase of combined nutritional and exercise intervention. CR = Calorie restriction: 80% energy intake from Ctrl mice, progressively increased to 100%. Exercise for LI[1] = speed and inclination incremental protocol on a treadmill (see exercise protocol section). LI[2]; extended phase of intervention. Pair-feeding strategy (isocaloric in respect to Ctrl mice). Exercise for LI[2] = constant moderate speed and inclination (see section 3.1.4).

3.1.2 Animal experimental groups

In the first step towards achieving the different experimental groups, 6 weeks old mice were randomly assigned to either the control group (*Ctrl*) or the pathological group (*Pat*) for the coming 16 weeks.

***Ctrl* group** (control group): mice were fed *ad libitum* with a standard chow diet (StdD) (section 3.1.3 for details) provided by the animal facilities.

***Pat* group** (diet-induced pathological group): mice were fed *ad libitum* a high-fat diet (HFD) with 45% of energy content from fat to achieve the pathological state (section 3.1.3 for details). *Inclusion criteria* for the pathological group were set as follows: overweight (threshold at BW >40g), glucose intolerance and insulin resistance.

After 16 weeks on a HFD, a subgroup of *Pat* mice (randomly selected) were assigned to perform a combined nutritional and exercise intervention divided into two successive stages from which we got the 2 groups; intervention group (*Int*) and extended (or long-term) intervention group (*LTint*), as follows:

***Int* group** (1st phase intervention): At the beginning of the intervention, animals were moved to individual cages for control of food intake. The first phase of intervention was for 5 weeks where animals were fed a high-fat, but customized formula diet (section 3.1.3 for details). During this phase, daily energy intake went progressively from 85% in kcal of the average determined for an *ad libitum*-fed *Ctrl* animal in the first week to 100% in the last week. The intervention diet was also combined with a 5-days a week incremental exercise training protocol (detailed in section 3.1.4).

***LTint* group** (2nd phase intervention): Based on the results from *Int* group, specifically the exhibited irreversibility in phenotype of pancreas and eWAT (check section 1.6), an extension of the intervention for another 5 weeks was initiated. In this second phase, mice were fed the same high-fat customized formula diet. For the animals to sustain their weights, food intake was likewise controlled by limiting the daily intake to an isocaloric intake in respect to *Ctrl* animals over the whole extended period (pair-feeding strategy). To sustain a certain level of physical activity, mice

followed an exercise program adjusted to an alternate-day workout with a fixed moderate speed and inclination (detailed in section 3.1.4).

3.1.3 Diets

Three different diets were used in this study: the standard chow diet, *StdD* (Teklad Global 14% Protein Rodent Maintenance Diet, Harlan Laboratories); the high-fat diet, *HFD*, with 45% of energy content from fat (D12451, OpenSource Diets, Research Diets Inc; New Brunswick, NJ, USA); and the customized intervention diet, *IntD* (Preliminary Formula Rodent Diet, OpenSource Diets, Research Diets Inc; New Brunswick, NJ, USA). The latest formula provided also 45% of energy content in form of fat, but with several modifications in terms of macronutrient source, such as the replacement of sucrose by corn-starch, and lard by flaxseed and olive oils. The nutritional composition of the different diet formulas is described in Table 2.

		Standard diet (StdD)	High fat diet (HFD)	Intervention diet (IntD)
Caloric Density (kcal/g)		2.9	4.7	4.7
Protein (%)		20	20	20
Carbohydrates (%)		67	35	35
Fat (%)		13	45	45
Total carbohydrates				
Source (%)	Corn starch		21.1	63.8
	Maltodextrin		28.9	36.2
	Sucrose		50	-
Total fat				
Source (%)	Soy bean oil		12.3	-
	Lard		87.7	-
	Flaxseed oil		-	55.6
	Olive oil		-	44.4
Composition (%)	Saturated fat	17.6	31.7	11.8
	Monounsaturated fat	20.6	35.6	43.8
	Polyunsaturated fat	61.8	32.7	44.4

Table 2: Dietary nutritional composition. Energy density and macronutrient distribution for each diet supplied, and comparison between HFD and IntD macronutrient source.

3.1.4 Exercise protocol

The exercise protocol was performed on a treadmill (Exer-6M Open Treadmill for Mice and Rats with Shocker and Software 2-102 M/m, Columbus

Instruments). An acclimatization period that started mid first week of intervention, allowed already calorie restricted mice to familiarize with the treadmill for 20 min a day at low speed and no inclination. At the beginning of the following week, an incremental 5-week exercise training was initiated as detailed in Figure 18. With the progressive weight loss and training, the animals became capable of a better performance reaching a speed of 20m/min from an 8m/min start at an inclination of 10°.

For the second phase of the intervention, the exercise protocol was set at a lower frequency and intensity. Instead of 5 days per week, the animals ran on the treadmill for 3 days per week at a 16m/min speed and 5° inclination constantly for the whole period of this phase.

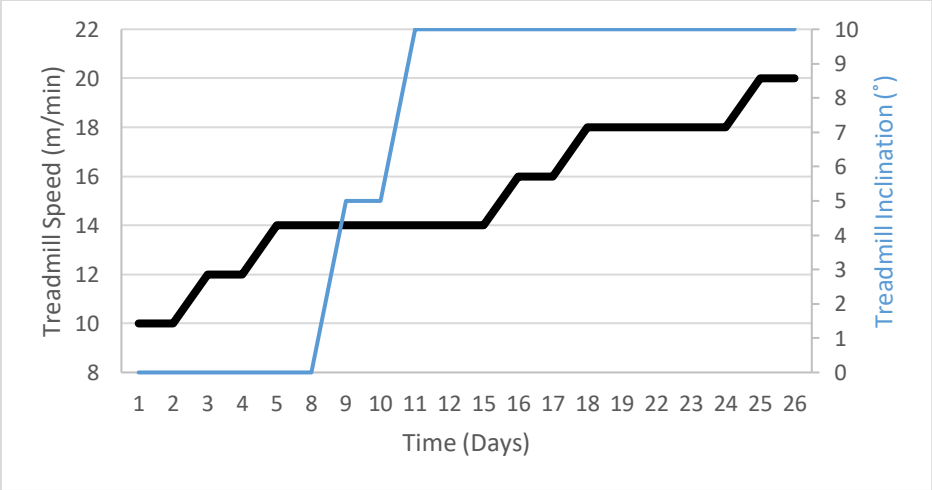

Figure 18: Exercise training protocol for the first phase of intervention. Treadmill speed is represented by the thick black line and the degree of inclination by the thinner blue line. Exercise protocol is preceded by a 3-day acclimatization period where the animals run for a few minutes at low speed (around 8m/min) without inclination.

3.1.5 Animal monitoring

For the initial 16 weeks dietary allocation, animals were weighed weekly using always the same weighing scale. Food intake per cage was monitored weekly and individual average daily intake was calculated considering 3 mice were housed in each cage. As for the intervention periods, animals were weighed on a daily basis in order to ensure weight evolution criteria.

3.2 Determination of in-vivo glucose homeostasis parameter

For an evaluation of glucose homeostasis at a systemic level an intraperitoneal glucose tolerance test (IGTT) was performed. This test was usually done 2 weeks prior to the date of the end-point experiments. An IGTT allowed the evaluation of the tolerance of conscious mice to a bolus glucose as well as systemic insulin sensitivity by measuring the time-resolved glucose clearance from the blood after the intraperitoneal administration of glucose.

3.2.1 Intraperitoneal Glucose Tolerance Test (IGTT)

Animals were fasted overnight (16h) and blood glucose was measured at t=0min with a GlucocardG+ meter (A-Menarini Diagnostics). Next, an intraperitoneal bolus of D-Glucose (2g/Kg of mouse BW) freshly diluted in saline solution was administered. Blood glucose was measured and recorded post-injection at different time-points (15, 30, 60, 120min post-injection).

3.3 Animal endpoint experiments for ex-vivo determinations

Ctrl and *Pat* animals were sacrificed at the age of 22 weeks, after 16 weeks on a *StdD* or *HFD*, respectively. *Int* animals with 5 weeks of intervention and *LTint* animals with 10 weeks of intervention were sacrificed at 27 and 32 weeks of age, respectively. Animals were sacrificed at the same time of day which would make the mice from the *Int* and *LTint* groups fasted for around 16h before their sacrifice. Tissue collection and terminal methods were equally applied for all animals.

3.3.1 Anesthesia procedure

Avertin was the anesthetic solution used for such endpoint procedures. The stock solution was prepared by mixing 10g of 2,2,2-Tribromo ethanol (BR_2CH_2OH) 99+%(GC) (Sigma Aldrich T48402-25G) with 10 mL Tertiary amyl alcohol (2 Methlbutan-201) (Sigma Aldrich 240486-100mL). The diluted solution (2%) used for injecting the mice was prepared from 200µL of stock solution diluted into 10 mL of dH_2O and then warmed in a water bath at 60ºC for 1h to facilitate dissolution. Approximately, 0.02 mL of diluted then heated avertin solution per g of body weight (BW) was intraperitoneally injected (20 times the BW expressed in µL).

3.3.2 Tissue collection

For the whole study, the previous data leading to the work done in this thesis, a wide set of tissues were collected from anesthetized animals and studied such as some skeletal muscles (*Tibialis anterior*, *Soleus* and *Extensor digitorum longus*), pancreas, heart, brown adipose tissue and others. In this thesis, tissues were excised from mice in the following order: skeletal muscle *Gastrocnemius* from the hindlimbs, subcutaneous (sWAT) and epididymal (eWAT) adipose tissue, liver and finally hypothalamus. After collection, adipose tissue depots and liver tissues were weighed and either kept in buffers for spontaneous *in vivo* assays or immediately frozen with liquid nitrogen.

3.4 Lipidomics

3.4.1 Sample preparation for NMR metabolomics

The frozen liver, eWAT, gastrocnemius, and hypothalamus tissues were pulverized using mortar and pestle. For each of WAT, gastrocnemius and hypothalamus, 30-70 mg, 20-40 mg and 10-25 mg of powder, respectively, were mixed with methanol and ultrasonicated. Chloroform was added in 2 steps to final 1:1 concentration and then water to get 1:2:2 (water:methanol:chloroform). After centrifugation, the upper aqueous phase (methanol/water) was separated from the lower organic phase and both were collected and stored. For the liver samples, 50-100 mg of liver powder was mixed with ice-cold acetonitrile:water (1:1), ultrasonicated, centrifuged and the aqueous upper phase was collected. After 3 repeats, the collected and combined aqueous supernatant was frozen and lyophilized. The resultant pellet was dried and extracted with chloroform:methanol (2:1) by ultrasonication and centrifuged. The upper lipidic phase was collected and dried under N_2 stream. For the measurement experiment, the organic extract was reconstituted in 700uL of $CDCl_3$/CD_3OD (2:1) solution (containing 1.18 mM tetramethylsilane, TMS). The supernatants from the newly formed solution were transferred into 5 mm NMR tubes.

The different protocols for sample preparation between liver and the other tissues, mainly the use of acetonitrile (liver), could affect the detection of some polar lipids. However, the detected metabolites in liver could be compared to the other tissues.

3.4.2 Nuclear Magnetic Resonance (NMR) metabolomics analysis

^{1}H-NMR spectra were recorded at 310K on a Bruker Avance III 600 spectrometer (Bruker, Billerica, USA) operating at a proton frequency of 600.20MHz using a 5mm CPTCI triple resonance (^{1}H, ^{13}C, ^{31}P). A 90° pulse with water presaturation sequence (zgpr) was used. Thus, a 50Hz power irradiation was used during recycling delay and mixing time to pre-saturate the solvent. 256 transients

were collected into 64 k data points for each ^{1}H spectrum, being the spectral width set as 12kHz (20 ppm). The exponential line broadening applied before Fourier transformation was of 0.3 Hz. The frequency domain spectra were manually phased and baseline-corrected using TopSpin software (version 2.1, Bruker, Billerica, USA).

3.4.3 NMR data analysis

^{1}H-NMR data acquisition was performed as previously described (191). Metabolite identification was performed using lipid standards and according to literature (192). After baseline correction, specific ^{1}H-NMR regions identified in the spectra were integrated using the AMIX 3.8 software package. Then, each integration region was normalized by proton number and then, by the tissue weight used from each sample. Data (pre-) processing, data analysis, and statistical calculations were performed in RStudio (R version 3.0.2).

3.5 Transcriptomics studies in adipose tissue

For in-depth exploration of adipose tissue behavior, bulk tissue transcriptomic approaches were applied. Data acquisition was performed at a different institutional research platforms and analyzed by expert collaborators. The next generation RNA-sequencing for transcriptomic analysis was performed at the Centre Nacional d'Anàlisis Genòmica (CNAG, www.cnag.crg.eu) in collaboration with Dr. Jose I. Martin-Subero, Dr. Marta Kulis and Dr. Vicente Chapaprieta (Biomedical Epigenomics Group, IDIBAPS).

3.5.1 RNA extraction and quantification

Pulverized epididymal and subcutaneous white adipose tissue samples were mixed with TRI Reagent® (T9424 Sigma) by means of 1 mL/50-100 mg of tissue (volume of tissue should not exceed 10% of TRI Reagent volume). Tissue was

further mechanically homogenized by adding a small quantity of magnetic beads (0.5 mm diameter zirconium oxide ZrO_2 for BulletBlender, Next Advance). A centrifugation step (5 min, 16000g, 4°C) was performed at this point to remove the fatty layer on the surface of the aqueous phase. 0.2 mL of chloroform was added per mL of TRI Reagent, and the mixture was shaken and centrifuged (15 min, 12000g at 4°C) to allow phase separation. The resulting aqueous phase, containing RNA, was transferred to a fresh tube, mixed with 0.5 mL 2-propanol, shaken vigorously and centrifuged (10 min, 12000g, 4°C) for RNA pellet precipitation. The supernatant was removed and the RNA pellet washed twice by adding 1mL of 75% Ethanol with a centrifugation step in between (5 min, 7500g, 4°C). RNA pellet was dried by airdrying and resuspended in 30 µL of RNAase free water. RNA concentration (ng/µL) and purity (RIN) were quantified first using the Nanodrop 1000 Spectrophotometer (ThermoFisher Scientific), and then Bioanalyzer 2100 (Agilent Technologies).

3.5.2 RNA sequencing and data analysis

Extracted RNA samples were sent to CNAG Sequencing Unit and were sequenced by standard Illumina protocol in an Illumina HiSeq 2000 system (Illumina, Inc.). Obtained raw sequence files (.fastq files) underwent quality control analysis using FASTQC (http://www.bioinformatics.babraham.ac.uk/projects/fastqc/), and reads were aligned to the Mouse Genome version July 2007 (NCBI37/mm9) using TopHat version 2.1.1, allowing for unique alignments to the genome and up to two mismatches. The resulting alignments were summarized by Ensembl gene identifiers to evaluate number of uniquely aligned reads per transcript and per sample (raw read counts). RNAseq data were analyzed using the limma package version 1.8.2 available through the Bioconductor open source (https://www.bioconductor.org/packages/release/bioc/html/limma.html). The raw read counts were used as input to form a differential gene expression list (DGEList) object combining the counts and associated annotation. Scale normalization was applied and the calculation of normalized signal was performed

by voom function of the limma package. DGE analysis was performed pair-wise between different experimental conditions (FDR<0.05).

3.5.3 Characterization of macrophages phenotypes

Based on the RNAseq data and a list of macrophages markers and their secretory factors, characterization of macrophages in WAT was conducted. A list of the specific markers for the different macrophage phenotypes (M1, M2a, M2b, M2c, M2d, Mox y Mme) had been created based on PubMed search by the group of María del Mar Malagón in the Instituto maimónides de Investigación Biomédica de Córdoba (IMIBIC). The list, displayed in Table 3, comprises cell surface markers, intracellular markers, and secreted factors (cytokines and chemokines).

	Marker		Secretion	
	Cell surface	Intracellular	Cytokine	Chemokine
M1	MHC II	COX2	TNFa	CCL2
	Il-1R	NOS2 / iNOS	IL-1b	CCL3
	TLR2	IRF5	Il-6	CCL4
	TLR4	STAT1		CCL5
	NOS2 / iNOS			CCL8
	SOCS3			CCL9
	CD36 / SR-B3			CCL11
	CD80 / B7-1			CCL19
	CD86 / B7-2			CCL20
	CD68 / SR-D1			CXCL1
	FCG-RII / CD32			CXCL2
	FCG-RIII / CD16+			CXCL3
	IFNg-R			CXCL5
				CXCL9
				CXCL10
				CXCL11
				CXCL13
				CXCL16
				CX3CL1
Mox	HMOX-1			
	SRXN-1			
	TXNRD-1			
	GST-O			
	GCLM			
Mme	PLIN2			
	ABCA-1			

	Marker		Secretion	
	Cell surface	Intracellular	Cytokine	Chemokine
M2a	MHC II	IRF4	IL-10	CCL1
	CD163	STAT6	IL-1R	CCL2
	Msr1 / SRa1	PPARg	TGFb	CCL17
	Mrc1 / CD206			CCL22
	TGM2			CCL24
	IL-1R II			CCL26
	CLEC10a / CD301			CXCR1
	CLEC7a / Dectin-1			CXCR2
	FCE-R1a			
M2b	MHC II	COX2	IL-6	CCL1
	CD86 / B7-2	IRF4	IL-10	CCL20
	IL-4Ra	SOCS3	TNFa	CXCL1
		SPHK	CSF3/ G-CSF	CXCL2
			CSF2/ GM-CSF	CXCL3
			IL-1b	
			TGFb	
M2c	CD163	IRF4	TGFb1	CXCL13
	TLR1	SOCS3		CCR2
	TLR8	TLR8		
	IL-4Ra			
	Slamf1 / CD150			
	Mrc1 /CD206			
	Msr1 / SR-A1			
	Scarb1 / SR-B1			
	MERTK			
M2d		NOS2 / iNOS	IL-10	CCL5
			VEGF	CXCL10
			TGFb	CXCL16

Table 3: List of macrophages markers and secretion factors.

Due to the fact that the transcriptomics studies were done at different occasions, the absolute values of the results did not allow a direct comparison between the data sets from eWAT and sWAT. Hence, heatmaps were the representation of choice for these results, revealing a pattern of expression in between groups of the same depot.

Moving from lowest to highest level of expression for every gene, colors went from blue to white then red representing the largest expression level.

3.5.4 Expression of extracellular matrix components

Using the same set of data from RNAseq, the expression of various ECM components in WAT was evaluated. For a better focused study, not all identified ECM components were examined, the collagens and proteoglycans part of the core matrisome were assessed. The list of these ECM components comprising 79 genes was also prepared by the group of María del Mar Malagón in IMIBIC. The data here was represented similarly to macrophages data using heatmaps. Moving from lowest to highest level of expression for every gene, colors went from blue to white then red representing the largest expression level.

3.6 Adipose tissue morphological and immunohistochemical analysis

Histological examination of epididymal and subcutaneous adipose tissue and immunohistochemistry studies were performed in collaboration with Dr. Rebeca Fernandez (Translational research in diabetes, lipids and obesity research group, in the area of Liver, digestive tract and metabolism at the IDIBAPS), Dr Fransesc Viñals and Ferran Medina-Jover (Molecular Signalling group at IDIBELL), Dr. Josep Villena (Metabolism and Obesity lab of the Vascular Biology and Metabolism group, Vall D'Hebron Institut de Recerca).

3.6.1 Preparation of tissues for microscopy: paraffin blocs, tissue sections and staining

Once sWAT and eWAT depots were excised, a piece from each was moved into histology cassettes and fixed by immersion in 10% formalin at 4°C overnight.

The next day, the tissue samples in the cassettes were submitted to a dehydration process by immersion following steps detailed Table 4.

	Immersion time (min)	Repetition
PBS (1x)	10	2
Ethanol 70%	60	1
Ethanol 96%	15	1
Ethanol 96%	30	1
Ethanol 96%	60	1
Ethanol 100%	30	2
Ethanol 100%	60	1
Xylene	60	1
Paraffin at 65°C	Overnight	1

Table 4: Steps for sample dehydration and paraffin immersion.

Tissues were then moved to molds and covered in molten paraffin in a paraffin embedding station (Embedding Center, Dispenser + hot Plate, EG1160, Leica). The paraffin blocks were cooled at -80°C overnight previously to being cut with a microtome (Rotary Microtome, RM2135, Leica). 7 µm-thick sections of tissue were cut, moved instantly to water bath at 40°C and then placed on Poly-L-Lysine coated glass slides.

3.6.2 Hematoxylin and eosin (H&E) staining

After drying the tissue sections on the glass slides, paraffin removal and samples dehydration were done followed by H&E staining as detailed in Table 5 (a and b). The H&E staining allows to study the morphology of adipocytes, through the action of hematoxylin, a basic compound, that stains the nucleus in blue, and the counteractivity of eosin, an acid compound, that stains eosinophilic structures such as the cytoplasm in a pink color.

a

	Immersion time (min)	Repetition
Xylene	10	4
Ethanol 100%	5	3
Ethanol 96%	5	3
Ethanol 70%	5	1
Ethanol 50%	5	1
ddH_2O	few seconds	1

b

	Immersion time	Repetition
Harris Hematoxylin	10 min	1
Tap water	Until excess dye is removed	1
HCl	2 min	1
ddH_2O	Rinsing	1
Ammonia water	2 min	1
Tap water	Until excess dye is removed	1
Eosin	2 min	1
Ethanol 70%	5	1
Ethanol 96%	5	3
Ethanol 100%	5	3
Xylene	10	4

Table 5: H&E staining. Steps for paraffin removal and sample dehydration (a) followed by steps for H&E staining and sample dehydration (b).

After the slides dry (not completely), they were mounted by adding drops of DPX and covering the sample with coverslips avoiding bubbles.

3.6.3 Image acquisition and adipocyte cell size measurement

To obtain images of the H&E stained slides, HISTECH Pannoramic 250 FLASH II 3D Scanner with the digitization of preparations in clear field and fluorescence was used. The routine profile for clear field samples uses a Carl Zeiss Plan-Apochromat Lens (20x) with a frame rate of 130 fps. Software SlideViewer (Version 2.5) was used to visualize the resulting images and to take random photos of the samples at 10x magnification for further analysis. Fiji-ImageJ1.8 open-source software with Adiposoft plugin were used to measure the area of adipocytes in the images.

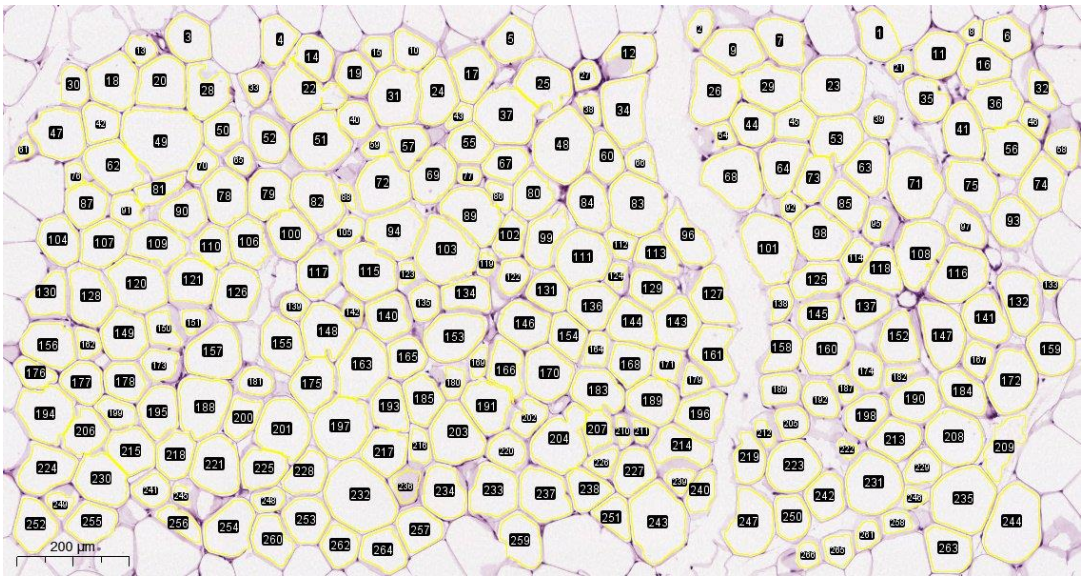

Figure 19: Adiposoft plugin result. An example of an image from eWAT stained with H&E processed with ImageJ and Adiposoft to measure adipocytes cell area.

3.7 Adipose-derived stem cells (ADSCs)

3.7.1 ADSC isolation

First, animals were dissected to collect sWAT and eWAT. The tissues were weighed and washed with DMEM/F12 (Gibco 31330038) + Penicillin-Streptomycin (P/S) (1%) or sterile Phosphate-buffered saline (PBS). It should be noted that to get enough cells from each group, it was necessary to pool tissues from several mice to reach at least 3 g of tissue for each sample. So, the number of pooled depots for each group were as follows: 3 or 4 for *Ctrl*, 2 for *Pat* and 5 or 6 for *LTint*.

From the next step forwards, all work was done with sterile conditions under the hood. Tissues were washed twice with media (DMEM/F12 + P/S) and then with curved scissors or sterile surgical blades, each tissue was minced until it was well homogeneous (a paste) to facilitate enzymatic digestion. The minced tissue was emptied into a falcon containing approximately per 1 g of WAT tissue, 1.5 mL of digestion buffer (previously warmed at 37 °C).

	Initial concentration	Final Concentration in Digestion buffer	Volume or weight added to 10 mL of final volume
HEPES	1.5 M, pH 7.4	100 mM	666.5 µL
NaCl	5 M	123 mM	246 µL
KCl	1 M	5 mM	50 µL
$CaCl_2 \cdot 2H2O$	0.5 M	3 mM	260 µL
Glucose (MW 180)		5 mM	9 mg
BSA (not fatty acid free)		1.5%	150 mg
Collagenase Type I* (Sigma, C0130)		1 mg/ml	10 mg

Table 6: Composition of digestion buffer.
* Added just before use

Next, samples were incubated at 37 °C under agitation for at least 20 minutes (until the tissue was fully digested). sWAT took 5-10 min more than eWAT for full digestion. An equal volume of complete media (DMEM/F12 + 10% fetal bovine serum (FBS) + 1% P/S) was added once the mixture was homogeneous to stop the digestion process. To discard pieces of tissue that had not been digested well, the total volume was passed into another falcon through filters of 250 µm (nylon mesh filters 125 mm Ø, net pore: 250 µm, thickness: 160 µm, 100 UD) (Dilabo S.A NY2500125). Samples were left standing for 3-5 min to allow mature adipocytes to separate, float upwards. Using a 20 mL syringe with a G-19 needle, liquid layer below the adipocytes was collected and passed through a 70 µm cell strainer. It was important to start collecting the solution from bottom to top to avoid the upper layer that would cause the collapse of the cell strainer with large adipocytes. Samples were centrifuged at 900g for 10 minutes at room temperature, supernatant was discarded and pellet resuspended in red cell lysis buffer for 10 min (approx. 1m L per 1g of tissue).

	Initial concentration	Final Concentration in Lysis buffer	Volume or weight added to 10 mL of final volume
NH_4Cl	0.5 M	155 mM	3.1 mL
$KHCO_3$	0.5 M	10 mM	200 µL
EDTA	0.5 M	0.1 mM	2 µL

Table 7: Composition of red cell lysis buffer.

Cells were washed with complete media (double cell lysis volume) and then centrifuged at 900g for 8 minutes at room temperature. Supernatant was aspirated and pellet resuspend in complete media (approx. 2 ml per 1g of tissue) then seeded in 6 well plates (2 ml/well). Cells were incubated at 37°C and 5% CO_2.

3.7.2 Cell culture

Every 24-48h, media was refreshed for cells until confluency was reached. Cells were passed by trypsinizing until passage 2 or 3 were reached to either freeze or use for assays. Cells were frozen at a density of 600.000 cells/mL minimum and a maximum of 2.000.000 cells/mL in the freezing media used (50% HyCro 2x cryopreservation medium (SR30001.02) with 50% complete media).

3.7.3 Samples preparation and Fluorescence-activated Cell Sorting (FACS)

- Cells were trypsinized, counted and divided to get 250.000 cells per tube. One extra aliquot to be used as blank was included
- Samples were centrifuged at RT for 5 min at 200g
- 0.5 mL of PBS (without Ca^{2+}/Mg^{+}) was added to wash the cells and then centrifuged again
- Pellet was resuspended in 100 µl PBS
- Antibodies were added as follows in 100 µl of volume:

Antibody	Source, Product code	Volume
PE- Ly-6A/E (SCA1)	BD, 562059	2 µl
FITC- CD45	BD, 553079	1 µl
APC- CD29	MACS, 130-102-557	1 µl

Table 8: Antibodies used for FACS.

- Samples were incubated for 20 min in the dark at RT
- 0.5 mL of PBS was added to wash the cells and then centrifuged
- Pellet was resuspended in 400 µl PBS
- Samples were stored at 4°C

Last, in order to characterize ADSCs separated from the stromal vascular fraction of WAT, a 2-laser FACSCanto II (BD Biosciences, Eysins, Switzerland) cytometer equipped with a 488-nM and 633-nM laser was used. The data was analyzed with the BD FACSDiva Software (version 6.1.3).

3.7.4 Agilent Seahorse XFe96 Cell Mito Stress Test

This assay allows the study of key parameters of mitochondrial function of cells seeded in a plate through direct measurement of the oxygen consumption rate (OCR) of the cells.

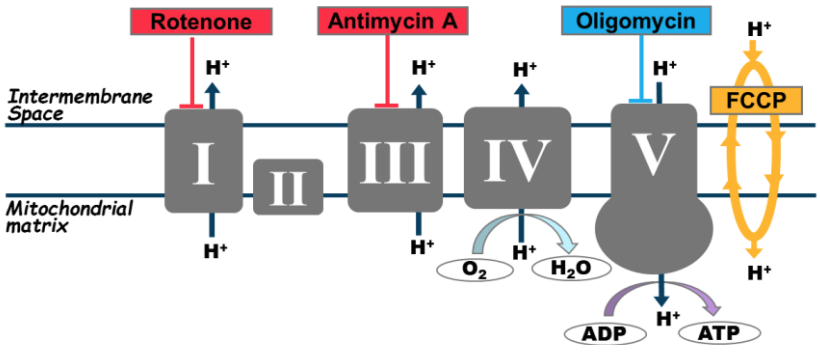

Figure 20: Illustration of the concept behind the Seahorse assay. Illustration of the complexes of the electron transport system (ETS) and the target of action of the modulators used during the Seahorse XF Cell Mito Stress Test. (Agilent Seahorse XF Cell, Mito stress Test Kit User Guide, Kit 103015-100).

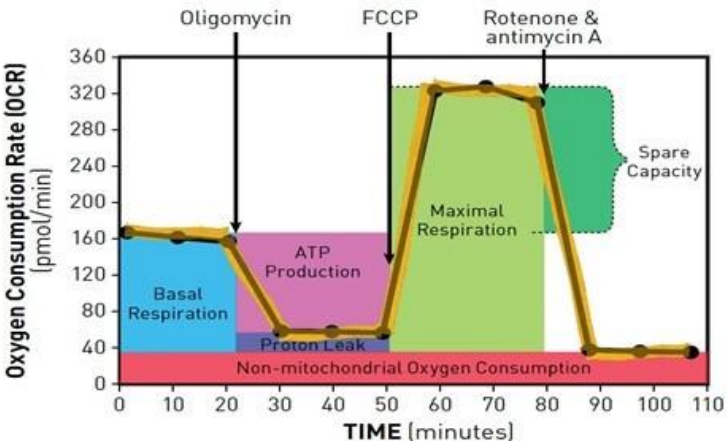

Figure 21: Illustration of the key parameters of mitochondrial function during the test. (Agilent Seahorse XF Cell, Mito stress Test Kit User Guide, Kit 103015-100).

Day previous to the experiment:

1. 80 µL of each sample in complete media was seeded in the seahorse plates (96 wells) at a density of 10.000 cells/ well
2. After seeding the seahorse plate, it was left on a flat surface at room temperature for 1 h to avoid edging of cells
3. A maximum of 100 µL of complete media was added to each well (total 180 µL) and the plate was moved to incubator at 37 °C and 5% CO_2
4. The sensory cartridge was hydrated by adding 200 µL of water per well and incubated at 0% CO_2
5. In addition, around 80 µL of DMEM/RPMI medium (no phenol red, no bicarbonate) and the supplements: L-glutamine, glucose and pyruvate (1 mL of each) were added and incubated at 0% CO_2

Day of the experiment:

1. Plate with cells was placed in incubator at 37°C, 5% CO_2
2. Water in sensory cartridge was discarded. Then, 200 µL of calibrant medium per well were added and sensory cartridge was incubated at 0% CO_2. The cartridge was incubated for at least 1 h before loading injections (detailed in next steps)
3. On software:
    a. Heater was turned on and set at 37°C ± 0.5°C
    b. Mito Stress test template was used and injection strategies were loaded.
    c. Groups were generated according to seeded samples and were assigned to the corresponding wells.
    Blanks were assigned to either of the 4 corner wells
4. Assay Medium was prepared as follows:

Reagent	Final Concentration	Volume (total 80 mL)
Seahorse XF DMEM/RPMI medium	-	77.6 mL
Seahorse XF glucose 1 M	10 mM	0.8 mL
Seahorse XF pyruvate 100 mM	1 mM	0.8 mL
Seahorse XF L-glutamine 200 mM	2 mM	0.8 mL

Table 9: Assay media composition.

5. Cells in plate were washed twice with Assay media then 180 µL were added per well and plate was incubated at at 0% CO_2 for 1 h maximum before beginning of the experiment.
6. Stock solutions of reagents were prepared.
   Using the stock from O2K reagents, the following preparation was done:

Reagent	Initial Stock Concentration	Final required concentration	Volume of Initial Stock	Final Volume (completed with assay media)
Oligomycin	5 mM	100 µM	18 µL	900 µL
Carbonyl cyanide-4 (trifluoromethoxy) phenylhydrazone (FCCP)	1 mM	100 µM	60 µL	600 µL
Rotenone/ Antimycin A	1 mM/ 1 mM	50 µM/ 50 µM	30 µL/ 6 µL	600 µL

Table 10: Reagents preparation for injection ports.

Calculations for the required volume of each reagent at the required concentration was based on:

a) Volume needed = number of wells x volume per port (check Table 11).
b) And optimal concentration of reagents chosen for this cell type (check Table 12).

				Add to port volume (µL)	
Port	Standard assay	Modified assay	Port concentration	96 well	24 well
A	Oligomycin	Test compound*	10X	20	56
B	FCCP	Oligomycin	10X	22	62
C	Rot/AA	FCCP	10X	25	69
D	—	Rot/AA	10X	27	75

Table 11: Volume per port.

	Final well (µM)	Stock solution volume (µL)	Media volume (µL)	10X (Port) (µM)	Volume added to port (µL)
Port A Oligomycin	0.5	150	2,850	5	20
	1.5	450	2,550	15	20
	2.5	630	1,890	25	20
Port B FCCP	0.125	37.5	2,962.5	1.25	22
	0.25	75	2,925	2.5	22
	0.5	150	2,850	5	22
	1.0	300	2,700	10	22
	2.0	600	2,400	20	22
Port C Rot/AA	0.5	300	2,700	5	25

Table 12: Preparation of required concentrations.

7. When the cartridge with calibrant had been incubated for at least 1 h, injections were filled in ports with proper reagent and proper volume.
8. Software was run.
   Calibration plate with loaded cartridge was placed in the tray. Calibration took 15-30 min.
9. Once calibration was done, calibration plate was replaced by samples plate and assay started.

   Results were normalized to the number of cells seeded per well during preparation of Seahorse plate.

3.8 Statistical analysis

All statistical analyses were performed using GraphPad Prism 8.4.2 (GraphPad Software Inc.). Results were expressed as Mean±SEM. The statistical significance among experimental groups is assessed using one-way ANOVA, unless contrary indicated, and differences between means were subsequently tested by Tuckey post-hoc test. Data curation involved the removal of values tested as outliers in punctual situations. A p-value <0.05 was considered significant in all cases, meaning a confidence interval of 95% and setting significance level at $\alpha=0.05$.

RESULTS

4.1 Characterization of experimental groups (phenotype)

4.1.1 BW and tissue weights increased after HFD and decreased with *Int* and *LTint* groups

In the first step towards identifying the effects of lifestyle modifications on specific processes in certain tissues, the characterization of the distinct groups of our model was due. Our 4 experimental groups were subjected to different diets, food intake patterns and physical activity protocols which promoted particular phenotypes. Starting with body weight, before the mice were split into groups, at the age of 6 weeks, they had an average BW of 22.3±0.25g. By the time the mice were sacrifice, *Pat* group had a significantly higher BW in comparison to all other 3 groups. The final BW was 32.37±0.65g for *Ctrl* mice, 42.28±0.89g for *Pat* mice, 32.82±0.58g for *Int* mice and 32.11±0.47g for *LTint* mice (Figure 22). In addition to BW, at the time of sacrifice, the weight of some tissues of interest (liver, sWAT, eWAT) was recorded for the same animals. A similar pattern to the one of final BW was seen with tissue weights. Compared with the *Ctrl* group, the *Pat* group showed an increase in tissue weights that was reduced after intervention and long-term intervention. In the case of the liver, weight in *Pat* group was significantly increased compared to *Ctrl* and *LTint* with values being 1.3±0.06g for *Ctrl*, 1.6±0.07g for *Pat*, 1.4±0.06g for *Int* and 1.2±0.03g for *LTint*. For eWAT and sWAT, *Pat* group showed significantly increased tissue weights compared to all others. The weight of eWAT for all groups was the following: 0.9±0.06g for *Ctrl*, 2.2±0.09g for *Pat*, 0.8±0.1g for *Int* and 0.8±0.07g for *LTint*. While sWAT weight among groups was distributed in such a way: 0.8±0.05g for *Ctrl*, 2.3±0.1g for *Pat*, 1.2±0.15g for *Int* and 0.9±0.08g for *LTint* (Figure 23).

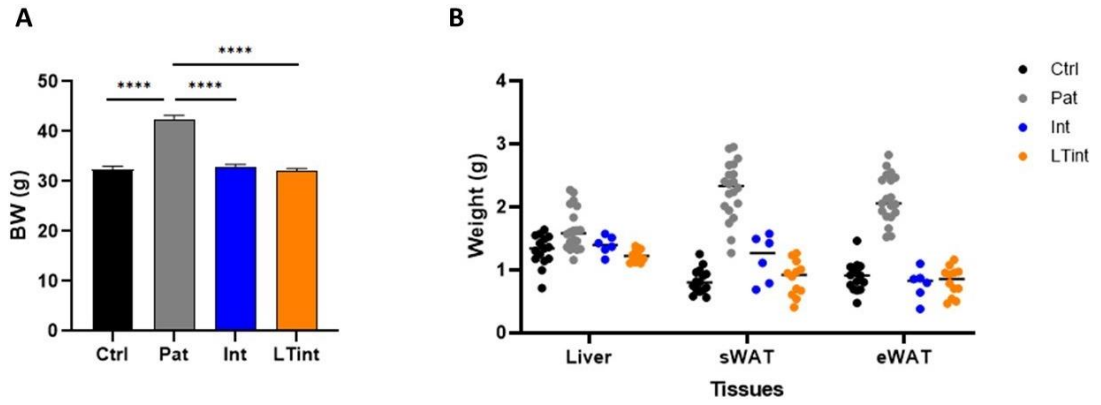

Figure 22: BW and tissue weights. A: Final BW of 4 groups. Ctrl n=15; Pat n=20; Int n=6; LTint n=12. B: Tissue weights of sWAT, eWAT and liver for the same animals in A.
Mean±SEM, ANOVA One-way, Post-hoc Tukey; *p<0.05, **p<0.01, ****p<0.0001.

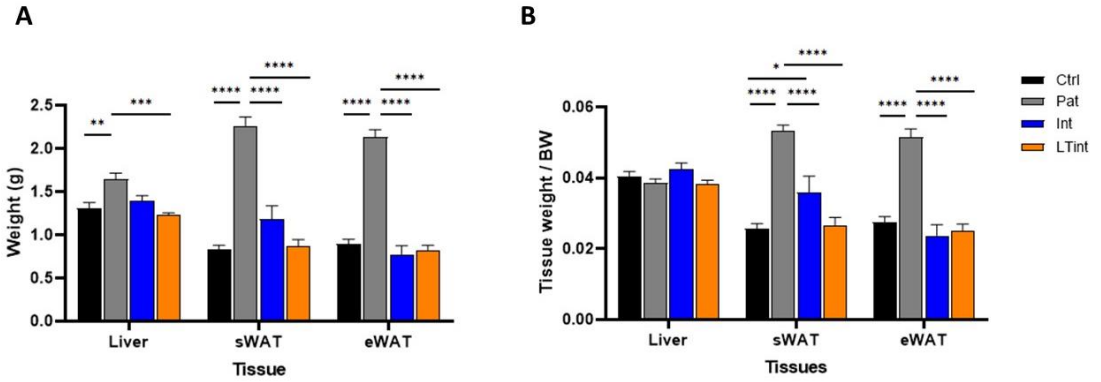

Figure 23: Tissue weights before and after normalization to BW. A: Tissue weights of sWAT, eWAT and liver without normalization to BW. Ctrl n=15; Pat n=20; Int n=6; LTint n=12. B: Same tissue weights of liver, sWAT and eWAT with normalization to BW.
Mean±SEM, ANOVA One-way, Post-hoc Tukey; *p<0.05, **p<0.01, ****p<0.0001.

It is worth mentioning that when the tissue weights were normalized to BW, no differences between groups were seen in liver weight. However, regarding eWAT and sWAT, the same pattern of increase in *Pat* group and a significantly decrease in *Int* and *LTint* groups was observed.

4.1.2 HFD induced glucose intolerance that was partially reverted after the interventions

The alterations observed in the food intake and the physical activity of the mice in the experimental groups were expected to have consequences on systemic

glucose homeostasis and insulin sensitivity. In this line, IGTTs were performed to assess and better describe the phenotype in our model. Considering the stress an IGTT imposes on the mice, it was preferred to avoid repeating the procedure for the same animals in a short range of time. For that reason, IGTT data for *Int* group from our recent cohorts was missing. For the sake of describing glucose homeostasis in all groups, we will use IGTT data from previous cohorts showing the groups *Ctrl*, *Pat*, and *Int* while using results from recent cohorts to show data from the groups *Ctrl*, *Pat*, and *LTint*. Observing the curves created by plotting time points 0, 15, 30, 60 and 120 minutes, it was clear that *Pat* group was the most glucose intolerant and insulin resistant. *Int* and *LTint* mice showed a marked improvement in insulin sensitivity and the capacity for glucose clearance which suggests that the observed hyperglycemia in the *Pat* group induced by HFD was reversed following both phases of interventions (Figure 24).

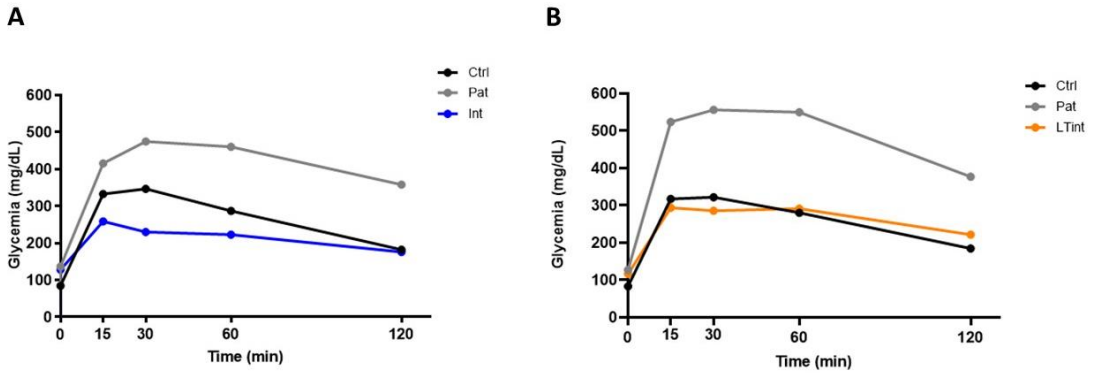

Figure 24: IGTT. A: IGTT results from previous cohorts representing experimental groups Ctrl, Pat and Int. Ctrl n=82; Pat n=168; Int n=32. B: IGTT results from current cohorts representing experimental groups Ctrl, Pat and LTint. Ctrl n=12; Pat n=12; LTint n=11.
Mean±SEM, ANOVA One-way, Post-hoc Tukey; *p<0.05, **p<0.01, ****p<0.0001.

For the IGTT protocol, mice were fasted for 16 h before recording blood glucose levels at time-point 0. The fasting glycemia from previous cohorts and from current ones was represented in Figure 4. Comparing fasting glycemia from *Ctrl*, *Pat*, and *Int* mice, an increase after HFD from 85 to 137 mg/dL was observed, with the first phase of intervention showing a non-recovered value of 132 mg/dL. When assessing groups *Ctrl*, *Pat*, and LTi*nt* in current cohorts, it was demonstrated that even after the second phase of intervention, fasting glucose levels did not regress back to *Ctrl*

values. The fasting glycemia was 83, 127 and 117 mg/dL for *Ctrl*, *Pat*, and LTi*nt* mice, respectively.

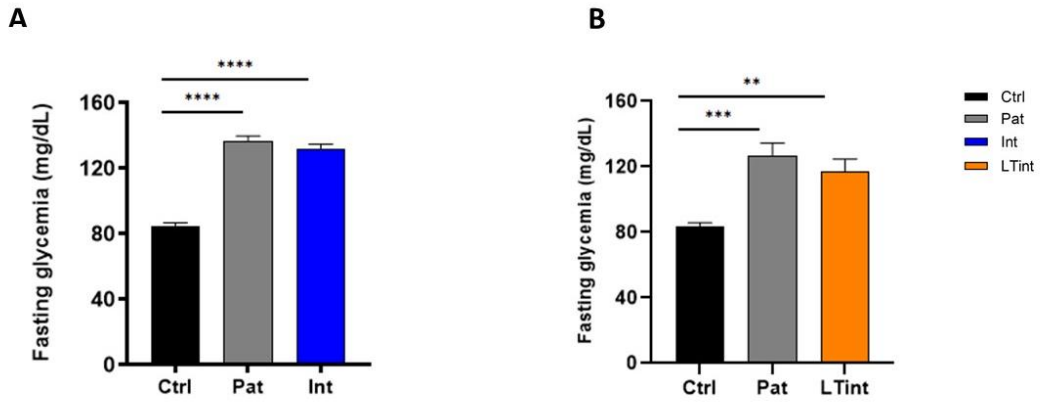

Figure 25: Fasting glycemia. A: Blood glucose levels after 16 h of fasting from previous cohorts. Ctrl n=82; Pat n=168; Int n=32. B: Blood glucose levels after 16h of fasting from current. Ctrl n=12; Pat n=12; LTint n=11.
Mean±SEM, ANOVA One-way, Post-hoc Tukey; *p<0.05, **p<0.01, ****p<0.0001.

4.2 Effects of HFD followed by a switch to a healthier lifestyle on tissue-specific lipidomic profile

For a better description of our experimental groups, various assays and investigations were conducted and reported in the first manuscript for the LiMa project (191). In order to fill some of the gaps in the systemic studies, in the next section, we focus on the lipidomics studies performed on several insulin-sensitive tissues in the experimental groups *Ctrl*, *Pat* and *Int*.

4.2.1 Lipid profile revealed a tissue-specific characteristic

In the initial part of this study, before introducing the different experimental groups, it was of interest to highlight the distinctive lipid profiles of the tissues from lean healthy mice (*Ctrl* group). Hence, firstly, the lipidomics data from the 4 insulin-

sensitive tissues – liver, eWAT, gastrocnemius and hypothalamus – of *Ctrl* mice was investigated (Figure 26).

At first glance, 3 major observations could be made: (1) eWAT and liver are the tissues with the highest content of glycerolipids (Figure 26A–C), whereas (2) eWAT presented the highest FA content (Figure 26H–O) and (3) hypothalamus showed the highest content in sterol lipids, and phosphoglycerolipids (Figure 26E–G, P–V). Evaluating each lipid of the glycerolipids, it was shown that triglycerides (TAG) were present at higher levels in eWAT than in liver and gastrocnemius muscle (Figure 26A). In addition, diglycerides (DAG) were more elevated in eWAT than in liver (Figure 26B), and monoglycerides (MAG) were mainly detected in liver (Figure 26C), while free glycerol was only detected in eWAT (Figure 26D). As for sterol lipids, hypothalamus had the highest content in total cholesterol (Chol) and free cholesterol (FC) compared to the other 3 tissues (Figure 26E, F), and only in hypothalamus and liver that esterified cholesterol (CE) was detected (Figure 26G). The peak in the spectra of the NMR representing total cholesterol included both free cholesterol and esterified cholesterol. Then, two different peaks in the spectra allowed the quantification of FC and EC independently. Evaluating the FA content in the tissues of interest, the major observation was that most FAs had their highest content in eWAT, lowest in gastrocnemius with liver and hypothalamus in second place. This was the case for unsaturated fatty acids (UFA) (Figure 26H), polyunsaturated FAs (PUFA) (Figure 26I), oleic acid (Figure 26J), arachidonic and eicosapentaenoic acids (ARA-EPA) (Figure 26N) and omega3-docosahexaenoic acid-EPA-Linolenic (n3.D-E-L) (Figure 26O). Some exceptions were linoleic acid that was almost absent in hypothalamus (Figure 26K) and linolenic acid that was only detected in eWAT (Figure 26L). Also, docosahexaenoic acid (DHA) was higher in liver and hypothalamus than in gastrocnemius, and not detected in eWAT (Figure 26M). Regarding phosphoglycerolipids, most of them had their highest content in hypothalamus – like phosphocholine (ChoP), phosphatidylethanolamine (PE), sn-glycerophosphocholine (sn-GPC) and plasmalogen – and not all were detected in the 4 tissues (Figure 26P-T). The content of sphingomyelin (SM) was significantly higher in the hypothalamus than in the other evaluated tissues (Figure 26U).

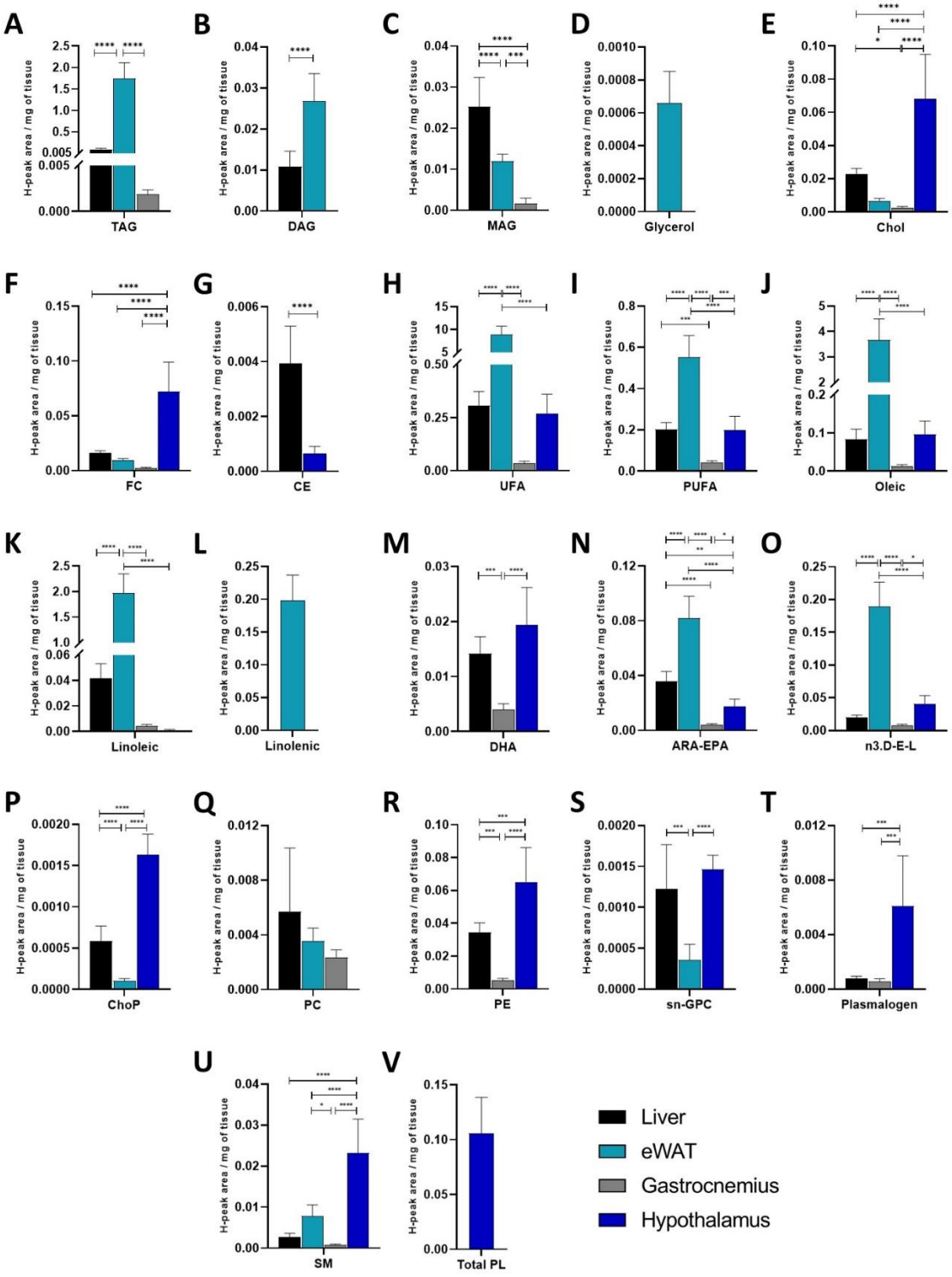

Figure 26: Lipid profiles of liver, eWAT, gastrocnemius and hypothalamus in healthy lean mice. Comparison of the presence of glycerolipids (A–D), sterol lipids (E–G), fatty acids (H–O), phospholipids and sphingolipids (P–V) in 4 different tissues from *Ctrl* mice. Liver n=8; eWAT n=8; gastrocnemius n=8; hypothalamus n=7. Y-axis values indicate proton-based NMR peak area normalised to sample weight (H-peak area/mg of tissue).
Mean±SEM, ANOVA One-way, Post-hoc Tukey; *p<0.05, **p<0.01, ****p<0.0001.

In the next part, we assessed the lipid profile and tissue distribution changes associated to high-fat feeding and the nutritional and exercise intervention following the HFD.

4.2.2 Lipid profile of hypothalamus was not altered by HFD and nutritional and exercise intervention

In the hypothalamus, the HFD and nor the intervention that followed seemed to evoke alterations in the levels of FA (Figure 27A, B), sterols (Figure 27C) nor phospholipids and sphingomyelin content (Figure 27D, E).

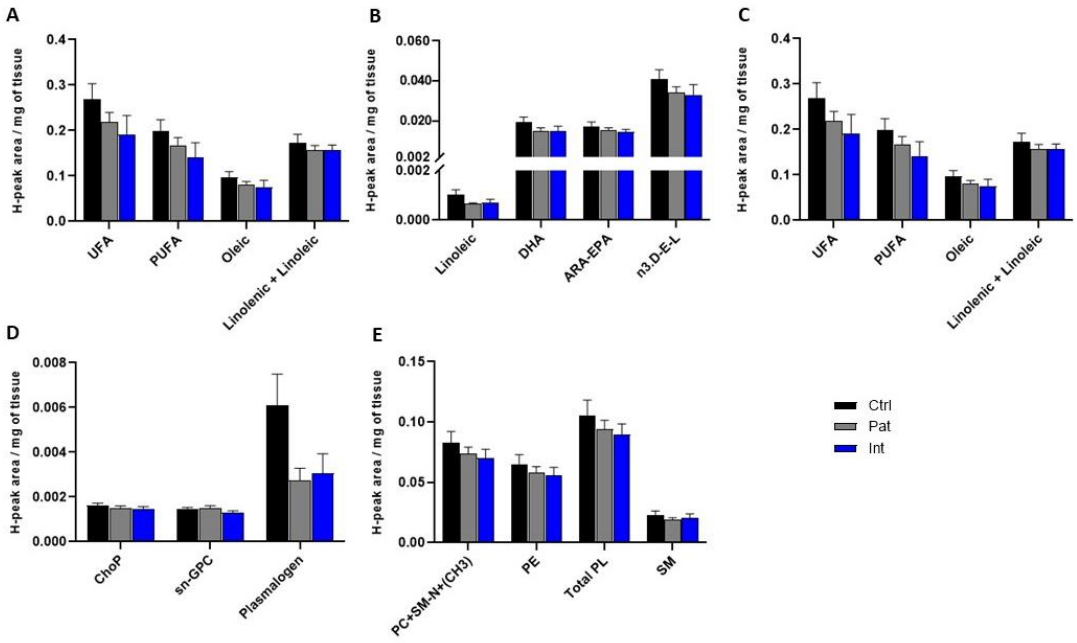

Figure 27: Alterations in metabolite lipid profile in hypothalamus. Representation of the changes induced by HFD and the nutritional and exercise intervention following the HFD, on the presence of (A, B) fatty acids, (C) sterol lipids and (D, E) phospholipids and sphingolipids in the hypothalamus. Ctrl n=7; Pat n=8; Int n=8. Y-axis values indicate H-peak area/mg of tissue.
Mean±SEM, ANOVA One-way, Post-hoc Tukey; *p<0.05, **p<0.01, ****p<0.0001.

4.2.3 Lipidome of gastrocnemius was sensitive to modifications in energy balance

The lipid profile of gastrocnemius skeletal muscle was investigated in consideration of the changes stimulated by HFD and the nutritional and exercise intervention that followed. An increased content of TAG (Figure 28A) and several fatty acids like UFA, oleic acid and linoleic acid (Figure 28B) was observed in the *Pat* group. The HFD-induced increase in content was reversed in the *Int* group where TAG, UFA, oleic acid and linoleic acid had similar values to the *Ctrl* group. The content of other FAs was differently modified; (1) no changes were observed with PUFA (Figure 28B), and DHA (Figure 28C), (2) ARA-EPA levels were decreased in *Int* compared to *Ctrl* group (Figure 28C) and (3) n3.D-E-L levels increased with the *Int* group in comparison to *Ctrl* and *Pat* groups (Figure 28C). Across the 3 experimental groups, no modifications in the content level were detected in sterols (Figure 28D) and phospholipids and SM (Figure 28E, F). These results suggest that the lipid profile of the gastrocnemius is reflective of modifications in energy intake, and do not mimic the composition of the administered diet (Section 3.1.3 for details on diets).

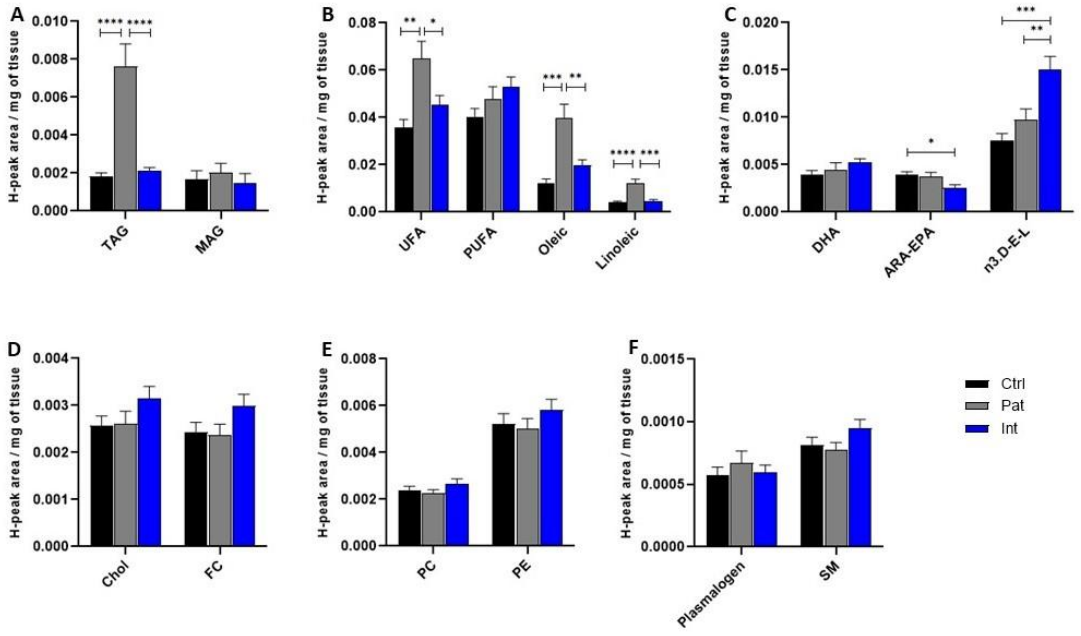

Figure 28: Alterations in metabolite lipid profile in gastrocnemius. Representation of the changes induced by HFD and the nutritional and exercise intervention following the HFD, on the

presence of (A) glycerolipids, (B, C) fatty acids, (D) sterol lipids and (E, F) phospholipids and sphingolipids. Ctrl n=8; Pat n=7; Int n=7. Y-axis values indicate H-peak area/mg of tissue.
Mean±SEM, ANOVA One-way, Post-hoc Tukey; *p<0.05, **p<0.01, ****p<0.0001.

4.2.4 The alterations in most lipid classes content in liver were greatly guided by the energy balance

Examining the lipidome of the liver throughout the changes induced by HFD and the intervention phase, a trend of increase in the *Pat* group and decrease to *Ctrl* values in the *Int* group was revealed in most lipids. This pattern was observed in TAG (Figure 29A), DAG (Figure 29B) and fatty acids UFA, PUFA, oleic, linoleic (Figure 29C), DHA and ARA-EPA (Figure 29D) and Chol and CE levels (Figure 29E). Fatty acids n3.D-E-L content had increased with the *Pat* group but without reversibility after the intervention (Figure 29D). In the case of phospholipids, the levels of content of each lipid were affecting differently across the groups. A decrease in ChoP levels in *Int* group compared to the *Ctrl* group and in plasmalogen in the *Int* group compared to the other groups was observed (Figure 29F). No change in PC content was found and HFD seemed to stimulate a decrease in content in *Pat* group which is reversed with an increase to *Ctrl* values in the *Int* group (Figure 29G). SM levels were reduced with both *Pat* and *Int* groups (Figure 29F). Altogether, these results demonstrate that the liver lipidome underwent substantial alterations induced by the stress of the HFD that were susceptible to changes upon intervention. Hence, it suggests that the content of lipids in the liver mostly reflect the energy balance and body composition; after a high-fat feeding, the levels of most lipids are increased and reduced after a lifestyle intervention that includes nutritional and energy constraints.

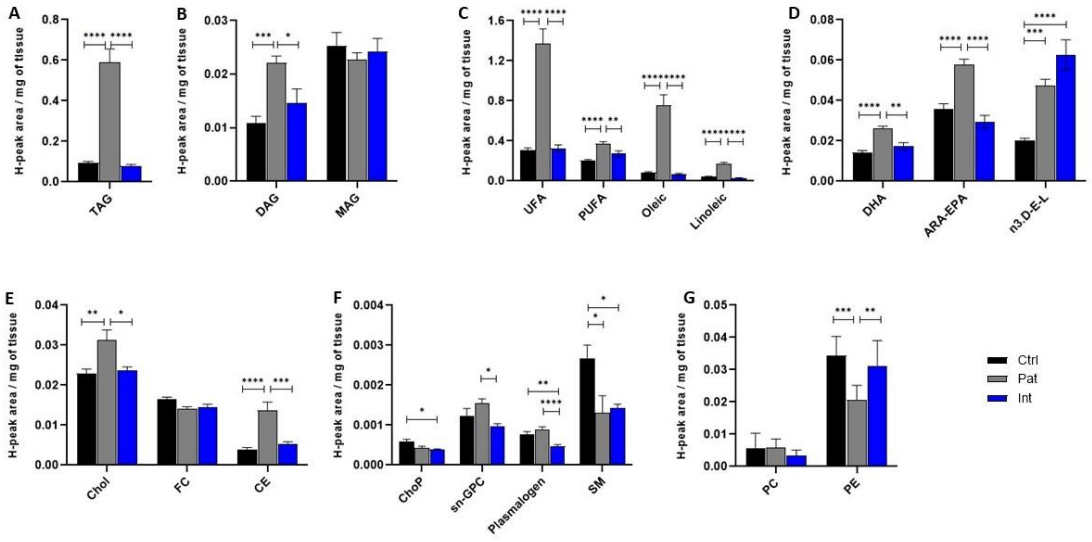

Figure 29: Alterations in metabolite lipid profile in liver. Representation of the changes induced by HFD and the nutritional and exercise intervention following the HFD, on the presence of (A, B) glycerolipids, (C–E) fatty acids, (F) sterol lipids and (G, H) phospholipids and sphingolipids. Ctrl n=8; Pat n=8; Int n=7. Y-axis values indicate H-peak area/mg of tissue.
Mean±SEM, ANOVA One-way, Post-hoc Tukey; *p<0.05, **p<0.01, ****p<0.0001.

4.2.5 Lipid profile of eWAT mirrored the composition of the administered diets

For the final part of this section, the lipidome of insulin-sensitive tissue eWAT was examined. Starting with glycerolipids and in the exception of free glycerol, no changes in content levels were seen (Figure 30A, B). As for fatty acids, the intervention seemed to evoke a massive rise in content levels of PUFA, linolenic and n3.D-E-L significant to both *Ctrl* and *Pat* groups (Figure 30D, E). On the other hand, linoleic acid and ARA-EPA content was decreased with HFD and further declined after the interventions (Figure 30D, E). An increase in content of Chol and FC induced by HFD was seen in the *Pat* group and no recovery was recorded in the *Int* group (Figure 30F). Phospholipids and SM reveal a trend of an increase in content moving from *Ctrl* to *Pat* and then *Int* that was only significant between *Ctrl* and *Int* groups for sn-GPC, PC and SM (Figure 30G, H). The mentioned alterations in eWAT suggest that the lipidome of eWAT is highly dependent upon the administered diet and not the energy balance since both HFD and IntD (details on diets in section 3.1.3) had equal fat content (45% higher than Chow diet) but IntD contained more unsaturated fat than HFD.

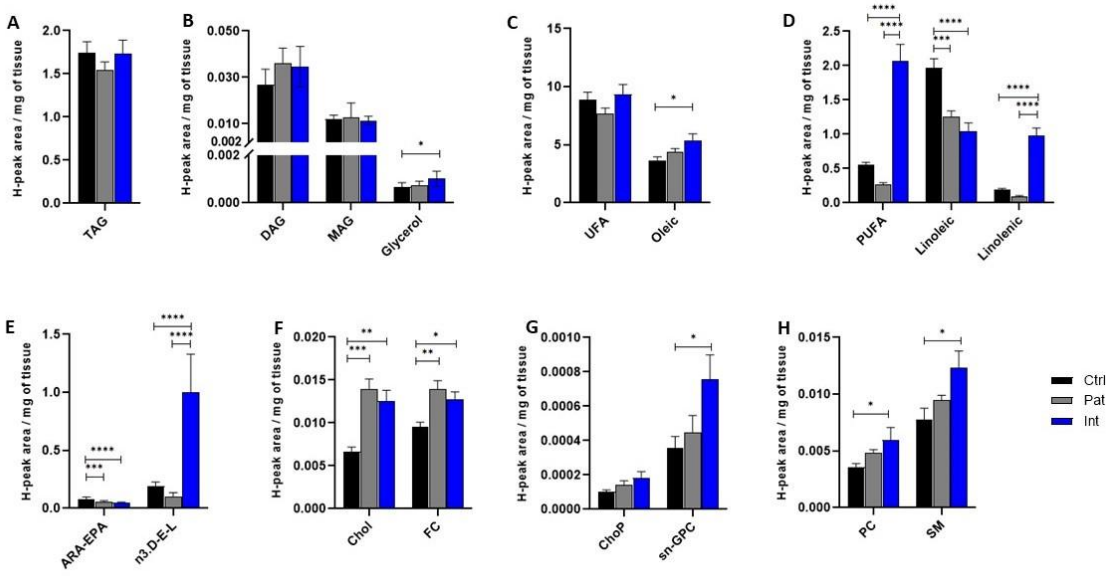

Figure 30: Alterations in metabolite lipid profile in eWAT. Representation of the changes induced by HFD and the nutritional and exercise intervention following the HFD, on the presence of (A, B) glycerolipids, (C, D) fatty acids, (E) sterol lipids and (F, G) phospholipids and sphingolipids. Ctrl n=8; Pat n=8; Int n=7. Y-axis values indicate H-peak area/mg of tissue.
Mean±SEM, ANOVA One-way, Post-hoc Tukey; *p<0.05, **p<0.01, ****p<0.0001.

4.3 Adipose tissue morphology

4.3.1 Inflammation and fibrosis observed after HFD and the first phase of intervention in eWAT but not sWAT

With the focus of this thesis being on adipose tissue, the histology of both depots, eWAT and sWAT, was highlighted through staining with H&E. With hematoxylin staining the nucleus blue and eosin staining eosinophilic structures such as the cytoplasm in a pink color, we can clearly identify adipocytes with the cytoplasm and nucleus pushed to the side by lipid droplets. Assessing the morphology of the tissue in eWAT, the *Pat* group showed few crown-like structures (CLS) that are indicated by the blue circles. The tissue from *Int* demonstrated an extensive immune cell infiltration and signs of fibrosis pinpointed at by the red

arrows (Figure 31). Comparing the morphology of the tissue in the *LTint* group to the others, it seems to resemble the tissue in the *Ctrl* group. In contrast, the sWAT depot lacks altogether the inflammatory response seen in eWAT (Figure 32). All groups of sWAT exhibit a similar absence of immune cell infiltration, CLS and signs of fibrosis.

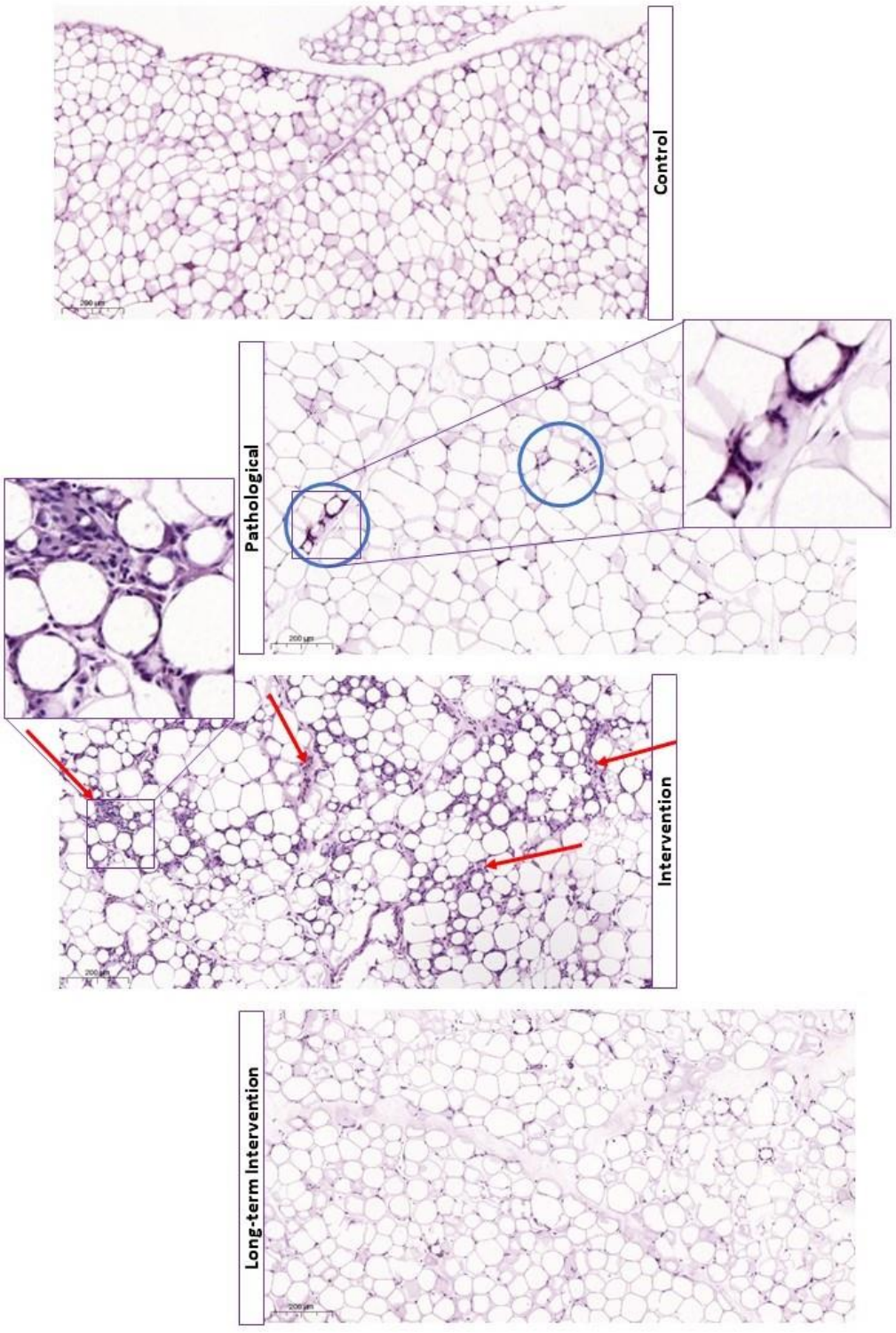

Figure 31: H&E of eWAT. Microscopy of eWAT stained by H&E showing the morphology of the tissue for the 4 experimental groups. The blue circles engulf CLS and the red arrows point to areas of massive alterations in the tissue.

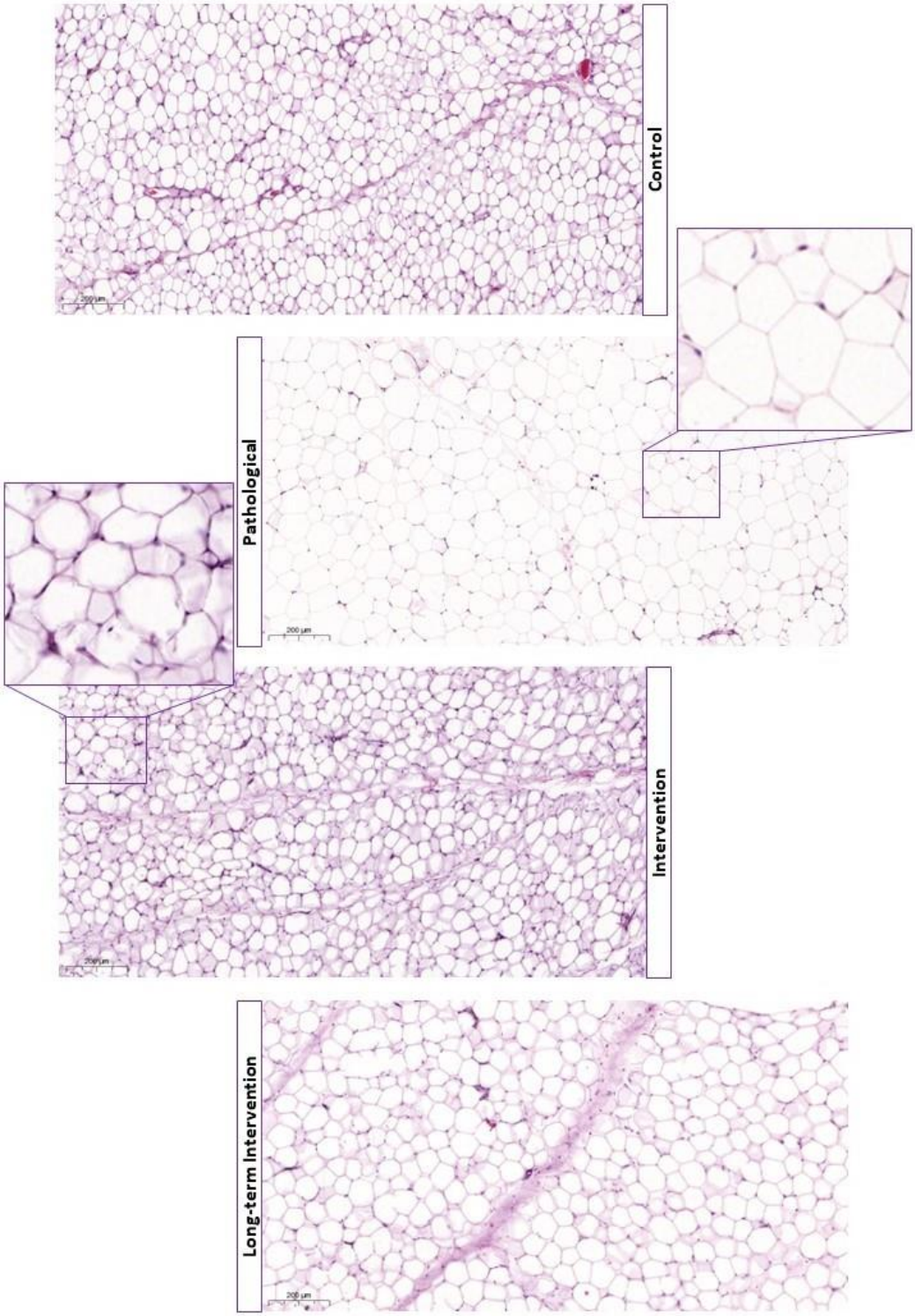

Figure 32: H&E of sWAT. Microscopy of sWAT stained by H&E showing the morphology of the tissue for the 4 experimental groups.

4.3.2 Adipocytes were hypertrophic after HFD with cell size area reduced faster in eWAT than sWAT with intervention

An additional readout was achieved using microscopy images for the same H&E stained samples, where adipocytes cell area was estimated. The cell area of adipocytes in these depots was set up to 1600 μm^2. The frequencies of cells with a cell area belonging to the following intervals were calculated: <50 μm^2, 50-100 μm^2, 100-200 μm^2, 200-400 μm^2, 400-800 μm^2, 800-1200 μm^2 and 1200-1600 μm^2. For both WAT depots, the peak in frequency for the *Ctrl* group was for cell area interval 100-200 μm^2. With the HFD-induced pathological phenotype, hypertrophy of cells in both depots was observed, so that the highest number of adipocytes have an area in the ranges 400-800 μm^2 and 200-400 μm^2 for eWAT and sWAT, respectively. With the interventions, the adipocytes cell area recovered control values, i.e., the greatest number of cells belong again to the interval 100-200 μm^2 (Figure 33A, B).

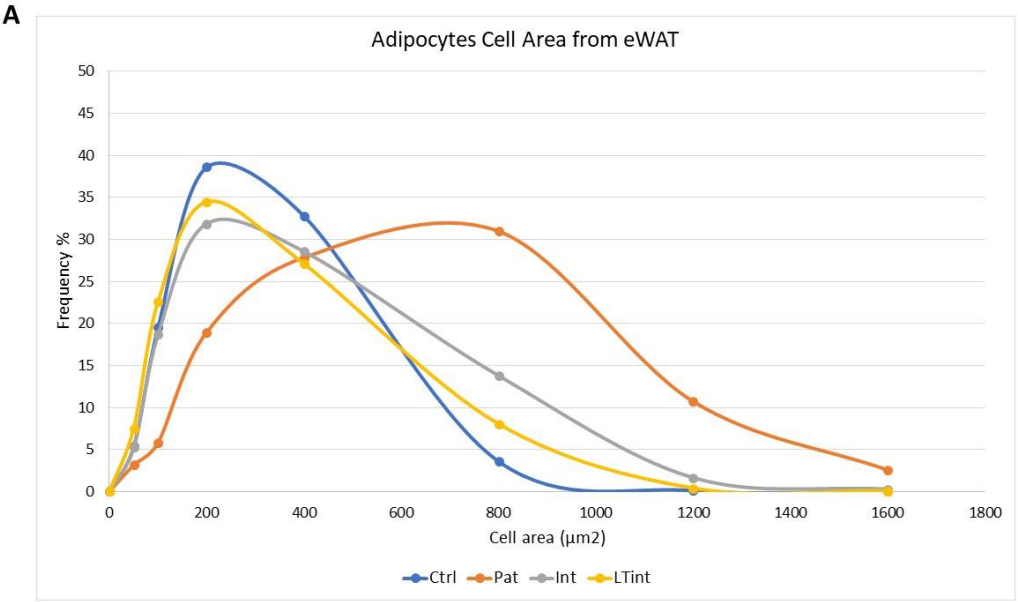

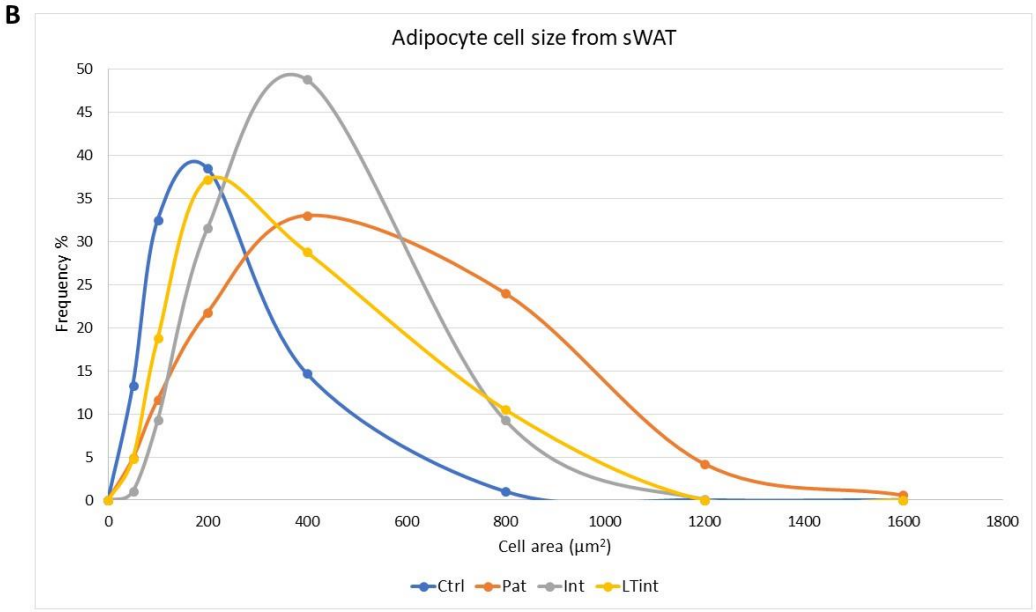

Figure 33: Frequency of adipocytes with assigned cell area intervals. A: Adipocytes from eWAT. Ctrl n=4; HFD n=8; Int n=4, LTint n=4. B: Adipocytes from sWAT. Ctrl n=4; Pat n=8; Int n=4; LTint n=4.

In order to highlight the differences between eWAT and sWAT, data representing each group from each depot were illustrated side by side. As shown in Figure 34, eWAT adipocytes had a tendency to have larger cell areas, as observed for *Ctrl* group and *Pat* group where the frequency of larger cells was slightly higher. Major differences between depots were observed in the *Int* group. sWAT adipocytes seemed to be less distributed and with the highest frequency reaching almost 50% in the cell area interval 200-400 µm^2. In contrast, eWAT adipocytes in the same experimental group had the highest frequency at the cell area interval 100-200 µm^2.

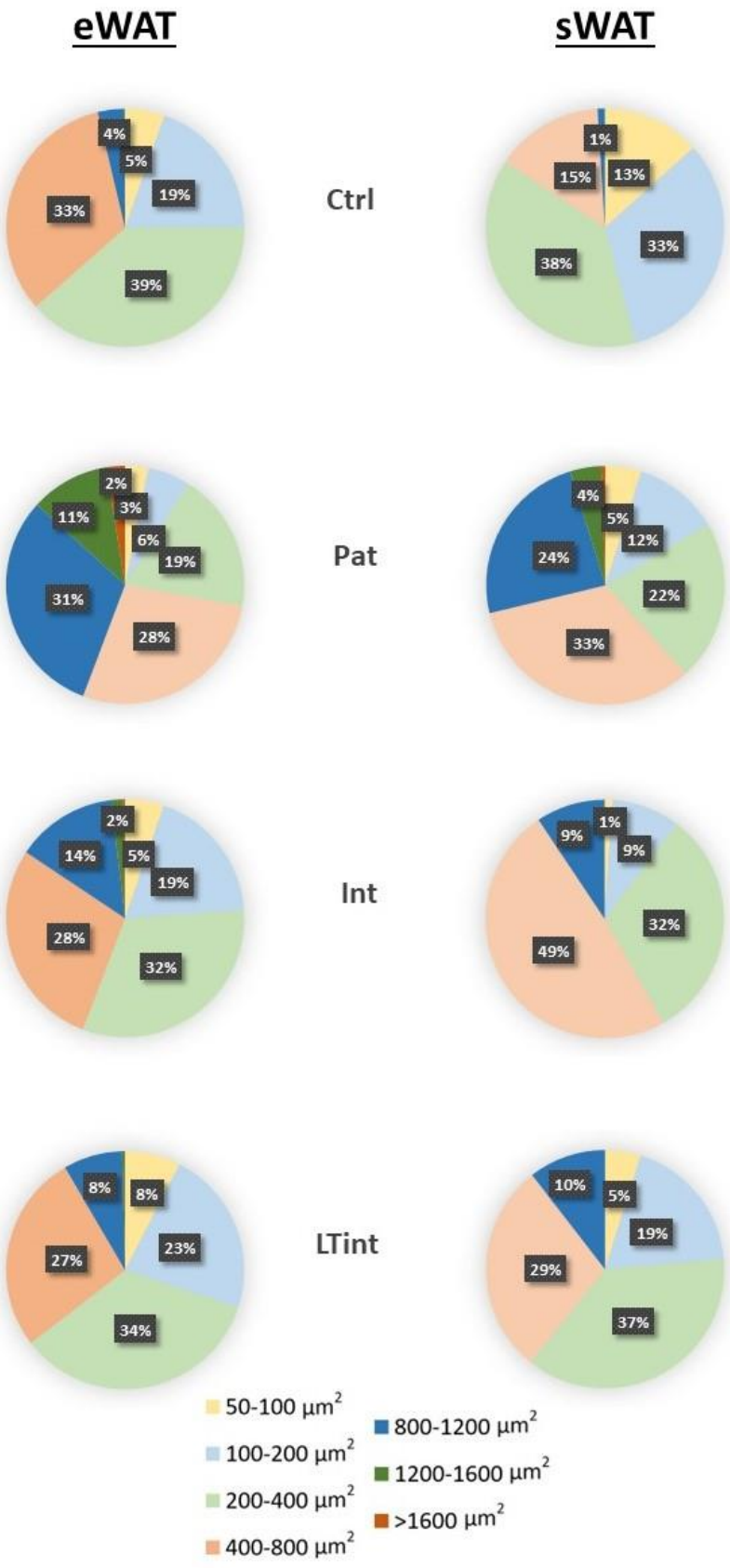

Figure 34: Comparative graphs between eWAT and sWAT adipocytes cell area from the 4 experimental groups. The cell area of adipocytes in each group illustrated by frequency of cell area intervals. Ctrl n=4; Pat n=8; Int n=4; LTint n=4.

4.4 Stromal vascular fraction of WAT

4.4.1 Adipose-derived stem cells can be efficiently separated from whole adipose tissue

Classical procedures for isolation of adipose-derived stem cells (ADSC) include the separation of adipocytes from the stromal vascular fraction (SVF) as a first step. Since various cell types comprise the SVF of WAT, it is important to validate the efficiency at which ADSCs are separated from WAT. For this purpose, the final population of cells obtained upon completion of the protocol depicted in Section 3.7.1, was incubated with several antibodies allowing their characterization. Specifically, we employed three antibodies: CD45 – a marker for all hematopoietic cells, CD29 – a marker for mesenchymal stem cells, and Sca1 – a marker for progenitor fibroblast-shaped cells.

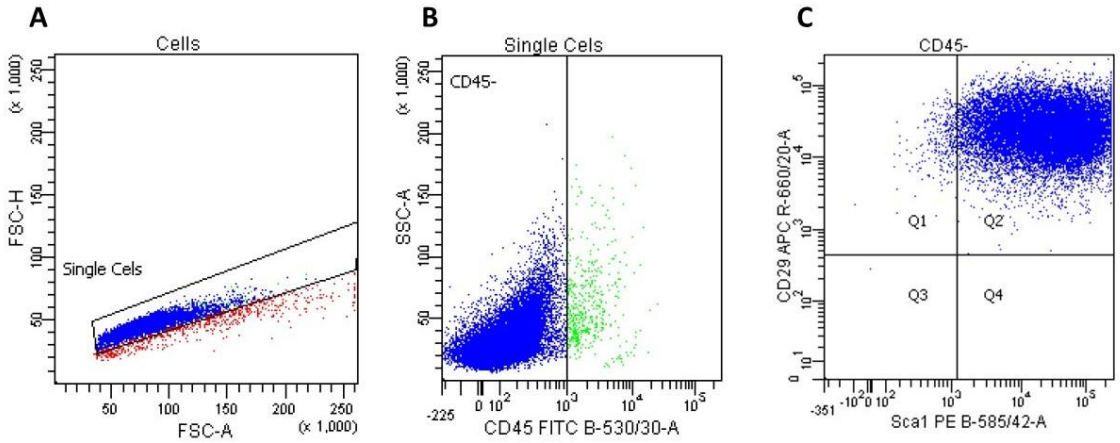

Figure 35: Characterization of the cell population separated from SVF to get ADSCs. This figure is an example of the FACS results from one of the samples of sWAT. The cells of interest were recognized as CD45- CD29+ and Sca1+ single cells.

In the first step of the FACS processing, viable cells were sorted followed by single cells (Figure 35A). Out of this population, CD45- cells found in the left side of the second panel of Figure 9 (Figure 35B) were segregated. Then, the ADSC population

was identified from those cells as the CD29+ and Sca1+ cells found in the second quadrant (Q2) of the third panel (Figure 35C). The percentage of CD45- CD29+ Sca1+ cells out of the total number of single cells was chosen to determine the content of our samples in ADSCs. To test the efficiency of the protocol, samples from control mice were used. For samples from eWAT, CD45- CD29+ Sca1+ cells accounted for by 82% of all single cells whereas from sWAT, they were at 94%.

4.4.2 Mitochondrial function of ADSCs is reduced with LTint in eWAT and with Pat in sWAT

Taking into consideration results of high-resolution respirometry experiments done on eWAT and sWAT by previous projects (section 1.6), it was decided to assess mitochondrial function of ADSCs. The test chosen for this readout was the *Seahorse Mito Stress Test* (section 3.7.4) where oxygen consumption rate (OCR) is measured 3 times at each of the 4 respiratory states. The 4 respiratory states are routine respiration (OCR with no interventions), proton leak (induced by the addition of oligomycin), maximal respiration (induced by ionophore FCCP), and the residual oxygen consumption ROX (induced by inhibitors rotenone and antimycin A). For this assay, not all experimental groups were included. One of the reasons for the exclusion of some experimental part was based on the previous results from whole homogenate mitochondrial function studies (section 1.6). These results revealed a worsened mitochondrial function in eWAT after HFD which persisted after both phases of intervention (*Int* and *LTint*), whereas mitochondrial function recovered back to *Ctrl* values from the first phase of intervention in sWAT. Thus, it was decided to focus on the groups *Ctrl*, *Pat* and *LTint* for eWAT and *Ctrl* and *Pat* groups for sWAT.

As expected for all samples, OCR decreased after ATP synthase inhibition by oligomycin to reach its maximal values with stimulation by FCCP. Finally, ROX was achieved by inhibition of complex I and complex III through rotenone and antimycin A titration, respectively. Starting with eWAT, the 3 groups exhibited significant differences at routine respiration, with the highest OCR of 41 pmol/min for the *Ctrl* group followed by 33 pmol/min for the *Pat* group and lowest OCR of 23 pmol/min

for the *LTint* group. Throughout the remaining respiratory states, *Ctrl* and *Pat* ADSCs had higher OCR values compared to *LTint* group (Figure 36).

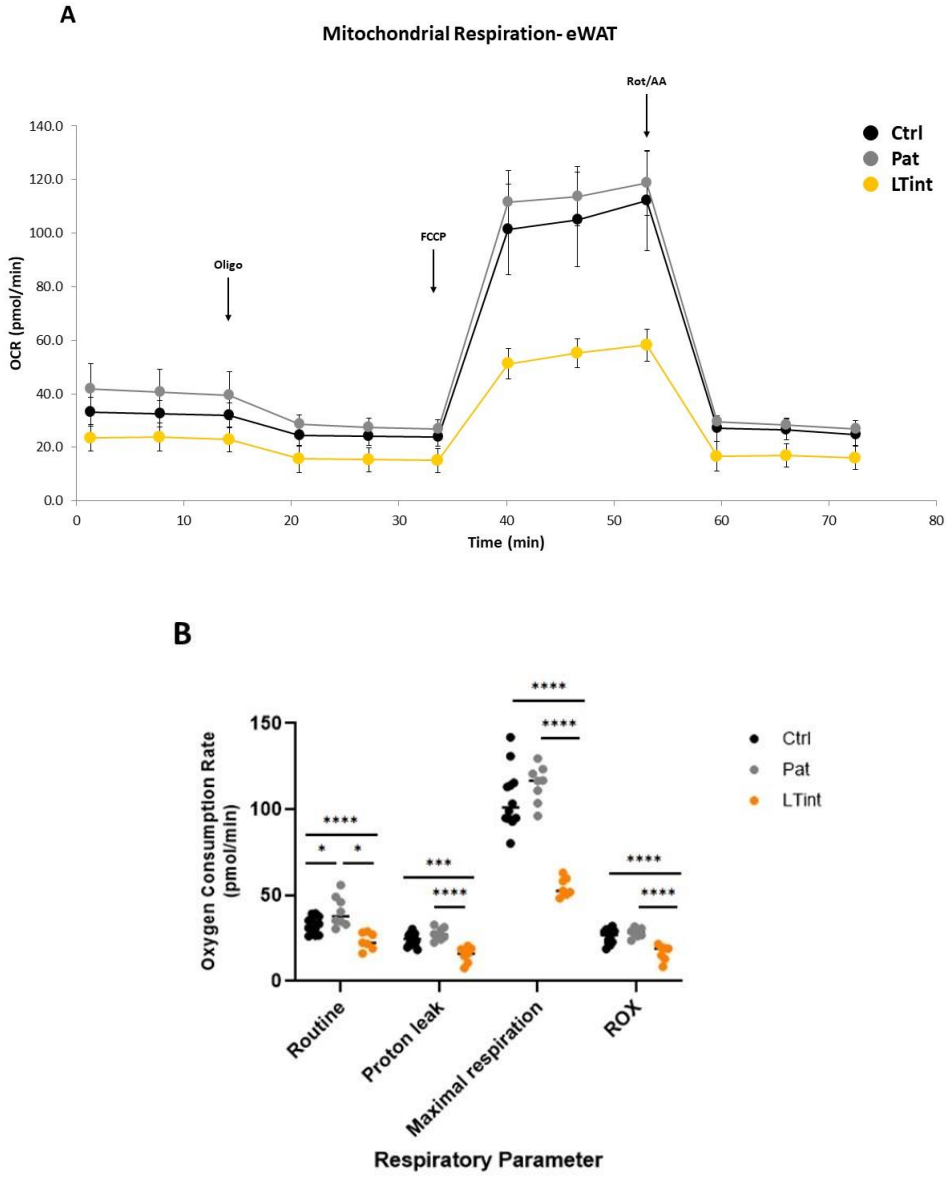

Figure 36: Mitochondrial function of ADSCs isolated from eWAT. A: Resulting representation of the OCR values during the protocol of Mito Stress Test. B: Average of the 3 measurements per sample in each respiratory state plotted. Ctrl n=12; Pat n=8; LTint n=7.

When evaluating mitochondrial function of ADSCs from sWAT, the same expected pattern generated by the titration of oligomycin, FCCP, rotenone and antimycin A was observed (Figure 37A). Throughout the assay and along the 4 respiratory states, ADSCs from *Ctrl* mice had significantly elevated OCR values in comparison to ADSCs

from *Pat* group. At the routine respiratory state, OCR of the *Ctrl* group and the *Pat* group were 18 and 13 pmol/min, respectively. The maximal respiration for the *Ctrl* group was 45 pmol/min and for the *Pat* group, it was 36 pmol/min (Figure 37B).

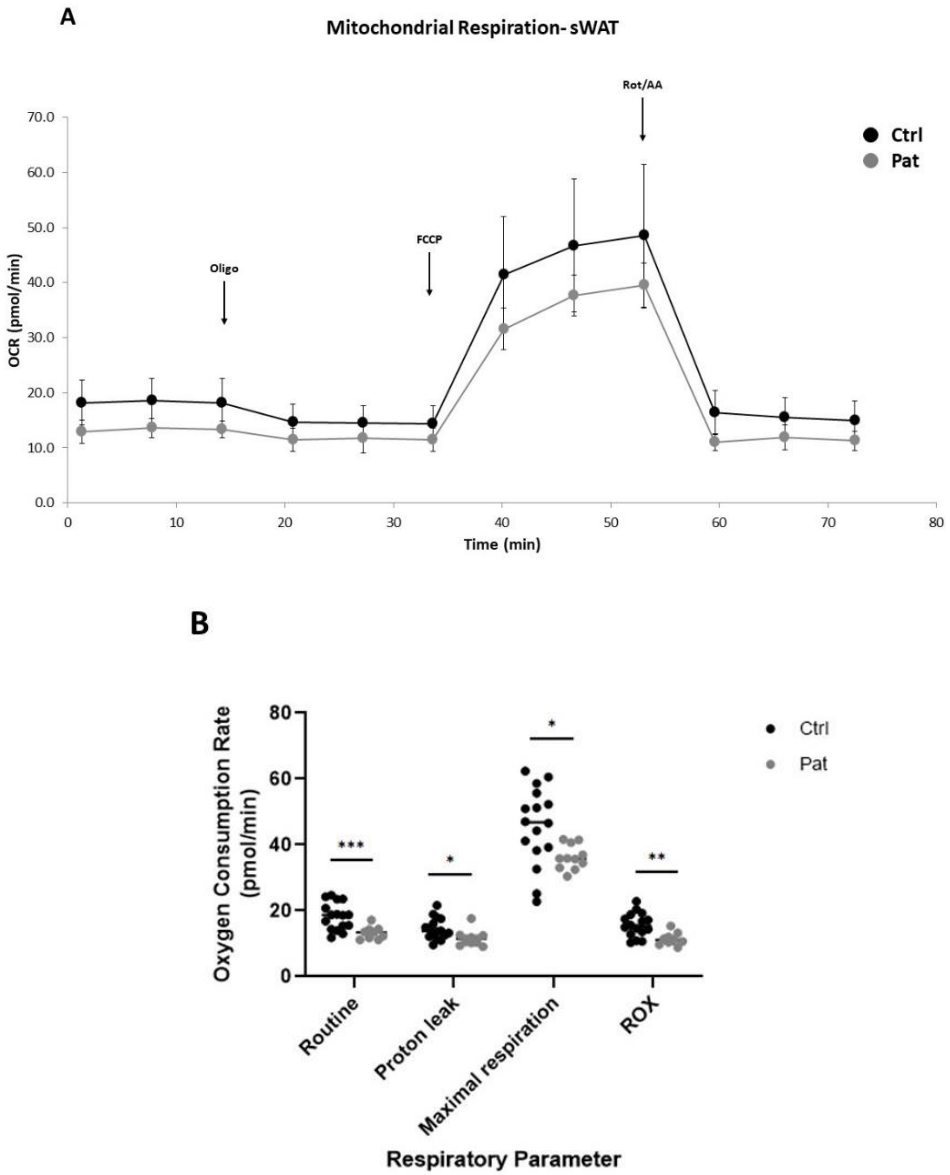

Figure 37: Mitochondrial function of ADSCs isolated from sWAT. A: Resulting representation of the OCR values during the protocol of Mito Stress Test. B: Average of the 3 measurements per sample in each respiratory state plotted. Ctrl n=16; Pat n=11.

Comparing the values from eWAT and sWAT, at every respiratory state and considering the experimental groups, OCR values for eWAT were superior to the values for sWAT. This was in correlation with results from the assessment of

mitochondrial function in whole WAT homogenate through high-resolution respirometry.

4.5 Macrophages phenotype characterization in white adipose tissue

Using transcriptomics data from RNAseq, the expression of both intracellular and surface markers and secretory factors (cytokines and chemokines) specific to different phenotypes of macrophages was evaluated (section 3.5.3). The transcriptomics studies were completed first for eWAT since it was the WAT depot demonstrating a major inflammatory profile and tissue remodeling. Thus, for eWAT, samples from the 4 experimental groups *Ctrl*, *Pat*, *Int* and *LTint* were assessed. While the samples from sWAT analyzed for transcriptomics studies were from the 3 groups *Ctrl*, *Pat*, and *LTint*.

For these studies, a literature search was performed for cell markers defining the different macrophage phenotypes, including the classical macrophage phenotypes (M1, M2), as well as different subtypes of these phenotypes (M2a, M2b, M2c, M2d) and other phenotypes that have been identified more recently: Mox and Mme. A total of 127 genes were selected (Table 3). Then, this gene list was searched in RNAseq database and expression changes were analyzed as a function of the different study conditions (*Ctrl*, *Pat*, *Int* and *LTint*) and a heatmap was built to show changes in gene expression in the different study conditions as compared to *Ctrl* group.

In the section below, each macrophage phenotype was reviewed separately. For every subsection, first, eWAT was evaluated, then sWAT and finally a comparative analysis between the two depots was illustrated. The order in which the genes were enumerated was from highest to lowest level of expression for each type of markers.

4.5.1 M1 macrophages

Based on the list in Table 3 (section 3.5.3), the expression of M1 specific genes was evaluated. In eWAT, 45 genes were identified and represented (Figure 38A). Most genes showed that HFD evoked a high increase of M1 markers which was partially reverted in *Int* group and for most of the selected genes, completely reverted in *LTint* group. Some of the genes demonstrating this pattern are *CD36*, *Fcgr3*, *Tlr2*, *Irf5*, *Ccl9* and *Cxcl19*. In the sWAT analysis, 29 specific genes for M1 macrophages were identified and represented (Figure 38B). It was difficult to recognize a certain pattern of alterations in the expression of M1 markers induced by HFD or the intervention in sWAT. For some genes, like *CD36* and *Cxcl10*, the highest level of expression was observed in the *Ctrl* group, while others like *Ccl3* and *Il1r2* were more highly expressed in *Pat* and *LTint* groups, respectively. In addition, the order by which the genes were enumerated in sWAT was different than that in eWAT, highlighting the occurrence of differences in the M1 macrophage population between depots.

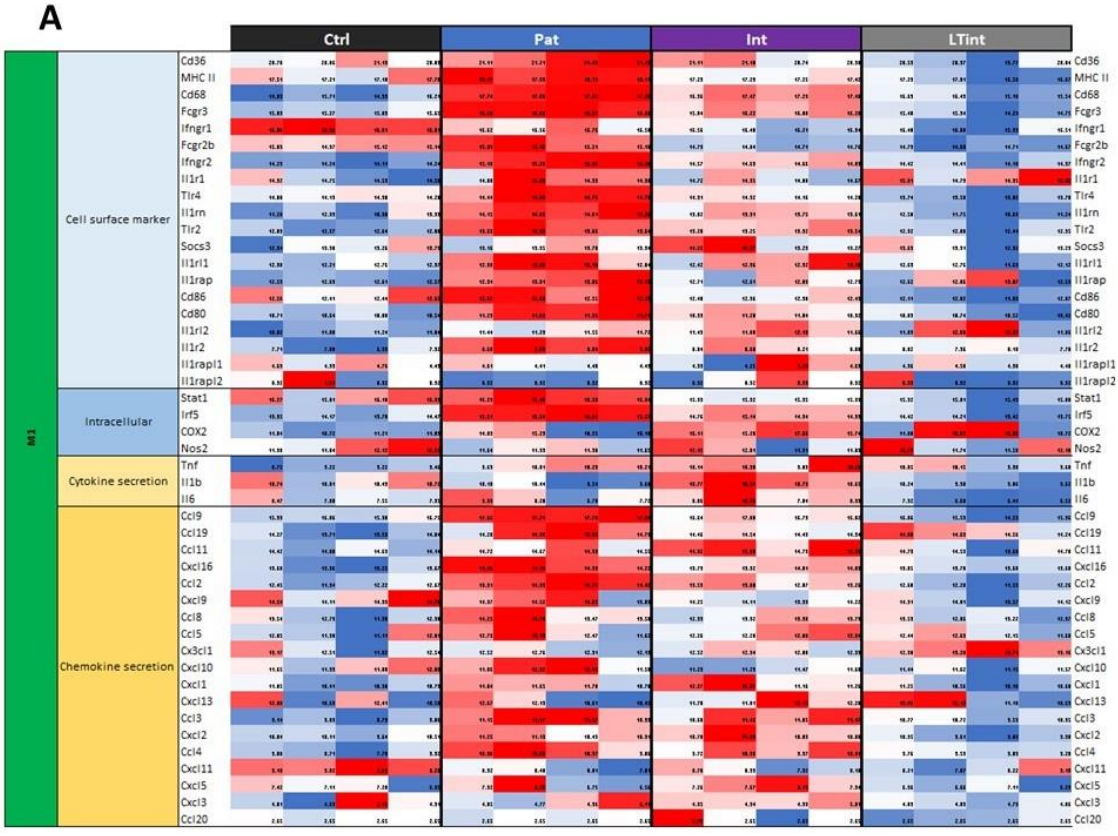

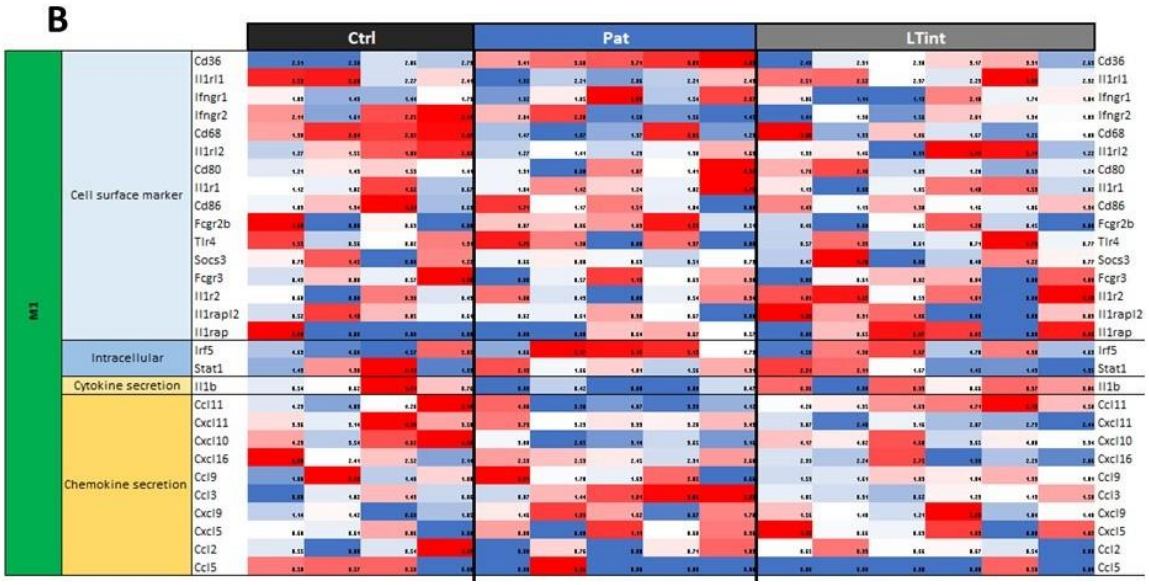

Figure 38: Expression levels of M1 marker genes. A: M1 markers and their expression in eWAT. Ctrl n=4; Pat n=4; Int n=4; LTint n=4. B: M1 markers and their expression in sWAT. Ctrl n=4; Pat n=5; LTint n=6.

To better emphasize on the dissimilarity in M1 markers within depots, the common genes expressed by both depots and by the same groups were plotted together. In a general view, in contrast to eWAT, the effect of HFD on increasing M1 marker expression did not stand out in sWAT. For example, CD68 expression increased in the *Pat* group and was decreased with *LTint* to values similar to the *Ctrl* group in eWAT, while in sWAT, the same cell surface marker had its highest expression in the group *Ctrl* then *LTint* and lowest in *Pat*.

As shown in Figure 39, it appears that eWAT is highly infiltrated by M1 macrophages in response to a HFD, an effect that is not observed in sWAT. An effect of *LTint* was observed in eWAT, with a clear decrease in the gene expression levels of M1 marker genes.

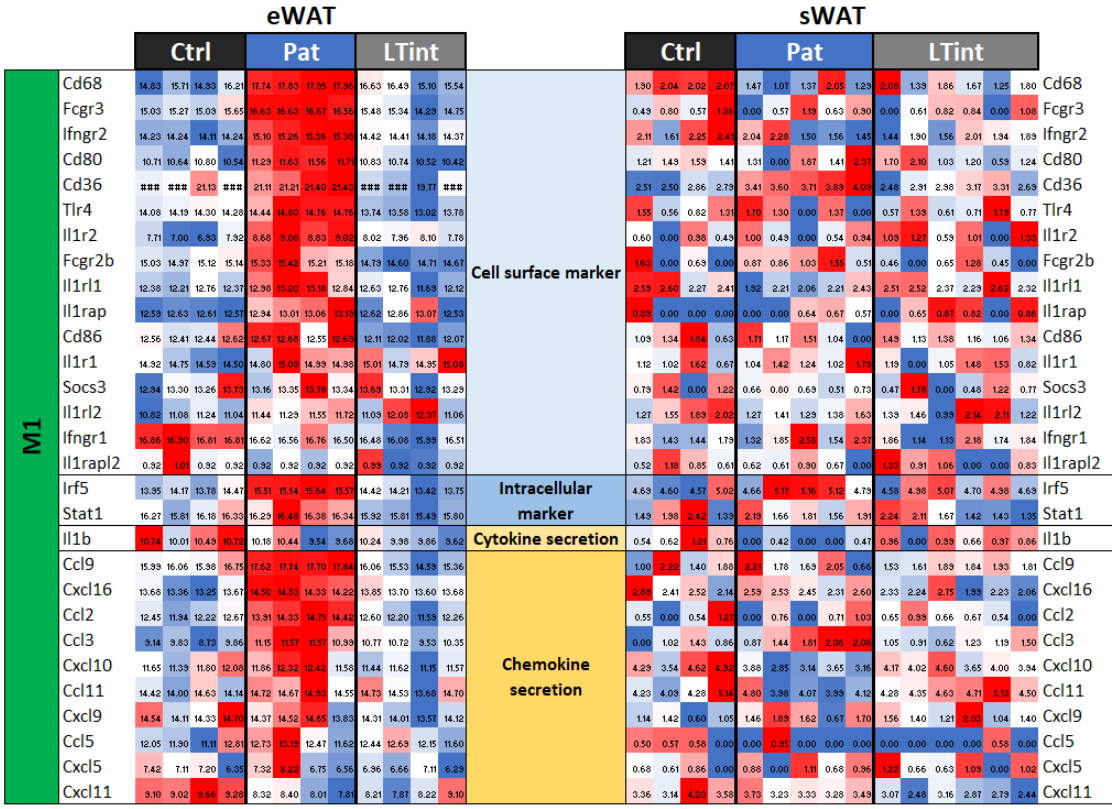

Figure 39: Comparative study of the expression of M1 marker genes in eWAT and sWAT. Common M1 markers between both depots and their expression in the 3 experimental groups Ctrl, Pat and LTint. For eWAT. Ctrl n=4; Pat n=4; LTint n=4. For sWAT. Ctrl n=4; Pat n=5; LTint n=6.

4.5.2 M2a macrophages

M2a macrophages, one of the many subtypes of M2 macrophages, have distinct markers and secretory factors that contribute to their function as wound-healing macrophages. In our data set, in eWAT, 25 genes representing M2a macrophages were identified (Figure 40A). Key cell surface marker *Mrc1* – also known as CD206 – was amongst the highest expressed genes. *Mrc1* expression was increased in the *Pat* group and declined after the interventions to reach its lowest expression with *LTint* group.

Other specific gene to M2a macrophages, CCL17, had its peak expression in *Int* mice and smallest in *Pat* mice. Even though, a single or dominant pattern of expression could not apply to all genes in eWAT, so that almost half of M2a genes had their highest level of expression in the *Pat* group and most had their lowest in *LTint* group.

In sWAT, the 17 genes identified showed no clear modifications evoked by the HFD or the interventions that affected the expression of all genes in the same manner (Figure 40B). For example, *Mrc1* and *CD209e* were among the few markers that demonstrated an increased level of expression in response to HFD that declines after *LTint*.

In Figure 41, the M2a genes expressed by both depots were plotted side by side to compare the alterations evoked by HFD and the interventions. For instance, intracellular marker of M2a macrophages, *Stat6*, had its peak level of expression in eWAT from *Pat* mice while it peaked in *LTint* mice in the case of sWAT.

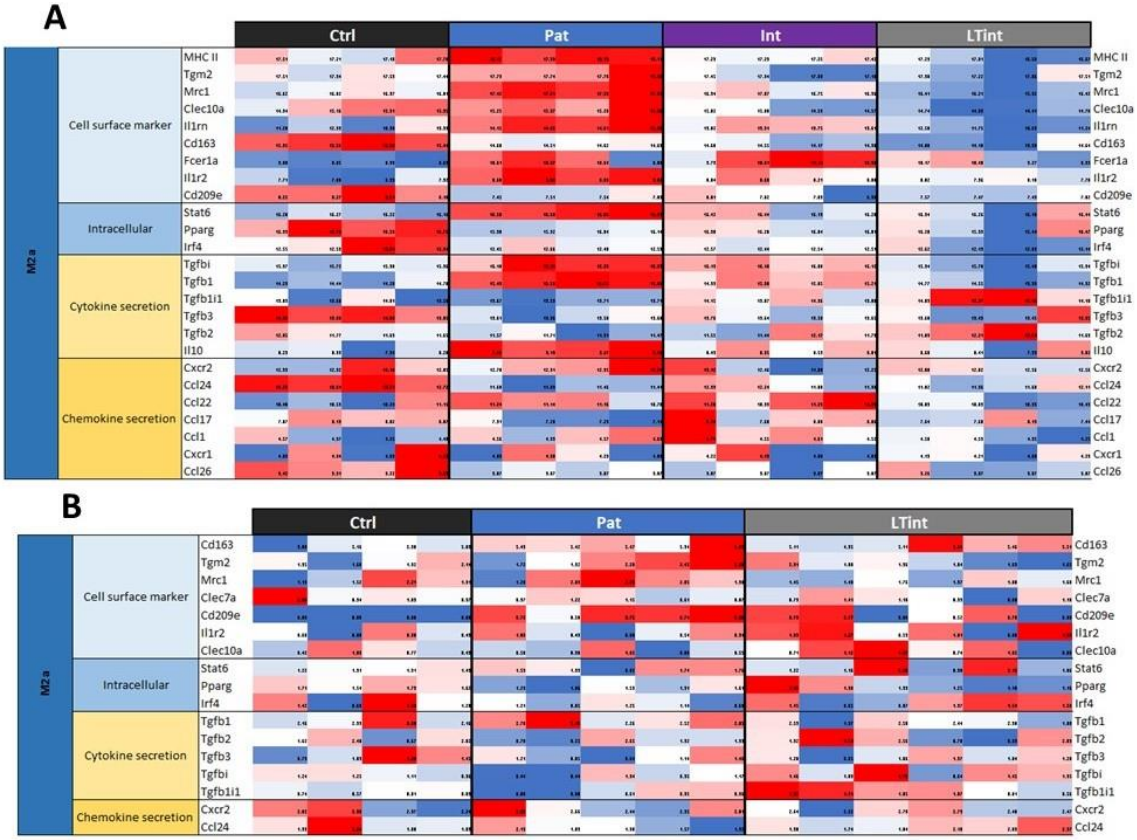

Figure 40: Expression levels of M2a marker genes. A: M2a markers and their expression in eWAT. Ctrl n=4; Pat n=4; Int n=4; LTint n=4. B: M2a markers and their expression in sWAT. Ctrl n=4; Pat n=5; LTint n=6.

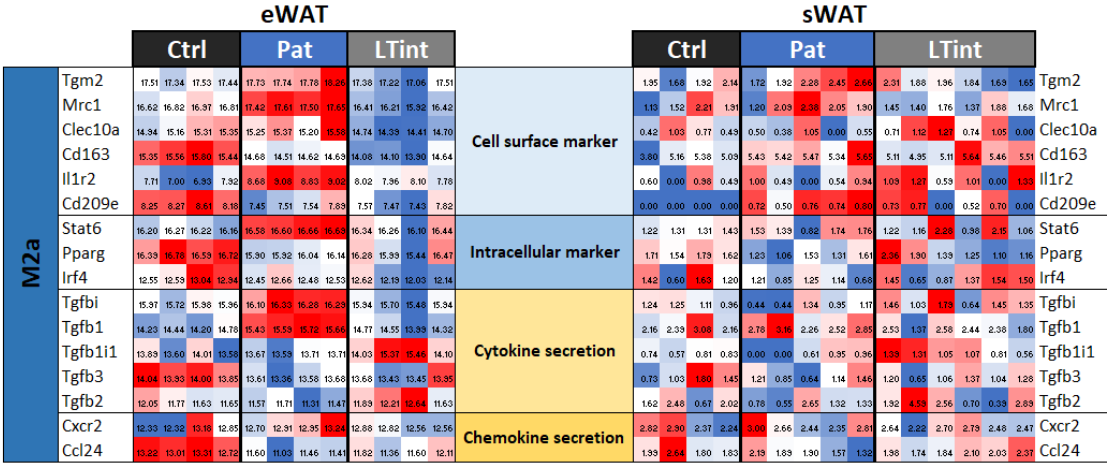

Figure 41: Comparative study of M2a marker genes between eWAT and sWAT. Common M2a markers between both depots and their expression in the 3 experimental groups Ctrl, Pat and LTint. For eWAT. Ctrl n=4; Pat n=4; LTint n=4. For sWAT. Ctrl n=4; Pat n=5; LTint n=6.

4.5.3 M2b macrophages

Subtype M2b macrophages are recognized as regulatory cells. In eWAT, 18 genes were identified as specific for M2b macrophages (Figure 42A). Amongst those genes, the level of expression was shown to be relevant to the type of the marker gene. The expression of cell surface markers such as key marker CD86, was highest in the *Pat* group while intracellular markers and secretory factors (cytokines and chemokines) increased after HFD but were at their peak level of expression with the *Int* group. In sWAT, 8 genes representing subtype M2b were detected (Figure 42B). For most genes, like the intracellular markers, *Sphk1* and *Sphk2*, the level of expression was highest either in *Ctrl* or *LTint* groups.

Comparing the changes in expression levels of M2b genes in the groups *Ctrl*, *Pat* and *LTint* between eWAT and sWAT, different trends were revealed (Figure 43). A particular example, in eWAT, *Sphk2* expression was increased after HFD but reversed in the *LTint* group while in sWAT, it was moderate in *Ctrl* group, declined after HFD and peaked with the *LTint* group.

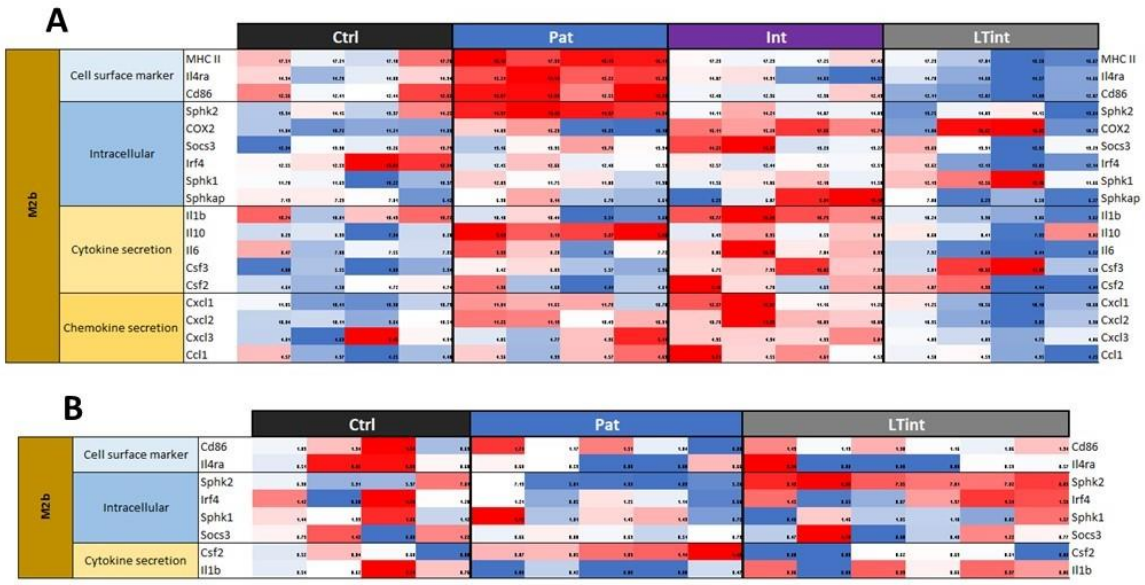

Figure 42: Expression levels of M2b marker genes. A: M2b markers and their expression in eWAT. Ctrl n=4; Pat n=4; Int n=4; LTint n=4. B: M2b markers and their expression in sWAT. Ctrl n=4; Pat n=5; LTint n=6.

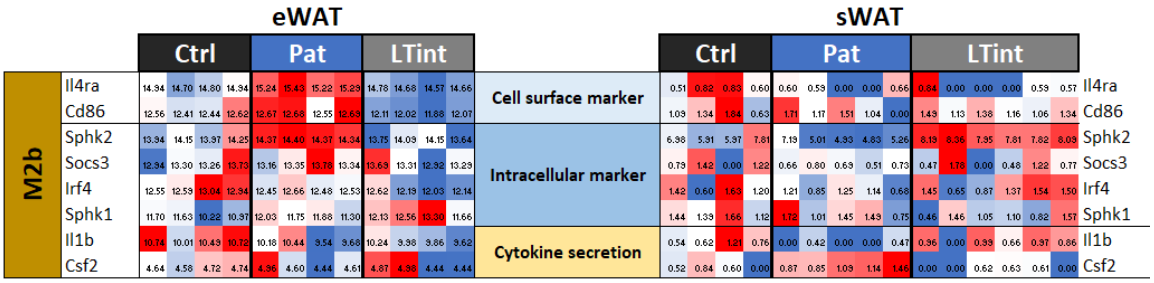

Figure 43: Comparative study of M2b marker genes between eWAT and sWAT. Common M2b markers between both depots and their expression in the 3 experimental groups Ctrl, Pat and LTint. For eWAT. Ctrl n=4; Pat n=4; LTint n=4. For sWAT. Ctrl n=4; Pat n=5; LTint n=6.

4.5.4 M2c macrophages

M2c macrophages display strong anti-inflammatory and pro-fibrotic activities. In eWAT, 13 genes were identified for M2c macrophages (Figure 44A). *Scarb1* was the most expressed factor, reaching its maximum in the *Pat* group. HFD seemed to evoke an increase in most of M2c genes that declined starting the first phase of intervention. Such a trend was not observed for the 10 genes representing

M2c expression in sWAT (Figure 44B). Thus, cell surface markers *Tlr1* and *Slamf1* had their highest expression in the *LTint* group.

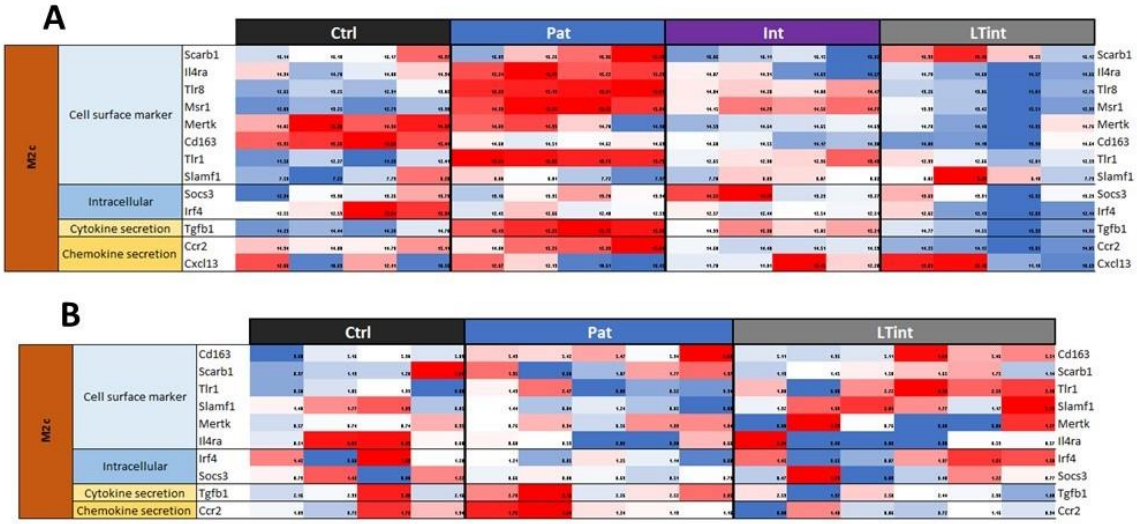

Figure 44: Expression levels of M2c marker genes. A: M2c markers and their expression in eWAT. Ctrl n=4; Pat n=4; Int n=4; LTint n=4. B: M2c markers and their expression in sWAT. Ctrl n=4; Pat n=5; LTint n=6.

The difference in trends observed between eWAT and sWAT was highlighted when the expression of the common genes from the same experimental groups *Ctrl*, *Pat* and *LTint* was represented side by side (Figure 45).

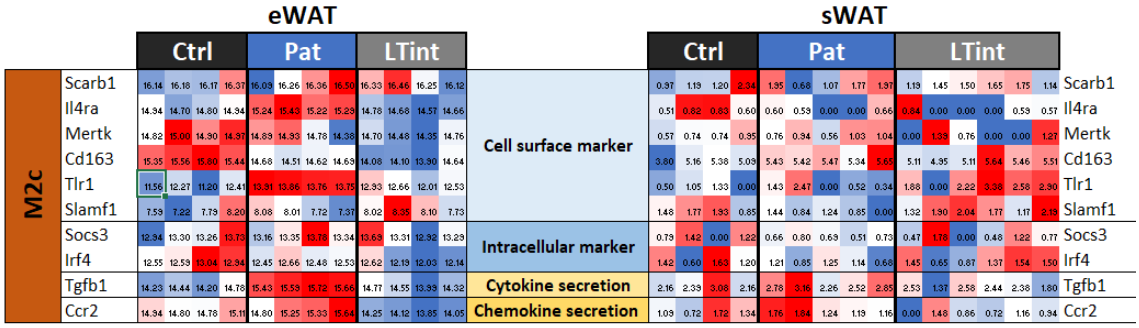

Figure 45: Comparative study of M2c marker genes between eWAT and sWAT. Common M2c markers between both depots and their expression in the 3 experimental groups Ctrl, Pat and LTint. For eWAT. Ctrl n=4; Pat n=4; LTint n=4. For sWAT. Ctrl n=4; Pat n=5; LTint n=6.

4.5.5 M2d macrophages

The last recognized subtype of M2 macrophages is the M2d macrophages which is also known as the tumor-associated macrophage type. The vascular endothelial growth factor (VEGF) is a cytokine secreted specifically by M2d cells in line with its function favoring tumor growth. A total of 13 genes were detected in eWAT as M2d genes (Figure 46A). *VEGFa* and *VEGFb* were at their highest level of expression in the *Ctrl* group and lowest in the *Pat* group and somewhere in between in the *Int* and *LTint* groups. In the sWAT depot, 11 M2d genes were identified and represented (Figure 46B).

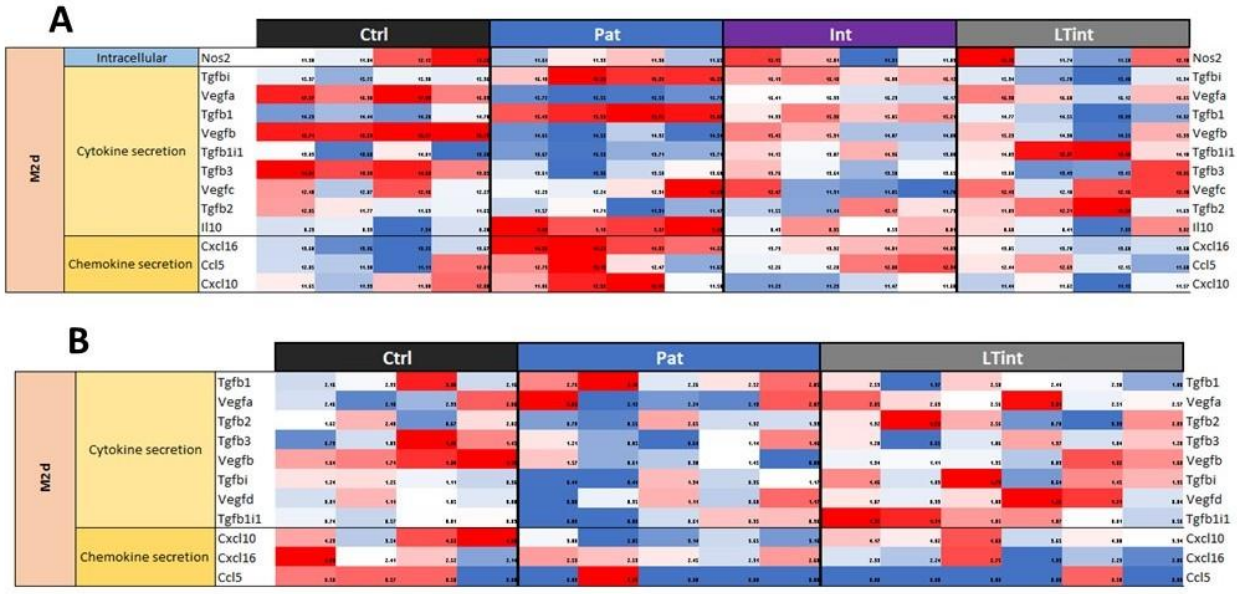

Figure 46: Expression levels of M2d marker genes. A: M2d markers and their expression in eWAT. Ctrl n=4; Pat n=4; Int n=4; LTint n=4. B: M2d markers and their expression in sWAT. Ctrl n=4; Pat n=5; LTint n=6.

When comparing the changes in gene expression induced by HFD or the interventions in both depots, it was shown that no unique trend could be shown to describe all genes in the same depot nor the same trend to describe the same gene in both depots (Figure 47).

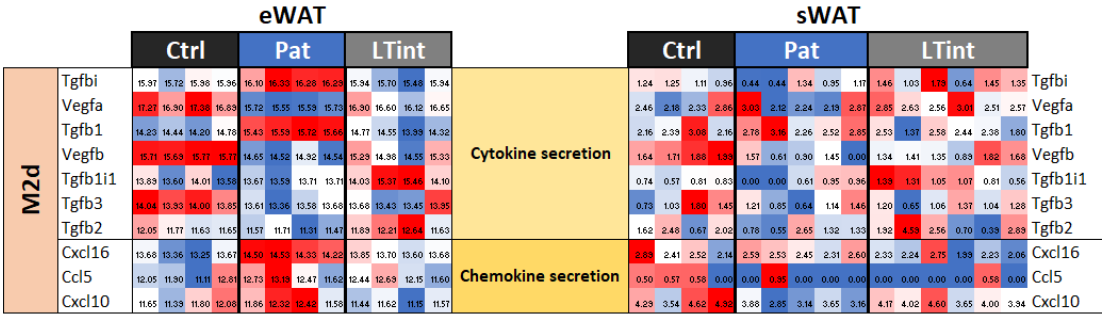

Figure 47: Comparative study of M2d marker genes between eWAT and sWAT. Common M2d markers between both depots and their expression in the 3 experimental groups Ctrl, Pat and LTint. For eWAT. Ctrl n=4; Pat n=4; LTint n=4. For sWAT. Ctrl n=4; Pat n=5; LTint n=6.

4.5.6 Mox and Mme macrophages

Besides M1 and M2 macrophages, in the recent years, new macrophage phenotypes have been accepted, including anti-oxidant macrophages (Mox) and metabolically activated macrophages (Mme). So far, 6 unique cell surface markers for Mox and 2 for Mme have been recognized, which were represented in both depots, eWAT and sWAT (Figure 48). In eWAT, the pattern observed for 6 out of the 8 genes was an increase in gene expression induced by HFD which partially recovered in *Int* group to reach similar values to *Ctrl* in *LTint* group (Figure 48A). In sWAT, a tendency towards an increased level of expression in the *Pat* group was noticed (Figure 48B).

Figure 48: Expression levels of Mox and Mme marker genes. A: Mox and Mme markers and their expression in eWAT. Ctrl n=4; Pat n=4; Int n=4; LTint n=4. B: Mox and Mme markers and their expression in sWAT. Ctrl n=4; Pat n=5; LTint n=6.

When the expression of markers genes for Mox and Mme was compared between eWAT and sWAT, we observed a similar pattern (increased levels in *Pat* group) in both depots, yet the changes were more consistent in eWAT than in sWAT (Figure 49).

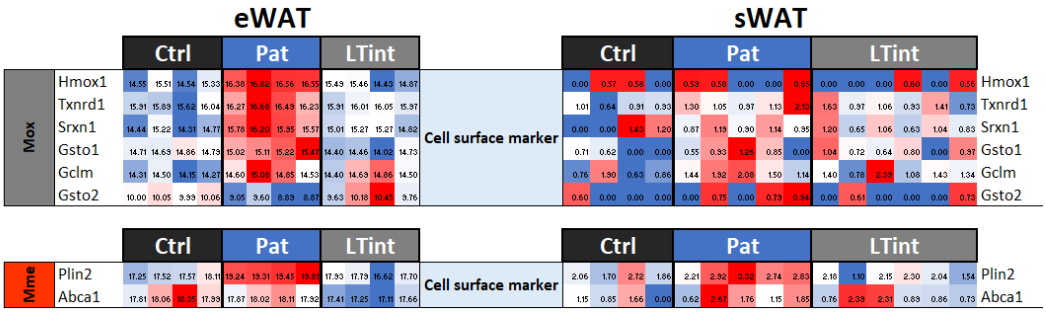

Figure 49: Comparative study of Mox and Mme marker genes between eWAT and sWAT. Common Mox and Mme markers between both depots and their expression in the 3 experimental groups Ctrl, Pat and LTint. For eWAT. Ctrl n=4; Pat n=4; LTint n=4. For sWAT. Ctrl n=4; Pat n=5; LTint n=6.

4.6 Extra cellular matrix characterization in white adipose tissue

The ECM components are divided into 3 major categories: the collagens, the proteoglycans and the glycoproteins. An ensemble of more than 1000 genes encode the ECM and ECM- associated proteins creating the matrisome. In the next section, genes encoding collagens and proteoglycans of the core matrisome in the WAT RNAseq dataset are explored. Hence, similarly to the data shown in the previous section, samples from the 4 experimental groups *Ctrl*, *Pat*, *Int* and *LTint* were assessed for eWAT while for sWAT it was samples from groups *Ctrl*, *Pat*, and *LTint*.

4.6.1 Collagens

There are various types of collagens and they can be formed of identical or distinct peptide chains. For example, type III collagen is a homotrimer meaning composed of 3 identical peptide chains while type VI collagen is composed of 3 distinct α-peptide chains. Hence, the nomenclature of the genes encoding the peptide chains: COL3A1 gene encodes for the alpha-1 peptide chain of type III collagen, COL6A1, COL6A2 and COL6A3 encode for the alpha-1, alpha-2 and the alpha-3 peptide chains of type VI collagen, respectively.

Based on the matrisome database (matrisomeproject http://matrisomeproject.mit.edu), we detected a total number of 42 collagen genes in eWAT (Figure 50A). The expression of around half of those genes increased to its maximum after HFD and declined after *Int* and *LTint*. Collagen III and collagen VI were amongst the genes demonstrating this pattern. The other majority of collagen genes showed a slight increase in expression with *Int* and peaked in *LTint* group, including *COL27A1*, *COL9A3*, *COL26A1* and *COL11A1*. Twenty-nine specific genes for core matrisome collagens were identified in sWAT, of which more than half, like *COL3A1*, *COL6A1* and *COL6A2*, had their highest level of expression in the *Pat* group (Figure 50B). The expression of another set of genes such as *COL27A1*, *COL4A3* and *COL4A4,* was increased the most in the *LTint* group.

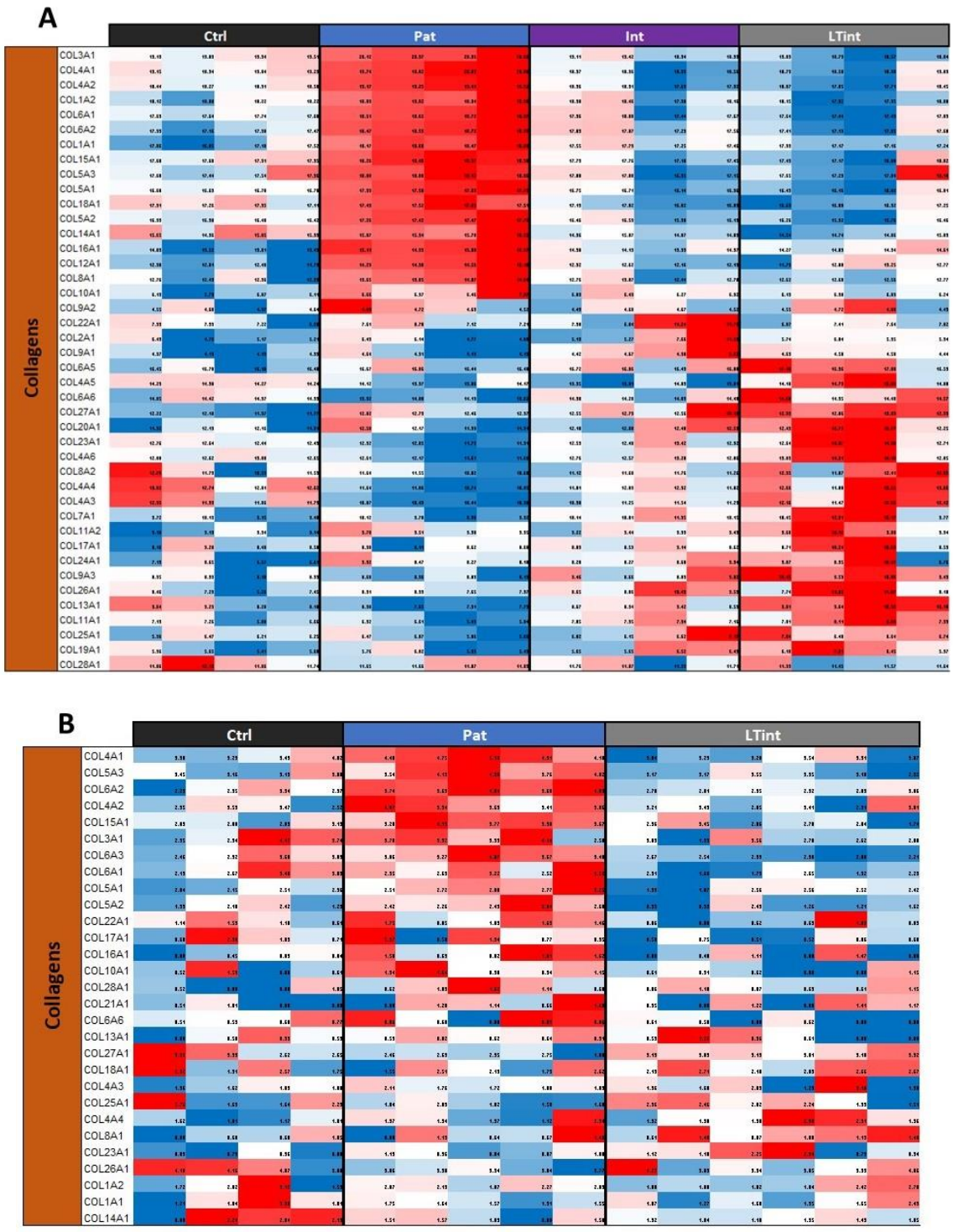

Figure 50: Expression of collagen ECM components. A: Genes encoding for collagens in the ECM and their expression in eWAT. Ctrl n=4; Pat n=4; Int n=4; LTint n=4. B: Genes encoding for collagens in the ECM and their expression in sWAT. Ctrl n=4; Pat n=5; LTint n=6.

In order to better illustrate a comparison between eWAT and sWAT, we examined the genes identified in both depots in the three groups available (*Ctrl*, *Pat*, and *LTint*) (Figure 51). Some genes revealed the same trend in response to HFD and *LTint*. For

instance, genes like *COL3A1*, *COL4A1* and *COL6A1* increased in expression levels upon HFD and then recovered with *LTint* in both depots. Genes such as *COL1A1* and *COL1A2* were at their highest expression level in the *Ctrl* group in sWAT.

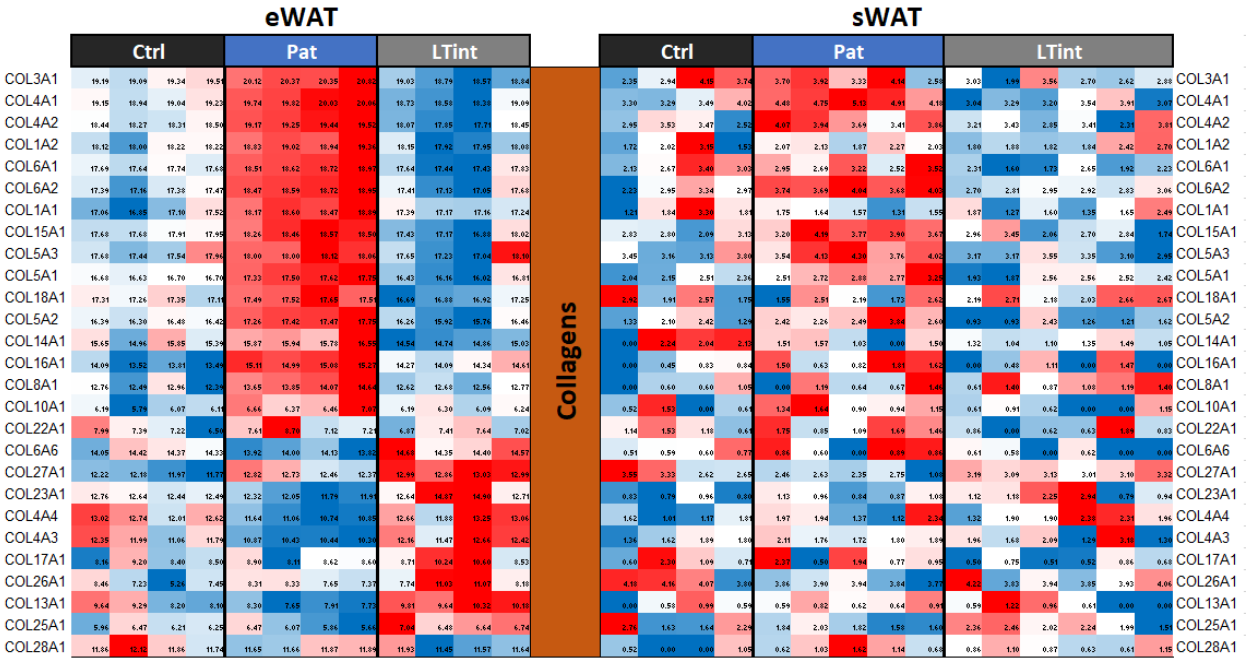

Figure 51: Comparative study of the expression of collagen ECM components between eWAT and sWAT. Genes encoding for collagens in the ECM common between both depots and their expression in the 3 experimental groups Ctrl, Pat and LTint. For eWAT. Ctrl n=4; Pat n=4; LTint n=4. For sWAT. Ctrl n=4; Pat n=5; LTint n=6.

4.6.2 Proteoglycans

Proteoglycans are another crucial component of the ECM contributing to the density and structure of the space in between cells, besides serving as a reservoir of growth factors. Thirty-five different genes encoding for proteoglycans were identified in eWAT (Figure 52A). HFD seemed to evoke an increase in the expression levels of 14 genes, including *HSPG2*, *LUM* and *VCAN*. Some other genes had their peak level of expression in the *Int* group, like *PRG2* and *HAPLN2*, while for many others this increase occurred in the *LTint* group (*SPOCK2*, *IMPG2*). In sWAT, a total number of 23 genes encoding proteoglycans were detected (Figure 52B). HFD seemed to cause an increase in the expression levels of genes such as *SPOCK1* and *LUM* while it decreased the expression of genes coding for the proteoglycans CHAD and DCN.

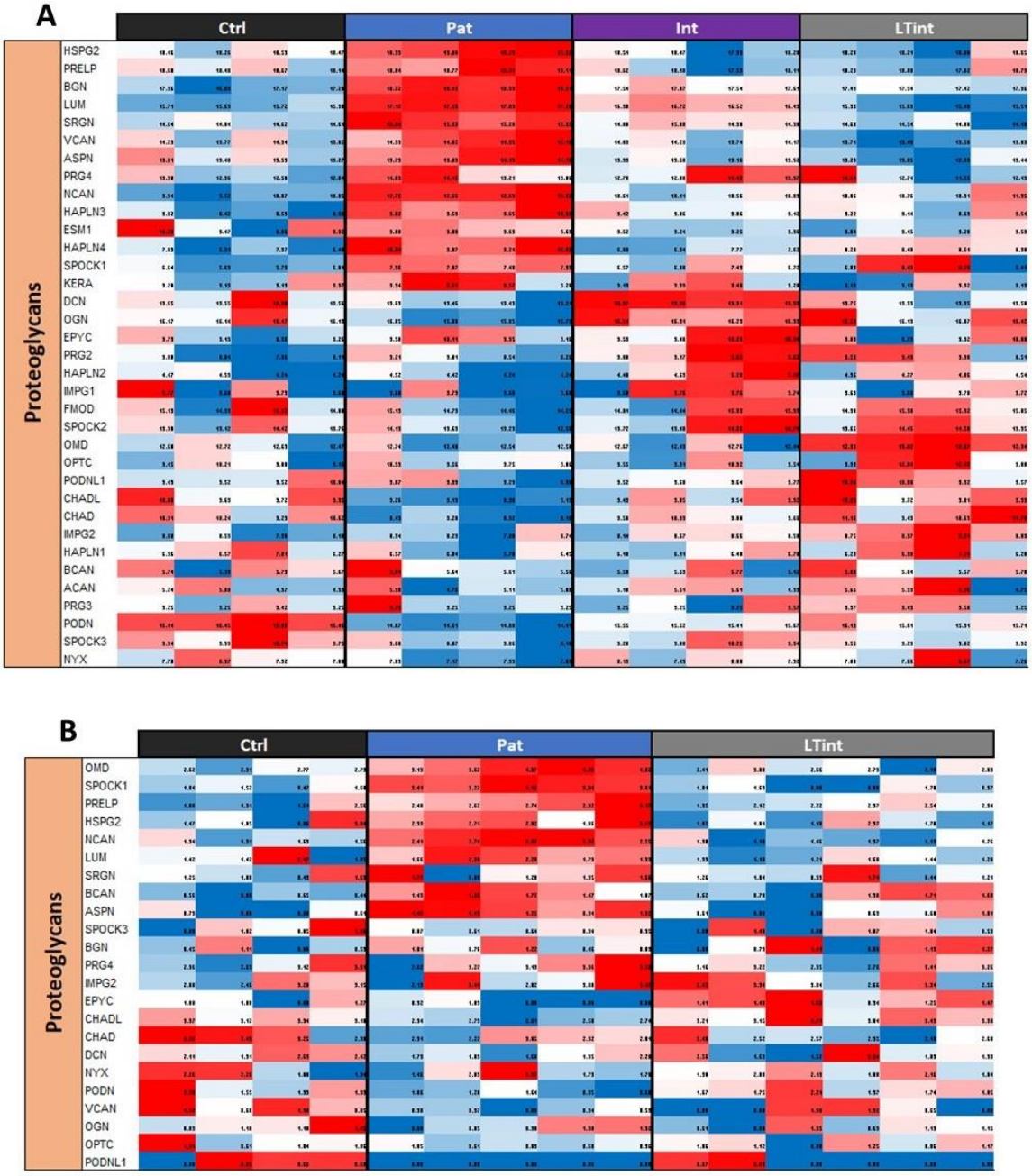

Figure 52: Expression levels of ECM proteoglycans. A: Genes encoding for proteoglycans in the ECM and their expression in eWAT. Ctrl n=4; Pat n=4; Int n=4; LTint n=4. B: Genes encoding for proteoglycans in the ECM and their expression in sWAT. Ctrl n=4; Pat n=5; LTint n=6.

In the same rationale used for collagens, a comparative analysis of proteoglycans in eWAT *vs.* sWAT was performed. As illustrated in Figure 53, many of the genes had the same trend in both depots, i.e., an amplification in the level of expression induced by HFD which was reverted in the *LTint* group. Examples of such genes are *PRELP*,

LUM and *ASPN*. Other genes like *OPTC*, *PODLN1* and *CHAD,* had their peak expression in the *LTint* group in eWAT while in sWAT, it was in the *Ctrl* group.

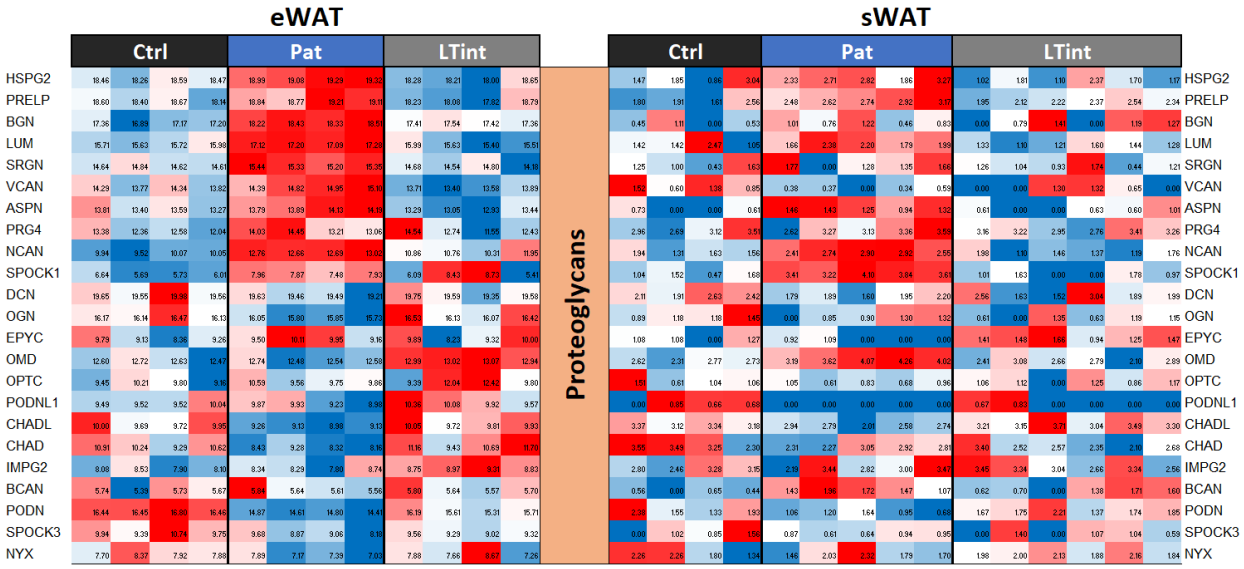

Figure 53: Comparative study of the expression of ECM proteoglycans between eWAT and sWAT. Genes encoding for proteoglycans in the ECM common between both depots and their expression in the 3 experimental groups Ctrl, Pat and LTint. For eWAT. Ctrl n=4; Pat n=4; LTint n=4. For sWAT. Ctrl n=4; Pat n=5; LTint n=6.

4.6.3 Collagens and proteoglycans in lean animals displaying an obese phenotype

Due to the extensive tissue remodeling observed in eWAT, another experimental group was added to the transcriptomics studies. The "*Lean obese*" mice were a group that was on a HFD for 16 weeks like the *Pat* group but demonstrated lower body weight gain and a healthy insulin responsive phenotype. In the purpose of a better description of the ECM modifications induced by HFD, we compared collagens and proteoglycans expression levels in this group with respect to *Ctrl* and *Pat* groups (Figure 54). Most of the genes encoding collagens like *COL3A1* and *COL6A1*, whose expression increased in the *Pat* group, also displayed increased levels in the *Lean obese* group (Figure 54A).

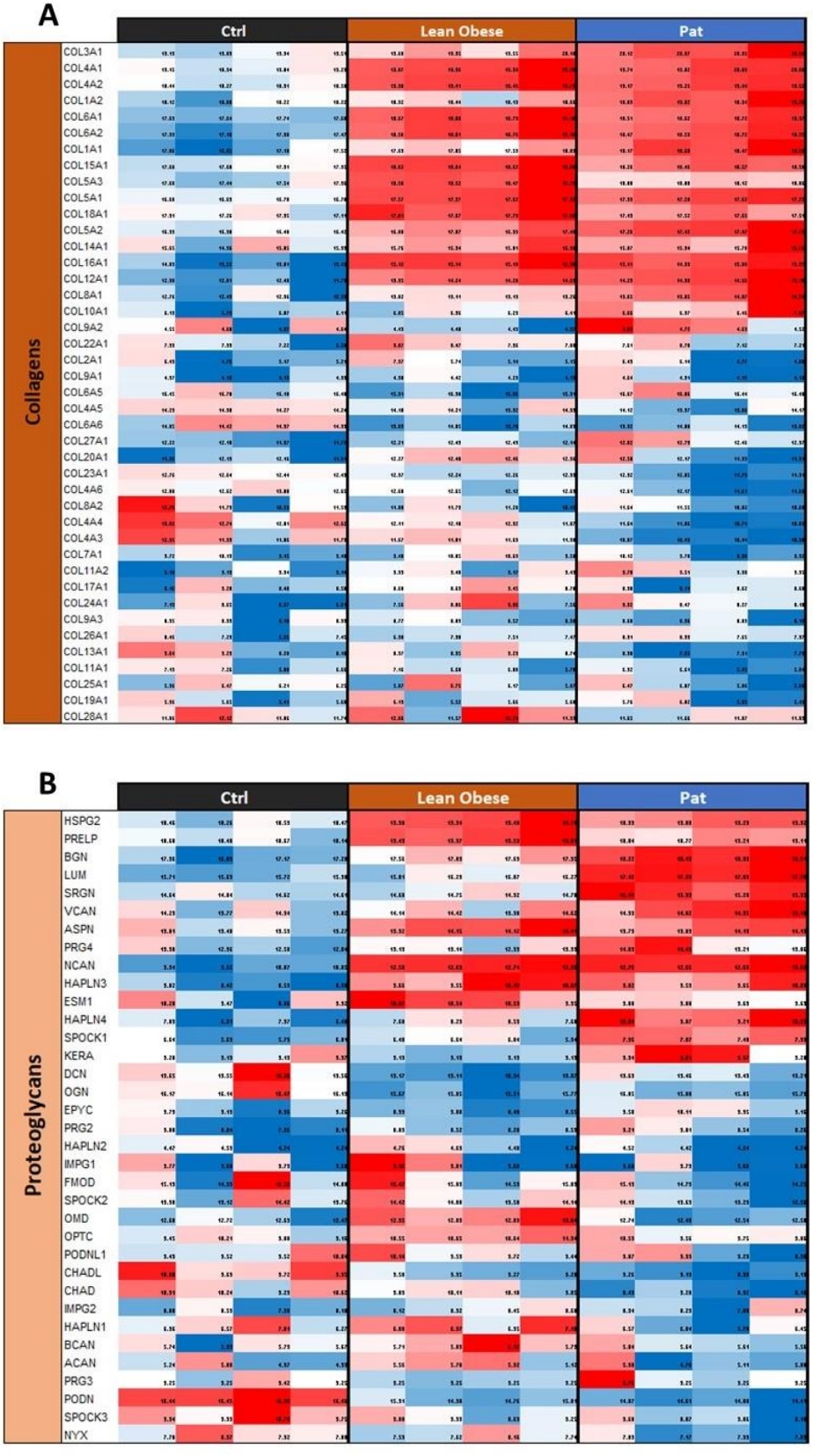

Figure 54: Comparative analysis of the expression of ECM genes in the Lean obese group vs. Crtl and Pat groups in eWAT. A: Genes encoding for collagens in the ECM and their expression in eWAT. Ctrl n=4; Lean obese n=4; Pat n=4. B: Genes encoding for proteoglycans in the ECM and their expression in eWAT. Ctrl n=4; Lean obese n=4; Pat n=4.

DISCUSSION

5.1 Animals phenotype

Diet-induced obesity (DIO) has been a topic of investigation for decades and over the years various models and protocols were chosen to achieve it. In our LiMa project, to create the intended effect of pathological obesity, C57BL6/J male mice were fed a HFD *ad libitum* for 16 consecutive weeks. Overweight, an increase in tissue weights like liver, eWAT and sWAT, hyperglycemia and glucose intolerance were among the reported features of DIO models which align with the literature (193–195). The lifestyle intervention performed in our experimental model seemed to successfully modify many of the phenotypic parameters from the first phase of intervention like BW and weights of tissues. After both phases of intervention, in *Int* and *LTint* groups, despite the recorded improvements in glucose tolerance and insulin sensitivity, an impairment in fasting glucose levels persisted.

Considering the various factors contributing to glucose homeostasis in particular and metabolism in general, the feeding patterns and strategies used in the experimental groups should be addressed. Due to our doubt that the sustained increase in fasting glucose levels in the *Int* and *LTint* groups might be a consequence of chronic exposition to long fasting periods on the liver, our discussion here will be restricted to two characteristics of our interventions which are calorie restriction (CR) and time-restricted feeding (TRF).

While the *Ctrl* and *Pat* groups were fed *ad libitum*, the weight loss strategy created for the *Int* and *LTint* groups generated different feeding patterns. In the purpose of controlling caloric intake in the *Int* and *LTint* groups, right after the treadmill workout, the food pellets were provided daily around 16:00-17:00. Observing the behavior of these groups of mice, we noticed that the pellets were consumed only few hours after the workout which meant that these mice were under large daily fasting periods that persisted throughout the intervention phases. A similar behavior was documented by Acosta-Rodríguez *et al*., that showed that mice under CR seemed to self-impose a temporal restriction of food intake (196). Even though, the access for food was for the whole 24h of the day, mice under CR finished the defined amount of food around 2h after the food was supplied. In the same study, the eating habits of mice being fed *ad libitum* were assessed. As anticipated for

nocturnal animals, the largest amount of food consumed was during the night with some eating urges scattered throughout the daytime. In an attempt to challenge the interplay between circadian rhythm, feeding behavior and metabolism, several research groups have pushed towards a high-fat consumption during light phase. A more pronounced diet-induced weight gain was reported as well as worsening glucose tolerance in comparison to the mice fed during the dark phase (197,198).

Modifications to the feeding strategy are expected to challenge metabolic homeostasis systemically. Besides CR or changing the timing of food intake, limiting the time-window of food availability while maintaining an isocaloric consumption has become a well-investigated strategy. It is defined as time-restricted feeding (TRF) and its metabolic benefits especially in the sense of prevention of DIO has been documented by many. Chaix *et al.* provided a HFD in a 9h window to young (3 months old) and older (12 months old) male mice and reported a significant prevention in BW gain compared to same age grouped mice eating *ad libitum* without time-restriction (199). In addition, TRF was associated to reduced fat mass, reduced hyperglycemia following a glucose tolerance test, and a quicker return to normal blood glucose levels. In tissue directed assays, it was revealed that liver of TRF mice showed a reduction in lipid droplets and TAG levels and alterations in the expression of key regulatory enzymes suggesting increased hepatic glucose utilization and inhibition of gluconeogenesis upon feeding (199). On the topic of TRF, Regmi *et al.* also assessed the importance of the initiation timing of TRF with early (initiated at lights off) and delayed initiation of TRF (4h after lights off). Reduced weight and fat mass was greater in both TRF groups in comparison to *ad libitum* but it was more pronounced in the early TRF group. TRF was found to improve glucose tolerance and prevent from diet-induced hepatosteatosis (200). Although TRF was eventually part of our feeding pattern in the *Int* and the *LTint* groups, on the hand, these mice were provided the food during the light phase. Based on the success of our intervention strategy in improving most of the diet-induced parametric alterations, we can conclude that the timing of the feeding could not overshadow the metabolic benefits of TRF in obesity.

An essential component in the strategy for weight loss in our study was the imposed CR after 16 weeks of HFD. In addition to the modifications implemented to the

composition of the consumed diets for the *Int* and *LTint* mice (details in section 3.1), the first intervention phase started with a 15-20% reduction of the daily caloric intake consumed by the *Ctrl* group. The caloric restriction was alleviated gradually until daily caloric intake was equal to that of the *Ctrl* group which would explain the dramatic decrease in BW during the first intervention phase followed by the flattening of the weight loss trend in the *LTint* mice. The benefits of CR on health have been documented by many studies conducted on humans and other animals including widely used rodents. In a simplified manner, calorie restriction by stimulating intense modifications at all levels from the transcriptome to whole animal physiology and behavior, improved life expectancy as well as the quality of life (155). Of interest to our study, CR promoted a switch from carbohydrate to lipid metabolism in several tissues possibly associated to the improved insulin sensitivity and reduced oxidative stress paralleled with an increase in autophagy (155). In order to sustain the healthy outcomes of the initial phase of our designed intervention and avoid further major alterations in physiological parameters, the mice were maintained a food intake isocaloric to that of the *Ctrl* group – a strategy known as pair-feeding. Along with the reported outcomes of pair-feeding by García-Gaytán *et al.* (201) we concluded that pair-feeding and not necessarily continuous and prolonged CR is enough to maintain the metabolic improvements already achieved.

Tackling the possible cause of the sustained elevated levels of fasting glycemia illustrated in *Int* and *LTint* groups, a new experimental group was introduced. The new pair-fed *Ctrl* group was under similar TRF conditions and interestingly it exhibited the same fasting hyperglycemia. In addition, changes to hepatic glycogen levels, to the expression of glucose metabolism-related genes, and to the reaction to gluconeogenic substrates (pyruvate tolerance test) were reported (data not shown). Hence, the data from the new experimental group, even though preliminary, could indicate that chronic long fasting periods stimulate a specific liver phenotype not associated solely to our *Int* and *LTint* protocols.

5.2 Tissue-specific lipidomic profiling

Prior to investigating the plasticity of lipid profiles when subjected to HFD followed by a first phase of intervention, a comparison between the lipidome of different insulin-sensitive tissues in lean subjects was drawn. A unique and tissue-specific lipid profile was revealed which was in agreement with previous studies (190,202–205). The detected differences between tissues at the level of content of each lipid species were reflective of the structure and function of each tissue. WAT being the principal site of storage and TAG being the major form of energy storage in the organism, it was found to be enriched at least ~4- to 30-fold in WAT as compared to any other tissue (190,202,205). Our data on TAG showed a minimum of an 18-fold rise in content in eWAT compared to liver and gastrocnemius. The entirety of the glycerolipids family was not detected in our data in the hypothalamus which is in contradiction to other studies (206,207). This could be attributed to the sensitivity of the technique. However, sterol lipids were most enriched in the hypothalamus potentially due to the role of sterol lipids in cellular membranes structures and the high cellular density in the brain (208). An important observation about sterol lipids was the high abundance of esterified cholesterol (CE) in the liver, the organ mainly responsible for cholesterol homeostasis. Free cholesterol, via the enzyme Acyl-CoA cholesterol acyltransferase (ACAT2), is esterified into cholesterol esters which are encompassed into lipoproteins (209). Fatty acids are major components of most lipid classes like glycerolipids, sterol lipids and phospholipids. Hence, eWAT containing the highest levels of FAs was consistent with the exceptionally elevated TAG levels in eWAT. Liver and hypothalamus were in second place in comparison, highlighting the major role of liver in lipid metabolism and the elevated cellular density of the hypothalamus reflected in an abundance of structural lipids such as phospholipids and cholesterol esters. Thus, as expected, phospholipids had their highest content in hypothalamus. In mammalian cells, the most abundant PLs that make up 60-80% of total PLs, are phosphatidylcholine (PC) and phosphatidylethanolamine (PE) (190,202,204,210) which is in compliance with our data revealing higher PE content to PC.

After establishing that each tissue had a unique lipid profile influenced by its function and structure, the plasticity of the lipidome was tested by subjecting the mice to opposing and sequential lifestyle routines: high-fat feeding (*Pat* group) followed by a switch to a healthy regime with changes in nutritional intake and physical exercise (*Int* group). In disagreement with several studies, the hypothalamus showed no modifications in its lipid profile in response to HFD and the intervention. Adopting for 6-8 weeks similar dietary high-fat feeding conditions to that of our model, a 2-3-fold rise in most lipid classes was induced in one study (207) and in another, the content in TAG, DAG, PC and some ceramides was amplified (206). Investigating lipid accumulation in the hypothalamus induced by high-fat feeding, Borg *et al*. determine fatty acids-enriched diets and not obesity itself to be the stimulus (206). Lipid accumulation, more accurately, the accumulation of certain specific lipid species is a hallmark of various disorders. For instance, long-chain ceramides in the brain are found to be elevated in Alzheimer's disease, arteriosclerosis, HIV and aging (206). To overturn the effect of HFD on the lipidome of the hypothalamus, two strategies were tested by two different investigations. An exercise training paralleled with HFD did not reverse the lipid accumulation induced by HFD (206) whereas, for a similar time period, a switch back to a low-fat diet was successful (207). The above-mentioned studies are based on results from mass spectrometry (MS) while our study was done via proton-based NMR which could explain the illustrated diversity in results between studies. Even though, in general, NMR is more quantitative than MS, it is also less sensitive. To clarify, NMR generates quantitative data on a lipid species as a whole whereas MS, a more sensitive technique, uncovers the abundance of the different molecules of the same lipid family – it detects the carbon chain length and degree of unsaturation of the lipids.

Skeletal muscles are crucial for the regulation of carbohydrate and lipid metabolism. The accumulation of intramyocellular lipids (IMCL) in skeletal muscle was initially the indicator for the development of insulin resistance (IR). However, several investigations have unveiled particular lipid intermediates abundance rather than total IMCL as more accurate indicator for skeletal muscle IR (181–184,211–213). An acute surge in plasma FAs causing decreased glycogen synthesis, insulin-stimulated IRS-1 tyrosine phosphorylation and PI3K activity, revealed FAs

as inhibitors of insulin-stimulated glucose uptake in skeletal muscle (181,182,211). Skeletal muscle IR is mainly induced by the lipid intermediates DAG and ceramides (214,215). It has been suggested that these intermediates are produced from intramyocellular triacylglycerols (IMTG) pools leading to the positive correlation between IMTG abundance and IR in skeletal muscle even though IMTG are considered metabolically inert with no direct regulatory role in proximal insulin signalling (216). An exception to this correlation is in the case of the "Athlete's paradox" where endurance-trained athletes despite an elevated IMCL content similar to the one in insulin-resistant obese and diabetic subjects, have highly insulin-sensitive skeletal muscles (215). The IMTG levels in the gastrocnemius on our model were increased by 3-fold after HFD. In addition, the *Pat* group showed a rise in content of several FAs like total UFA, oleic and linoleic acids. An increase in FA abundance could be attributed to an increase in lipid synthesis to fatty acid oxidation ratio. Several investigations have revealed defects, induced by lipid accumulation, in the mitochondrial machinery crucial for FA oxidation (217–219). Among some reported adaptations were a reduction in mitochondrial content in skeletal muscle without proof of diminished function or intrinsic modifications to the persisting mitochondria pool (220) or an increase in mitochondrial content promoting a boost in fatty acid oxidation capacity (221–223). Since our results illustrated a surge in FA levels, the most plausible interpretation is that the FA excess driven by overnutrition and ectopic lipid accumulation, could not be neutralized by an amelioration in mitochondrial oxidative capacity. In our study, with changes towards a healthier diet and intensified physical activity, IMTG and FA levels were reduced to values equal to *Ctrl* levels. The effect of exercise on muscle fibers in terms of utilization of IMTG and mobilization of IMCL contained in lipid droplets between sarcomeres creating an energy pool, is well documented (183,224–226). The detected FA content in our data is also reflective of the FAs comprised in the structure of esterified lipids. Hence, even though the content of sterol lipids and phospholipids was not different between the 3 groups, the FA part of these lipids could have altered accounting for some of the detected changes in FA levels. In addition, n3.D-E-L content seemed to increase after HFD and furthermore with the *Int* group. This result is consistent with findings in other studies demonstrating major alterations to FA lipid profile of skeletal muscle particularly when elevated

content of n-3 long chain poly-unsaturated fatty acids (LCPUFAs) was administered in the diet (227,228). Furthermore, another study revealed increased levels of n3-LCPUFAs when dietary linoleic acid was substituted with α-linolenic acid, a similarity in modifications of administered diets, HFD and IntD (229). A positive correlation between increased levels of n3-LCPUFAs and improved insulin action in skeletal muscle has been established (228).

A key regulator of metabolic pathways is the liver. It is at the center of FA synthesis and lipoprotein assembly. FA utilization by the liver occurs via 3 main pathways: containment in lipoproteins like very-low-density lipoprotein (VLDL), esterification into TAGs stored in lipid droplets and and β-oxidation by liver mitochondria (230). For FA storage and circulation, TAGs are considered the most common reliable form of energy compound (231). Hence, with an elevated positive energy balance, hepatic FA levels and hepatic TAGs accumulation are increased (232). The excessive accumulation of lipid droplets in the liver is directly linked to the development of non-alcoholic fatty liver disease (NAFLD), a common feature of obesity (230,233). Liver also is the major site for intracellular esterification of free cholesterol (FC). Neutralizing the toxicity of free cholesterol molecules, ACAT2 enzyme residing in the liver yields esterified cholesterols (CE) (209,232). In agreement with previously mentioned literature, data from the *Pat* group of our study revealed a 6-fold increase in TAG levels, and a rise in content of FAs, CE and total cholesterol. The changes induced by HFD on the phospholipids (PLs) and sphingomyelin (SM) content were very different between lipid species and could not be attributed to either the increase in energy balance or the diet administered which means phospholipids and SM interact distinctively in the liver. One remarkable observation was the reduction in PE levels in the *Pat* group which was documented as well by Trentzsch *et al.* when administering a lard-based HFD similar to ours (234). PE synthesis in the liver is driven by mitofusin-2 which is downregulated in HFD-fed individuals (235). Several studies have focused on the dynamics of lipid droplets in the liver and reported various outcomes when attempting to reverse hepatic lipid accumulation through exercise. While exercise induced a reduction in hepatic lipid content without necessarily a body weight loss (224,230,236), it was also found to reduce liver weight and lipid droplets but not the levels of intrahepatic TAGs (233). The benefits of exercise on hepatic fatty acid oxidation have been well

documented. Through exercise, crucial rate-limiting enzymes in FA oxidation are further activated like carnitine palmitoyl-CoA transferase I/II (CPT-1 and CPT-2) and acyl-coenzyme A dehydrogenase (ACD). Whereas, the expression of lipogenic enzymes such as acetyl-CoA carboxylase (ACC), fatty acid synthase (FAS), elongases and stearoyl-CoA desaturase 1 (SCD1) is reduced (230). A combination of exercise and changes in nutrition reversed the increase of TAGs, FAs and cholesterols levels induced by HFD in our model. Considering the diets used for each of our groups and their daily caloric intake, it can be suggested that hepatic glycerophospholipids, sterol lipids and FAs abundance is highly reflective of systemic energy balance. And most importantly, these results demonstrate a high-capacity plasticity of the liver lipidome since most alterations stimulated by HFD were reversed in the *Int* group.

WAT once regarded as solely a tissue for energy storage, is now considered a major regulator of metabolism. Energy is stored as TAGs in lipid droplets in WAT which also releases, via lipolysis, FAs to be utilized by other organs. In conditions of a sustained positive energy balance, extensive alterations of WAT structure and function occur. These alterations are highlighted by adipocyte hypertrophy, local hypoxia, low-grade inflammation and modified profile of adipokine synthesis and secretion (1,237). When the energy surplus surpasses the capacity of WAT to adapt and store it, excess FAs are deposited in non-adipose sites, mainly in the liver, skeletal muscle, heart and kidneys (238–241). A strong correlation between the ability of visceral WAT to expand and the degree of ectopic fat accumulation has been established (238,239,242). Impairments in insulin-stimulated glucose uptake in eWAT were observed while peripheral tissues continued to be insulin-sensitive in early stages of high-fat feeding (205). When high-fat feeding was extended, eWAT content in TAG, DAG, ceramides and sphingomyelin was amplified in mice (205) and rat models (243). The dietary fat composition of a HFD has been found to determine the degree of pathophysiology in diet-induced obesity. For instance, saturated fatty acids (SFAs), compared to unsaturated FAs (UFAs), promote a worse inflammatory profile in eWAT that is more challenging to improve not only in eWAT but systemically as well (241,243,244). Even though the HFD and IntD of our study have an equal percentage of fat (45%), the composition differs widely leading to a lesser consumption of SFA by *Int* mice and a higher UFA consumption (section 3.1.3). Comparing the diet composition to the FAs profile in eWAT of *Int* mice, we noticed

a striking similarity illustrated by a reduction in omega-6 FAs content (linoleic acid and ARA) and an increase in PUFA, linolenic acid and combined n3.D-E-L in the lipidome of eWAT. Thus, the singularity of the eWAT lipid profile among the other 3 insulin-sensitive tissues, is that it mirrors the exact composition of the administered diet regardless of the systemic energy balance. However, some of the results seen in eWAT lipidome could not be explained by the diet composition. Examining the eWAT content in PLs and SM, it tended to increase moving from *Ctrl* to *Pat* and *Int* groups. Tissue remodelling of eWAT characterized by adipocytes hypertrophy in the *Pat* group and by a massive immune cell infiltration in both *Pat* and *Int* groups could account for these modifications. As it was already mentioned, PLs and SM are major components of plasma membranes thus their levels can reflect the cellularity of a tissue. The tissue remodeling of eWAT in our study will be further discussed in the next section. The lack of reversibility observed in the lipidome of eWAT could also be attributed to an impairment in mitochondrial function in eWAT. It is well established that mitochondria are crucial for lipid metabolism, hence, a dysfunction in the mitochondrial machinery can greatly influence the capacity of a tissue to regulate lipid metabolism. In the LiMa project from which our study derives, a significant decrease in mitochondrial respiration of eWAT was recorded in the *Pat* mice and persisted with the *Int* group (details in section 1.6). Whereas in the tissues revealing a capacity to reverse the changes stimulated by the HFD on their lipid profile, no alterations in mitochondrial respiration in hypothalamus, glycolytic skeletal muscles and liver were detected in *Pat* and *Int* mice. Hence, the association between the dynamics of the lipid classes and the mitochondrial function can be further explored with a consideration of other organelles and processes involved in lipid metabolism such as the endoplasmic reticulum (ER), peroxisomes, lipid transport and recycling.

5.3 Adipose tissue morphology

Adipose tissue has a primary role in regulating energy homeostasis. Besides the numerous hormones produced by this tissue that control energy balance,

adipose tissue acts as an energy storage site and a sensor and manager of energy status. The different cell types of adipose tissue, namely (pre)adipocytes and immune cells, produce and release cytokines according to the energy status allowing the coordination between organs to achieve energy homeostasis. Hence, under sustained conditions of major alterations to energy balance, the adipose tissue undergoes structural and functional remodeling (105). An unparalleled ability to expand is a hallmark of white adipose tissue. Under conditions of acute or chronic positive energy balance, WAT adapts to facilitate the need for increased lipid storage. Energy accumulates as TAG in lipid droplets in adipocytes which expand along with the increased anabolic pressure (105,110,123,126).

The hypertrophy of adipocytes was clearly observed with histological analysis of WAT depots in our *Pat* group, either eWAT or sWAT. The cell area of adipocytes clearly increased in WAT of *Pat* mice compared to those from *Ctrl* mice. While adipocytes with cell area above 800 μm^2 only represented 1-4% of total adipocytes count in *Ctrl* mice, in the *Pat* group they represented 28 to 44% depending on the depot. In addition, in both *Ctrl* and *Pat* groups, adipocytes from eWAT seemed to be larger than those from sWAT which is in agreement with the study by Parlee *et al.* investigating cell area and volume of adipocytes from WAT of male mice (245). Enlarged adipocytes function differently and in an expanded WAT, they are more prone to be hypoxic, apoptotic and under mechanical stress from interactions with the ECM (105,116). Thus, a positive correlation between adipocytes size and glucose intolerance, insulin resistance, hyperinsulinemia, increased adipocyte death rate and inflammation of adipose tissue was well-established by several studies (111–114). Furthermore, metabolic function of whole tissue homogenates of eWAT and sWAT seemed impaired in the *Pat* group as reported by the antecedents of the LiMa project. Assessing the morphology of the tissue, eWAT of *Pat* mice contained crown-like structures (CLS) unlike sWAT of the same group. Crown-like structures are an aggregate of macrophages that surround apoptotic adipocytes in order envelope and ingest them (137,138,143). Signs of inflammatory response even though not very explicit in the *Pat* group were much more pronounced in the I*nt* group of eWAT. Massive immune cell infiltration and fibrosis were identified in eWAT of *Int* mice. In both humans and rodents, low-grade chronic inflammation is associated to a systemic burden of circulatory cytokines and acute phase proteins reflective of

other systemic inflammatory-related pathologies (246,247). Hence, adipose tissue is at the center of obesity-associated systemic inflammatory response. Thus, it can be suggested that adipose tissue health, specifically of eWAT, is particularly relevant for an understanding of metabolic plasticity in our model.

Even though WAT structure and function in obese subjects have been widely discussed in the literature, not much has been reported about WAT after weight loss especially with human subjects due to obvious challenges. Nevertheless, Magkos *et al.* demonstrated a rectification of insulin sensitivity at a tissue level, however, the adipose and systemic inflammatory profile persisted with moderate weight loss and was resolved after subsequent weight loss (248). A multi-phase longitudinal study on obese women conducted by Dominique *et al.* as well described, despite an improvement in insulin sensitivity, a sustained inflammatory profile in adipose tissue after weight loss which was only eliminated during a weight maintenance period (249–251). Schmitz et al. described an adipose tissue obesogenic memory as the responsible factor for the sustained inflammatory state despite weight loss (252). Although the mentioned studies have been performed for subcutaneous WAT (in exception of (252)), they appear to contradict with our findings of sWAT that exhibits a lack of inflammation throughout the different groups of our model. The reported results seem to be more representative of the profile of eWAT in our model where adipose tissue architecture is restored after *LTint*. The contradiction in results between our project and the above-mentioned studies could be accredited to differences in: 1) time exposition to the obesogenic environment, and 2) between mice models and humans.

Drawing a comparison concerning adipocytes cell size, it was revealed that sWAT was slower in the regression of the size of adipocytes. Whereas in eWAT, a faster achievement of adipocytes cell area similar to the *Ctrl* group does not necessarily mean a higher adaptive capability of eWAT. Intriguingly, the proportion of sWAT adipocytes with areas ~ 400 μm^2 was higher in the *Int* group than in *Pat* mice or *Ctrl* mice, an effect that was not observed in eWAT. Moreover, in contrast to that found for eWAT, sWAT adipocytes *LTint* mice did not fully recover a lean-like size distribution. In view of these findings, it is tempting to speculate that lipid spillover from eWAT upon tissue remodeling in *Int* and *LTint* animals may be stored, at least

temporarily, in sWAT. The smaller adipocytes accounted for in eWAT of *Int* mice could be attributed to the tissue remodeling stimulating the commitment and differentiation of precursor cells into adipocytes. Despite the fact that adipogenesis is mostly inhibited in adult subjects (121), considering the extensive damage to eWAT induced by HF-overnutrition, tissue regeneration mainly via adipogenesis could be responsible for the ability of eWAT to recover. This hypothesis is further discussed in the upcoming section.

5.4 Adipose-derived stem cells metabolic function

Adipogenesis in WAT is a highly regulated process that initiates as early as the embryonic period and proceeds during development to be activated in adult life when expansion and tissue regeneration are stimulated (56,109,119). Wang *et al.* adopted the Adipochaser method to track adipogenesis in eWAT and sWAT depots of mice in different stages of their life cycle and under different diets (119). Their first observation for mice under chow diet (lean mice) was that the rate of adipogenesis was very low equally in eWAT and sWAT which is in agreement with human studies reporting a 10% annual adipocytes regeneration in adults (111). In addition, it was demonstrated that at early stages of HFD exposure, hypertrophy was the principal process responsible for WAT expansion and further HFD exposure induced a high capacity for adipogenesis only in eWAT and not sWAT. It was also concluded that in comparison to sWAT and under various physiological challenges like HFD and cold exposure, eWAT had a relatively higher potential to undergo adipogenesis. All these observations re-enforce the idea of distinctive modes of action of the different WAT depots. This can be additionally highlighted by our own results regarding mitochondrial function of WAT depots. Respirometry assays of whole-tissue homogenates of WAT had shown an impairment in mitochondrial function in eWAT and sWAT induced by HFD which was ameliorated after the intervention only in sWAT but never in eWAT even with the prolongation of the intervention to a second phase (details in section 1.6). Taking into consideration the

state of eWAT depots after HFD shown in the histological analysis of the tissue and the seemingly normal tissue with the *LTint* mice, we were curious to identify the extent of the hidden metabolic derangements in WAT.

For this purpose, metabolic function of adipose-derived stem cells (ADSCs) was assessed via mitochondrial respiration. While no major differences were recorded between *Ctrl* and *Pat* groups of eWAT, in sWAT, at all 4 respiratory states, ADSCs from Ctrl mice showed higher mitochondrial respiration. In a study led on human ADSCs from lean and type II diabetic patients, it was demonstrated that ADSCs from diabetic subjects had a distinctive phenotype defined by a larger size, a swollen cytoplasm, a deformation of the nuclear membrane and a degeneration of mitochondrial cristae (253). The deformation and swelling of the nuclear membrane and the reported reduced expression of Emerin – a membrane protein found in the inner nuclear membrane – could influence chromatin structure degeneration and gene transcription. Along with the recorded decrease in mitochondrial enzyme activity, the data suggest a reduced adipogenic capability of ADSCs from type II diabetic patients (253). It has been established by several studies that adipogenesis imposes a high demand on cellular energy level which implies an amelioration of oxidative phosphorylation (OXPHOS) in mitochondria. Once committed to differentiation, stem cells switch from a general glycolytic state to a more oxidative metabolism (254–256). An enhanced mitochondrial respiration was paralleled with an increase in mitochondrial biogenesis (57,257–259). Thus, it can be suggested that appropriate mitochondrial function of mesenchymal stem cells is key to a healthy WAT expansion via adipogenesis. Interpreting the reduced mitochondrial respiration of ADSCs from the eWAT *LTint* group, it can be attributed to either a strong inhibition of hyperplasia in that tissue or an impairment in mitochondrial function in those cells. Assessing the remodelling of eWAT that was required from *Pat* and *Int* depots to achieve the morphology of tissue demonstrated by the *LTint* groups, it is highly unlikely that hyperplasia was inhibited. However, the results in sWAT could be attributed to a stronger inhibition of hyperplasia induced by HFD which is in line with several previous studies (119–121).

It is worthy to mention that subpopulations of adipose progenitor cells (APCs) has been identified in high-fat fed mice (260,261). The APCs were recognized as the

platelet-derived growth factor receptor b+ (PDGRFβ+) cells responsible for healthy hyperplastic expansion of WAT (262,263) whereas the other PDGRFβ+ subpopulation of cells was termed as fibro-inflammatory progenitors (FIPs). FIPs were distinguished from APCs due to their reduced adipogenic potential and elevated ability to induce a pro-inflammatory gene expression profile stimulated by HFD (264). Triggered by mitochondrial dysfunction in eWAT depots, progenitor cells would rely more on glycolytic pathways on account of mitochondrial respiration which is associated with an increase in pro-inflammatory gene expression – a phenomenon well described in the literature for immune cells (260). The investigations around metabolic function of ADSC in humans and mice have led to a common hypothesis: the restoration of mitochondrial function in progenitor cells could treat obesity-associated adipose tissue dysfunction.

5.5 Macrophages profile in WAT

Macrophages are key modulators of energy metabolism and mitochondrial function in adipose tissue. The polarization of adipose tissue macrophages (ATMs) is determined by other cells types and components of the adipose tissue; thus, a bi-directional relation exists between ATMs and the rest of adipose tissue components (265). In all WAT depots, ATMs have two distinct origins; they can be self-renewed and proliferating tissue-resident macrophages or infiltrating and in-situ proliferating macrophages recruited by monocytes (266). Quantifying ATMs population in lean and severely obese mice reported an augmentation from 10% to 50% of all WAT cells (266). Initially, ATMs were described based on the two-dimensional M1-M2 spectrum. But, following the progresses in the understanding of macrophages activation and polarization, the use of the M1/M2 ratio to define the inflammatory profile of AT has been challenged. Distinct populations of ATMs expressing unique markers and exhibiting specialized transcriptional profiles and functions have led to the notion of highly plastic macrophages with phenotypes defined by the interactions with their surrounding microenvironment (143,265,266).

In our model, when evaluating the expression of M1-specific genes, a pronounced upregulation of most genes upon HFD was demonstrated in eWAT, which is indicative of M1 macrophage infiltration of this tissue. When the results obtained from RNAseq analysis are compared to our histological results, it appears clear that an increase in the number of immune cells, namely M1-like macrophages forming CLS around damaged adipocytes, accompanies HFD-induced weight gain. This would sustain the inflammatory profile that has been attributed to diet-induced obesity. Some of the M1-associated genes, following the weight-loss strategy, showed a gradual downregulation that was modest in *Int* mice but complete in *LTint* mice. In visceral WAT, macrophages accumulation was attributed by Amano *et al.* to MCP-1 stimulated *in situ* proliferation and not the recruitment of migrating macrophages by monocytes (267). Additional investigations have shown that in the early stages of diet-induced WAT expansion, resident ATMs are less apoptotic and faster at proliferation (268,269). Our results are in line with Zamarron *et al*. that addressed ATMs profile in formerly obese mice, revealing a persisting high content in ATMs for up to 6 months after the weight loss despite a fat mass normalization. A pro-inflammatory profile was characterized by a persisting fibrosis and a high expression of TNF-α, Il-1b and IFN-γ (268). Lipid-rich M1-like CD11c+ ATMs were reported to appear in visceral WAT when it reaches its hypertrophic limit. Their presence was evidenced in eWAT earlier than sWAT suggesting a reduced capacity of adipocytes in eWAT to handle lipid oversupply (269). As a matter of fact, a clear M1-like gene fingerprint, as that observed in eWAT, was not clearly identified in sWAT, and CLS could only occasionally observed in sWAT. Notwithstanding these observations, some changes in macrophage phenotypes were observed also in sWAT. To be more specific, there seemed to be a loss of M2b marker genes and, to a lesser extent, of M2c marker genes in sWAT of *Pat* mice, which was recovered in *LTint* animals. Given the anti-inflammatory potential of both M2b and M2c macrophages (29,142), our observations suggest a loss of protection to inflammation in sWAT in response to HDF-induced obesity.

Notably, the pattern of M2 macrophage subtypes related to weight gain and subsequent loss was more clearly evidenced in eWAT. Thus, *Pat* up-regulated the expression of gene markers defining M2a, M2b and M2c macrophages, thus supporting the complexity of the immune response triggered in eWAT in response

to obesity. Moreover, according to our RNAseq analysis, the expression of these markers persisted in *Int* animals, which would account for the increased immune cell infiltration observed in the histological sections. In this scenario, anti-inflammatory M2a and M2b macrophages, together with M2c macrophages, responsible of phagocytosis of apoptotic cells and tissue remodeling, would help ameliorate eWAT structure and function in response to IntD, that would be finally achieved after long-term interventions. In addition, M2b and M2c macrophages, through their immunosuppression/immunoregulatory properties would also contribute to reduce HFD-induced immune response. The elevated levels of ATMs in expanding WATs cannot be solely credited to an increase in the classically activated M1 phenotype. The metabolically activated macrophages (Mme) were identified in obese WATs and they overexpress lipid-related genes such as *PLIN2* and *ABCA1*. Mme macrophages are characterized by an upregulated lipid metabolic profile suggesting that metabolic alterations, such as elevated FFAs, insulin and glucose levels, promote the polarization of macrophages into Mme (143,265,266). In our data, both *PLIN2* and *ABCA1* were found to be upregulated in eWAT and sWAT of *Pat* groups. Perilipin-2 (Plin2), a cytoplasmic lipid droplet scaffolding protein, is usually associated to its contribution in the development of non-alcoholic fatty liver disease (NAFLD). However, a study by Orlicky *et al.* has revealed that total depletion of Plin2 fully protected mice from diet-induced steatohepatitis, liver fibrosis, insulin resistance and adipose tissue inflammation whereas hepatocyte-specific Plin2 knockout did not protect against insulin resistance or adipose tissue inflammation (270). The role of ATMs and their derived inflammatory mediators in the development of insulin resistance in adipose tissue has been reviewed by several studies. ATMs mainly inhibit insulin signalling pathways in adipocytes via the release of pro-inflammatory cytokines that activate pro-inflammatory kinases (266). JNK is an example of a pro-inflammatory kinase which blocks insulin receptor downstream signalling through serine/threonine phosphorylation of insulin receptor substrates (147).

ATMs contribute to the regulation of adipose tissue metabolism in physiological and pathological conditions and the metabolic state of the adipose tissue affects the polarization of ATMs. The differentiation and effector function of macrophages are intricately linked to their intracellular bioenergetic pathways. In other words, lipid

production and utilization of ATMs differentiates their phenotypes. A generalized notion is that M1-like macrophages are predominately glycolytic for rapid ATP production whereas M2-like macrophages favor oxidative phosphorylation (OXPHOS) (271). M1-like macrophages via a glycolytic metabolism contribute to ROS generation, reduced glutathione and HIF-1α stabilization among others while M2-like macrophages suppress ROS production and HIF-1α expression through efficient coupling of the electron transport system (ETS) (272,273). Moreover, Boutens *et al.* showed that cytokine production by ATMs in lean tissues is mediated by FA, glucose, and glutamine utilization – a similarity to the metabolic profile of M2 macrophages – whereas cytokine production in obese tissues is supported by glycolysis – a similarity to the metabolic profile of M1 macrophages (274). Identification of the differential macrophages phenotypes under lean and obese conditions has been greatly driven by their glycolytic and OXPHOS capacities. For instance, macrophages with low glycolytic capacity and low OXPHOS predominately found in lean WAT are now recognized as Cd11b+ "Mox" macrophages (275) and Mme macrophages were differentiated in obesity due to their unique metabolic phenotype that was partially M1 and M2 like. Even though our results demonstrate an upregulation of most specific cell surface markers for Mox in eWAT and sWAT of *Pat* group it did not necessarily refute the previous statement that Mox are predominant in lean WAT. It just showed that Mox macrophages in expanding WATs are further activated which is in coordination with their principal function as handlers of oxidative stress. In addition, recent studies on ATMs from lean and obese mice and on co-cultures with AT explants, reported increases in glycolysis and OXPHOS of macrophages originating from obesity models thus introducing additional macrophages phenotypes (274,275). The metabolism of ATMs with all their existing phenotypes and how it engages with WAT metabolism in lean and obese conditions is still preliminary, however, the concept of metabolic flexibility of ATMs has been widely accepted.

Beyond diet-induced obesity, several investigations have been led to evaluate the adipose tissue profile induced by weight loss. One of the earliest mouse studies on the subject where weight loss was driven by calorie restriction, reported increased ATMs accumulation and increased lipolysis mostly in visceral adipose tissue in the early stages of weight loss that was only reduced after extended period of weight

loss (276). A positive correlation between ATM levels and the levels of circulating FFAs and adipose tissue lipolysis suggested lipolysis as the stimulator for ATM accumulation. To further test this theory, inducing lipolysis pharmacologically or through fasting was shown to rapidly increase adipose tissue chemoattractant activity, ATM accumulation and lipid uptake by ATMs (276). A later study, demonstrated, after 8 weeks of switching back to a chow diet inducing weight loss, a persisting insulin resistance and no reduction in ATMs population in eWAT. The same conclusion could not be made regarding sWAT since initially, the massive increase in ATMs population induced by HFD was not observed in sWAT (268). Moreover, the study by Schmitz et al. reported in visceral AT of mice of weight loss even higher levels of inflammatory cytokines than in that of obese mice maintained on HFD throughout the course of the study (252). All these results are in agreement with our findings; a macrophage-dominated inflammation induced by HFD is more pronounced in eWAT than sWAT and it is sustained through early periods of weight loss.

The modification to the population of macrophages in obesity and weight loss include the presence of distinctive phenotypes in each condition. Fisher et al. identified in visceral AT of obese mice 7 different clusters of macrophages based on their gene expression profile. They recognized the most abundant phenotype of ATMs by a profile of enriched lipid binding and metabolic processes. This same subpopulation of macrophages was lost after only 2 weeks of CR and it was replaced by a phagocytosis-favoring macrophages. These observations reveal that ATMs after CR, do not adopt again a lean phenotype but rather embrace a completely new profile (277). In a mouse model where lipolysis was induced in eWAT and sWAT via β-adrenergic stimulation, a population of ATMs acting as efferocytes was revealed. The role of these ATMs was the phagocytosis and clearance of dead cells in AT contributing to tissue remodeling (278).

5.6 ECM characterization in WAT

Tissue remodeling and the adaptation of adipose tissue to internal and environmental stimuli requires a communication among adipose tissue cells and the components of the extracellular matrix (ECM). Continuous remodeling of ECM and an elevated degree of ECM flexibility are key to maintain a healthy adipose tissue profile. During positive energy balance, an adaptive response of cellular and extracellular compartments in the expanding adipose tissue is required for prevention of lipid deposition and lipotoxicity (279). Adipose tissue is recognized for its loose connective tissue and for an ECM mostly composed of collagens. In rodents, usually the collagenous matrix is more developed in sWAT than visceral WAT (49,280). Dozens of collagens types have been identified along with the genes encoding their subunits. Collagens are categorized into 2 main types, the fibrillar and the non-fibrillar. Type I collagen (COL1) and COL3 are examples of collagens that organize into fibrils and assemble to generate mature collagen fibers. COL1 fibrils are responsible for the major structural framework of adipose tissue (50). The non-fibrillar collagens such as Fibril-associated collagens with interrupted triple helices (FACITs) instead of forming fibrils, they bind to collagen fibers creating mesh-like networks in the ECM. Type IV collagen is an example of FACITs that is the primary collagen present in basement membranes of AT cells. Along with COL4, type VI collagen is classified as network-forming collagen. Even though it exists in the ECM of other tissues, COL6 is considered specific to WAT and it was found to have a higher expression in visceral WAT than sWAT (49). COL6 microfibrils function as cellular anchors through binding to cells on one side – via integrins, cell surface proteoglycans and COL4 – and to the collagen fibers on the other side. These interactions allow the formation of the complex 3D network which maintains tissue structure and facilitates intracellular signaling pathways (281).

Several studies have reported an increased collagen deposition and fibrosis in WATs of diet-induced obese mice and humans (47,282). In our data and in both WAT depots, the *Pat* group demonstrated an upregulation of genes encoding COL1, COL4 and COL6. Song *et al.* showed an increase in COL1 in WAT of mice under HFD and revealed toll-like receptor 2 (Tlr2) as a possible mediator of COL1 deposition (283).

Chen *et al*. reported an increase in content in COL1 and COL4 in eWAT and sWAT of mice under HFD (284). In addition, Khan et al. demonstrated an enrichment of COL6 in eWAT and sWAT among other WAT depots of obese mice. In an attempt to disrupt ECM composition, a mouse model with *COL6* knockout was used and it revealed a weakening in ECM of the adipose tissue paralleled with substantial improvements in the metabolic phenotype and a reduction of adipose tissue inflammation (52).

When our RNAseq data and histological observations are viewed together, it seems likely that COL1, COL3, and COL6 are major collagens forming the network supporting extended eWAT in obese mice, and effect that was not observed for sWAT, thus reinforcing the occurrence of interdepot differences. In fact, COL1 was not modified in sWAT of *Pat* mice. Notably, COL4 which, as mentioned above, is a major component of basement membranes, was greatly increased in sWAT of obese mice, suggesting that the interface adipocyte-ECM is altered in this depot in obesity. When viewed together, our results indicate that, although in a distinct manner, both fat depots are altered in response to weight gain. In terms of collagen subtype content, it appears that though most collagens that increased in obesity tended to decrease after weight loss, other collagens behaved in an opposite way. These results are interesting in that they indicate that obesity-induced changes in the ECM are not fully recovered, even upon normal weight recovery.

Pathological fibrosis in WAT is a consequence of abnormal accumulation of collagen fibers and of non-fibrillar ECM components like proteoglycans (PGs) as well. An increased deposition of numerous PGs and their largest subfamily, the small leucine rich proteoglycans (SLRPs) has been illustrated in obese WATs of mice and humans (47,285–287). In agreement with these studies, we found that many of the SLRPs such as lumican, biglycan and asporin, had an increased expression level in the *Pat* group. Wolff *et al.* evaluated mice with silenced or over-expressed lumican and demonstrated that SLRP lumican plays an important role in systemic glucose homeostasis and the development of obesity-associated metabolic complications (288).

CONCLUSIONS

In our mouse model of diet-induced obesity, the acquired pathological phenotype was improved by our combined nutritional and exercise intervention promoting a weight-loss strategy followed by a maintenance phase. The mouse phenotype was set up through an in depth systemic and tissue specific characterization highlighted by few parameters such as body weight, weight of some insulin-sensitive tissues, glucose tolerance and insulin sensitivity.

In a step further to complete the phenotype of our experimental model, lipidomics studies on 4 insulin-sensitive tissues allowed us to conclude that:

I. Lipid profile is tissue-specific dictated by the structure and function of a tissue.

II. Liver and skeletal muscle gastrocnemius showed a lipid profile mimicking the changes in systemic energy balance, an indication that both tissues maintain their plasticity.

III. Lipidome of eWAT was not reflective of energy balance but of the nutritional content, mainly the fat composition, of the administered diet.

Following the rationale of previous findings of tissue-specific features that did not improve after the intervention, our focus was shifted towards white adipose tissue, more specifically, the impairments identified in epididymal white adipose tissue (eWAT). Investigations centered around eWAT and subcutaneous white adipose tissue (sWAT) allowed us to conclude that:

IV. Distinctively from sWAT, eWAT was subjected to a complete tissue remodeling stimulated by high-fat diet and tissue atrophy characterized by cell death, immune cell infiltration and fibrosis.

V. The deterioration of mitochondrial function in eWAT was evident furthermore by an impairment in mitochondrial respiration of adipose-derived stem cells after the implementation of the long-term intervention (LT intervention) suggesting a reduced ability of eWAT for healthy adipogenesis.

VI. Adipose tissue macrophages accumulated in expanding eWAT revealing obesity-associated metabolically activated phenotypes of macrophages.

VII. Weight loss induced by calorie restriction did not resolve the inflammatory profile in eWAT at the early stages thus requiring extended periods of intervention.

VIII. The gene expression of macrophages markers and their secretory factors in sWAT demonstrated less intense alterations in the adipose tissue macrophages phenotypes in comparison to eWAT.

IX. Extracellular matrix (ECM) was highly susceptible to internal and environmental stimuli manifested by major changes in expression of collagens and proteoglycans genes in WAT depots induced by high-fat feeding and the implementation of weight loss strategies.

The detectable regulations in numerous ECM components in sWAT at the pathological state, without major changes indicative of M1 macrophage infiltration of this fat depot in obese animals led to hypothesize:

Under high-fat feeding, changes to ECM may proceed macrophages accumulation, at least in sWAT, which open new scenarios for future research.

REFERENCES

1. Trayhurn P, Beattie JH. Physiological role of adipose tissue : white adipose tissue as an endocrine and secretory organ. Proc Nutr Soc. 2001;60:329–39.

2. Kahn CR, Wang G, Lee KY. Altered adipose tissue and adipocyte function in the pathogenesis of metabolic syndrome. J Clin Invest. 2019;129(10):3990–4000.

3. Lee M-J, Wu Y, Fried SK. Adipose tissue heterogeneity: Implication of depot differences in adipose tissue for obesity complications. Mol Asp Med. 2014;34(1):1–11.

4. Lumish HS, Reilly MO, Reilly MP. Sex Differences in Genomic Drivers of Adipose Distribution and Related Cardiometabolic Disorders Opportunities for Precision Medicine. Arterioscler Thromb Vasc Biol. 2020;40(January):45–60.

5. Carroll JF, Chiapa AL, Rodriquez M, Phelps DR, Cardarelli KM, Vishwanatha JK, et al. Visceral Fat , Waist Circumference , and BMI : Impact of Race / ethnicity. Obesity. 2008;16:600–7.

6. Wang W, Seale P. Control of brown and beige fat development. Nat Rev Mol Cell Biol. 2016;17(11):691–702.

7. Zwick RK, Guerrero-juarez CF, Horsley V, Plikus M V. Anatomical, physiological and functional diversity of adipose tissue. Cell Metab. 2019;27(1):68–83.

8. Hovey RC, Aimo L. Diverse and active roles for adipocytes during mammary gland growth and function. J Mammary Gland Biol Neoplasia. 2010;15(3):279–90.

9. Parmar H, Cunha GR. Epithelial-stromal interactions in the mouse and human mammary gland in vivo. Endocr Relat Cancer. 2004;11(3):437–58.

10. Medical M, Maridas DE, Rendina-ruedy E, Helderman RC, Demambro VE, Brooks D, et al. Progenitor recruitment and adipogenic lipolysis contribute to the anabolic actions of parathyroid hormone on the skeleton. FASEB J. 2019;33:2885–98.

11. Cawthorn WP, Scheller EL, Learman BS, Parlee SD, Simon BR, Mori H, et al. Bone marrow adipose tissue is an endocrine organ that contributes to increased circulating adiponectin during caloric restriction. Cell Metab. 2014;20(2):368–75.

12. Park A, Kim WK, Bae K. Distinction of white , beige and brown adipocytes derived from mesenchymal stem cells. World J Stem Cells. 2014;6(1):33–42.

13. Cushman SW. Structure-function relationships in the adipose cell. I . Ultrastructure of the Isolated Adipose Cell. J Cell Biol. 1970;46:326–41.

14. Sarjeant K, Stephens JM. Adipogenesis. Cold Spring Harb Perspect Med. 2012;4:1–19.

15. Taittonen M, Ph D, Laine J, Savisto N. Functional brown adipose tissue in healthy adults. New Engl J Med. 2009;360(15):1518–25.

16. Cypess AM, Lehman S, Williams G, Tal I, Rodman D, Goldfine AB, et al. Identification and importance of brown adipose tissue in adult humans. New Engl J Med. 2009;350(15):1509–17.

17. Li Y, Wang D, Ping X, Zhang Y, Zhang T, Wang L, et al. Local hyperthermia therapy induces browning of white fat and treats obesity. Cell. 2022;185(6):949–66.

18. Berry DC, Stenesen D, Zeve D, Graff JM. The developmental origins of adipose tissue. Development. 2013;140:3939–49.

19. Majka SM, Barak Y, Klemm DJ. Adipocyte Origins : Weighing the Possibilities. Stem Cells. 2012;29(7):1034–40.

20. Giordano A, Smorlesi A, Frontini A, Barbatelli G, Cint S. White, brown and pink adipocytes: The extraordinary plasticity of the adipose organ. Eur J Endocrinol. 2014;170(5):159–71.

21. Bacakova L, Zarubova J, Travnickova M, Musilkova J, Pajorova J, Slepicka P, et al. Stem cells: their source, potency and use in regenerative therapies with focus on adipose-derived stem cells – a review. Biotechnol Adv [Internet]. 2018;36(4):1111–26. Available from: https://doi.org/10.1016/j.biotechadv.2018.03.011

22. Zakrzewski W, Dobrzyński M, Szymonowicz M, RybaK Z. Stem Cells: Past, Present and Future. Stem Cell Res Ther. 2019;10:1–22.

23. Amira Ragab EL Barky* EMMA and TMM. Stem Cells, Classifications and their Clinical Applications. Am J Pharmacol Ther [Internet]. 2017;1(1):1–7. Available from: www.scireslit.com

24. Uccelli A, Moretta L, Pistoia V. Mesenchymal stem cells in health and disease. Nat Rev Immunol. 2008;8(9):726–36.

25. Mushahary D, Spittler A, Kasper C, Weber V, Charwat V. Isolation, cultivation, and characterization of human mesenchymal stem cells. Cytom Part A. 2018;93(1):19–31.

26. Murphy MB, Moncivais K, Caplan AI. Mesenchymal stem cells: Environmentally

responsive therapeutics for regenerative medicine. Exp Mol Med [Internet]. 2013;45:1–16. Available from: http://dx.doi.org/10.1038/emm.2013.94

27. Chen L, Tredget EE, Wu PYG, Wu Y, Wu Y. Paracrine factors of mesenchymal stem cells recruit macrophages and endothelial lineage cells and enhance wound healing. PLoS One. 2008;3(4):1–12.

28. Ren G, Zhang L, Zhao X, Xu G, Zhang Y, Roberts AI, et al. Mesenchymal Stem Cell-Mediated Immunosuppression Occurs via Concerted Action of Chemokines and Nitric Oxide. Cell Stem Cell. 2008;2(2):141–50.

29. Mantovani A, Sica A, Sozzani S, Allavena P, Vecchi A, Locati M. The chemokine system in diverse forms of macrophage activation and polarization. Trends Immunol. 2004;25(12):677–86.

30. Konopleva M, Konoplev S, Hu W, Zaritskey AY, Afanasiev B V., Andreeff M. Stromal cells prevent apoptosis of AML cells by up-regulation of anti-apoptotic proteins. Leukemia. 2002;16(9):1713–24.

31. Rehman J, Traktuev D, Li J, Merfeld-Clauss S, Temm-Grove CJ, Bovenkerk JE, et al. Secretion of Angiogenic and Antiapoptotic Factors by Human Adipose Stromal Cells. Circulation. 2004;109(10):1292–8.

32. Strioga M, Viswanathan S, Darinskas A, Slaby O, Michalek J. Same or not the same? comparison of adipose tissue-derived versus bone marrow-derived mesenchymal stem and stromal cells. Stem Cells Dev. 2012;21(14):2724–52.

33. Hsiao STF, Asgari A, Lokmic Z, Sinclair R, Dusting GJ, Lim SY, et al. Comparative analysis of paracrine factor expression in human adult mesenchymal stem cells derived from bone marrow, adipose, and dermal tissue. Stem Cells Dev. 2012;21(12):2189–203.

34. Ding DC, Chou HL, Hung WT, Liu HW, Chu TY. Human adipose-derived stem cells cultured in keratinocyte serum free medium: Donor's age does not affect the proliferation and differentiation capacities. J Biomed Sci [Internet]. 2013;20:1–11. Available from: Journal of Biomedical Science

35. Bourin P, Bunnell BA, Casteilla L, Dominici M, Katz AJ, March KL, et al. Stromal cells from the adipose tissue-derived stromal vascular fraction and culture expanded adipose tissue-derived stromal/ stem cells: a joint statement of the International Federation for Adipose Therapeutics (IFATS) and Science and the International S.

Cytotherapy. 2013;15(6):641--648.

36. Mazini L, Rochette L, Amine M, Malka G. Regenerative capacity of adipose derived stem cells (ADSCs), comparison with mesenchymal stem cells (MSCs). Int J Mol Sci. 2019;20(10):1–30.

37. Guzik TJ, Skiba DS, Touyz RM, Harrison DG. The role of infiltrating immune cells in dysfunctional adipose tissue. Cardiovasc Res. 2017;113(9):1009–23.

38. Choe SS, Huh JY, Hwang IJ, Kim JI, Kim JB. Adipose tissue remodeling: Its role in energy metabolism and metabolic disorders. Front Endocrinol (Lausanne). 2016;7:1–16.

39. Huh JY, Park YJ, Ham M, Kim JB. Crosstalk between adipocytes and immune cells in adipose tissue inflammation and metabolic dysregulation in obesity. Mol Cells. 2014;37(5):365–71.

40. Catrysse L, van Loo G. Adipose tissue macrophages and their polarization in health and obesity. Cell Immunol [Internet]. 2018;330(October 2017):114–9. Available from: https://doi.org/10.1016/j.cellimm.2018.03.001

41. Michailidou Z, Gomez-Salazar M, Alexaki VI. Innate Immune Cells in the Adipose Tissue in Health and Metabolic Disease. J Innate Immun. 2022;14:4–30.

42. Haka AS, Barbosa-Lorenzi VC, Lee HJ, Falcone DJ, Hudis CA, Dannenberg AJ, et al. Exocytosis of macrophage lysosomes leads to digestion of apoptotic adipocytes and foam cell formation. J Lipid Res. 2016;57(6):980–92.

43. Molofsky AB, Nussbaum JC, Liang HE, Dyken SJV, Cheng LE, Mohapatra A, et al. Innate lymphoid type 2 cells sustain visceral adipose tissue eosinophils and alternatively activated macrophages. J Exp Med. 2013;210(3):535–49.

44. Brestoff JR, Kim BS, Saenz SA, Stine RR, Monticelli LA, Sonnenberg GF, et al. Group 2 innate lymphoid cells promote beiging of adipose and limit obesity HHS Public Access. Nature [Internet]. 2015;519(7542):242–6. Available from: www.nature.com/reprints

45. Bonnans C, Chou J, Werb Z. Remodelling the extracellular matrix in development and disease. Nat Rev Mol Cell Biol [Internet]. 2014;15(12):786–801. Available from: http://www.ncbi.nlm.nih.gov/pubmed/25415508%0Ahttp://www.pubmedcentral.nih.gov/articlerender.fcgi?artid=PMC4316204

46. Mariman ECM, Wang P. Adipocyte extracellular matrix composition, dynamics and role in obesity. Cell Mol Life Sci. 2010;67(8):1277–92.

47. Crewe C, An YA, E SP. The ominous triad of adipose tissue dysfunction: inflammation, fibrosis, and impaired angiogenesis. J Clin Invest [Internet]. 2017;7(1):74–82. Available from: https://www.ncbi.nlm.nih.gov/pmc/articles/PMC5199684/pdf/jci-127-88883.pdf

48. Ruiz-Ojeda FJ, Méndez-Gutiérrez A, Aguilera CM, Plaza-Díaz J. Extracellular matrix remodeling of adipose tissue in obesity and metabolic diseases. Int J Mol Sci. 2019;20:1–25.

49. Mori S, Kiuchi S, Ouchi A, Hase T, Murase T. Characteristic expression of extracellular matrix in subcutaneous adipose tissue development and adipogenesis; Comparison with visceral adipose tissue. Int J Biol Sci. 2014;10(8):825–33.

50. Zöller N, Schreiner S, Petry L, Hoffmann S, Steinhorst K, Kleemann J, et al. Collagen I Promotes Adipocytogenesis in Adipose-Derived Stem Cells In Vitro. Cells. 2019;8(302):1–13.

51. Divoux A, Clément K. Architecture and the extracellular matrix: The still unappreciated components of the adipose tissue. Obes Rev. 2011;12(5):494–503.

52. Khan T, Muise ES, Iyengar P, Wang Z V., Chandalia M, Abate N, et al. Metabolic Dysregulation and Adipose Tissue Fibrosis: Role of Collagen VI. Mol Cell Biol. 2009;29(6):1575–91.

53. Aikio M, Elamaa H, Vicente D, Izzi V, Kaur I, Seppinen L, et al. Specific collagen XVIII isoforms promote adipose tissue accrual via mechanisms determining adipocyte number and affect fat deposition. Proc Natl Acad Sci U S A. 2014;111:3043–52.

54. Karamanos NK, Theocharis AD, Neill T, Lozzo R V. Matrix modeling and remodeling: a biological interplay regulating tissue homeostasis and diseases. Matrix Biol. 2019;75–76:1–11.

55. Theocharis AD, Manou D, Karamanos NK. The extracellular matrix as a multitasking player in disease. FEBS J. 2019;286(15):2830–69.

56. Ghaben AL, Scherer PE. Adipogenesis and metabolic health. Nat Rev Mol Cell Biol [Internet]. 2019;20(4):242–58. Available from: http://dx.doi.org/10.1038/s41580-018-0093-z

57. Tang QQ, Lane MD. Adipogenesis: From stem cell to adipocyte. Annu Rev Biochem. 2012;81:715–36.

58. Wang Q, Yan CL, Wang J, Kong J, Qi Y, Quigg RJ, et al. miR-17-92 cluster accelerates adipocyte differentiation by negatively regulating tumor-suppressor Rb2/p130. Proc Natl Acad Sci U S A. 2008;105(8):2889–94.

59. Kennell JA, Gerin I, MacDougald OA, Cadigan KM. The microRNA miR-8 is a conserved negative regulator of Wnt signaling. Proc Natl Acad Sci U S A. 2008;105(40):15417–22.

60. Scheja L, Heeren J. The endocrine function of adipose tissues in health and cardiometabolic disease. Nat Rev Endocrinol [Internet]. 2019;15(9):507–24. Available from: http://dx.doi.org/10.1038/s41574-019-0230-6

61. Fasshauer M, Blüher M. Adipokines in health and disease. Trends Pharmacol Sci. 2015;36(7):461–70.

62. Wang P, Mariman E, Renes J, Keijer J. The secretory function of adipocytes in the physiology of white adipose tissue. J Cell Physiol. 2008;216(1):3–13.

63. Hauner H. Secretory factors from human adipose tissue and their functional role. Proc Nutr Soc. 2005;64(2):163–9.

64. Blüher M. Importance of adipokines in glucose homeostasis. Diabetes Manag. 2013;3(5):389–400.

65. Cowley MA, Smart JL, Rubinstein M, Cerdán MG, Diano S, Horvath TL, et al. Leptin activates anorexigenic POMC neurons through a neural network in the arcuate nucleus. Nature. 2001;411(6836):480–4.

66. Marroquí L, Gonzalez A, Nĕco P, Caballero-Garrido E, Vieira E, Ripoll C, et al. Role of leptin in the pancreatic β-cell: Effects and signaling pathways. J Mol Endocrinol. 2012;49(1).

67. Maeda N, Shimomura I, Kishida K, Nishizawa H, Matsuda M, Nagaretani H, et al. Diet-induced insulin resistance in mice lacking adiponectin/ACRP30. Nat Med. 2002;8(7):731–7.

68. Kim JY, Van De Wall E, Laplante M, Azzara A, Trujillo ME, Hofmann SM, et al. Obesity-associated improvements in metabolic profile through expansion of adipose tissue. J Clin Invest. 2007;117(9):2621–37.

69. Yang Q, Graham TE, Mody N, Preitner F, Peroni OD, Zabolotny JM, et al. Serum retinol binding protein 4 contributes to insulin resistance in obesity and type 2 diabetes. Nature. 2005;436:356–62.

70. Rosen ED, M SB. Adipocytes as regulators of energy balance and glucose homeostasis. Nature [Internet]. 2006;444:847–53. Available from: https://www.ncbi.nlm.nih.gov/pmc/articles/PMC3624763/pdf/nihms412728.pdf

71. Smith U, Kahn BB. Adipose tissue regulates insulin sensitivity: role of adipogenesis, de novo lipogenesis and novel lipids. J Intern Med. 2016;280(5):465–75.

72. Luo L, Liu M. Adipose tissue in control of metabolism. J Endocrinol. 2016;231(3):R77–99.

73. Kojta I, Chacinska M, Blachnio-Zabielska A. Obesity, Bioactive Lipids, and Adipose Tissue Inflammation in Insulin Resistance. Nutrients. 2020;12:1–19.

74. Frühbeck G, Méndez-Giménez L, Fernández-Formoso JA, Fernández S, Rodríguez A. Regulation of adipocyte lipolysis. Vol. 27, Nutrition Research Reviews. 2014. 63–93 p.

75. Chouchani ET, Kajimura S. Metabolic adaptation and maladaptation in adipose tissue. Nat Metab. 2019;1(2):189–200.

76. Song Z, Xiaoli AM, Yang F. Regulation and metabolic significance of De Novo lipogenesis in adipose tissues. Nutrients. 2018;10(10):1–22.

77. Hill JO, Wyatt HR, Peters JC. Energy Balance and Obesity. Circulation. 2012;126(1):126–32.

78. Bo S, Fadda M, Fedele D, Pellegrini M, Ghigo E, Pellegrini N. A critical review on the role of food and nutrition in the energy balance. Nutrients. 2020;12(4):1–27.

79. Müller MJ, Enderle J, Bosy-Westphal A. Changes in Energy Expenditure with Weight Gain and Weight Loss in Humans. Curr Obes Rep [Internet]. 2016;5(4):413–23. Available from: http://dx.doi.org/10.1007/s13679-016-0237-4

80. Byrne NM, Wood RE, Schutz Y, Hills AP. Does metabolic compensation explain the majority of less-than-expected weight loss in obese adults during a short-term severe diet and exercise intervention. Int J Obes. 2012;36:1472–8.

81. Dulloo AG. Physiology of weight regain: Lessons from the classic Minnesota Starvation Experiment on human body composition regulation. Obes Rev.

2021;22:1–19.

82. Müller MJ, Enderle J, Pourhassan M, Braun W, Eggeling B, Lagerpusch M, et al. Metabolic adaptation to caloric restriction and subsequent refeeding: The Minnesota Starvation Experiment revisited. Am J Clin Nutr. 2015;102(4):807–19.

83. Bauer P V., Hamr SC, Duca FA. Regulation of energy balance by a gut-brain axis and involvement of the gut microbiota. Cell Mol Life Sci. 2016;73(4):737–55.

84. Steinert RE, Feinle-Bisset C, Asarian L, Horowitz M, Beglinger C, Geary N. Ghrelin, CCK, GLP-1, and PYY(3-36): Secretory controls and physiological roles in eating and glycemia in health, obesity, and after RYGB. Vol. 97, Physiological Reviews. 2017. p. 411–63.

85. Müller TD, Finan B, Bloom SR, D'Alessio D, Drucker DJ, Flatt PR, et al. Glucagon-like peptide 1 (GLP-1). Mol Metab [Internet]. 2019;30:72–130. Available from: https://doi.org/10.1016/j.molmet.2019.09.010

86. Persaud SJ, Bewick GA. Peptide YY: More than just an appetite regulator. Diabetologia. 2014;57:1762–9.

87. Judge A, Dodd MS. Metabolism. 2020;64:607–47.

88. Guo X, Li H, Xu H, Woo S, Dong H, Lu F, et al. Glycolysis in the control of blood glucose homeostasis. Acta Pharm Sin B [Internet]. 2012;2:358–67. Available from: http://dx.doi.org/10.1016/j.apsb.2012.06.002

89. Bar-Even A, Flamholz A, Noor E, Milo R. Rethinking glycolysis: On the biochemical logic of metabolic pathways. Nat Chem Biol. 2012;8(6):509–17.

90. Rabinowitz JD, Enerbäck S. Lactate: the ugly duckling of energy metabolism. Nat Metab. 2020;2(7):566–71.

91. Han HS, Kang G, Kim JS, Choi BH, Koo SH. Regulation of glucose metabolism from a liver-centric perspective. Exp Mol Med [Internet]. 2016;48(3):218–27. Available from: http://dx.doi.org/10.1038/emm.2015.122

92. Wu G. Amino acids: Metabolism, functions, and nutrition. Amino Acids. 2009;37(1):1–17.

93. Houten SM, Violante S, Ventura F V., Wanders RJA. The Biochemistry and Physiology of Mitochondrial Fatty Acid β-Oxidation and Its Genetic Disorders. Annu Rev Physiol. 2016;78:23–44.

94. Muoio DM, MacLean PS, Lang DB, Li S, Houmard JA, Way JM, et al. Fatty acid homeostasis and induction of lipid regulatory genes in skeletal muscles of peroxisome proliferator-activated receptor (PPAR) α knock-out mice. Evidence for compensatory regulation by PPARδ. J Biol Chem [Internet]. 2002;277(29):26089–97. Available from: http://dx.doi.org/10.1074/jbc.M203997200

95. Gibala MJ, Young ME, Taegtmeyer H. Anaplerosis of the citric acid cycle: Role in energy metabolism of heart and skeletal muscle. Acta Physiol Scand. 2000;168(4):657–65.

96. Owen OE, Kalhan SC, Hanson RW. The key role of anaplerosis and cataplerosis for citric acid cycle function. J Biol Chem [Internet]. 2002;277(34):30409–12. Available from: http://dx.doi.org/10.1074/jbc.R200006200

97. Zhao RZ, Jiang S, Zhang L, Yu Z Bin. Mitochondrial electron transport chain, ROS generation and uncoupling (Review). Int J Mol Med. 2019;44(1):3–15.

98. Nolfi-Donegan D, Braganza A, Shiva S. Mitochondrial electron transport chain: Oxidative phosphorylation, oxidant production, and methods of measurement. Redox Biol [Internet]. 2020;37:101674. Available from: https://doi.org/10.1016/j.redox.2020.101674

99. Gnaiger E. Mitochondrial physiology. Recent Adv Mitochondrial Med Coenzyme Q. 2018;13–30.

100. Lobo-Jarne T, Ugalde C. Respiratory Chain Supercomplexes: Structures, Function and Biogenesis. Semin Cell Dev Biol. 2018;76:179–90.

101. Bray GA, Kim KK, Wilding JPH. Obesity: a chronic relapsing progressive disease process. A position statement of the World Obesity Federation. Obes Rev. 2017;18(7):715–23.

102. Blüher M. Obesity: global epidemiology and pathogenesis. Nat Rev Endocrinol [Internet]. 2019;15(5):288–98. Available from: http://dx.doi.org/10.1038/s41574-019-0176-8

103. Qasim A, Turcotte M, de Souza RJ, Samaan MC, Champredon D, Dushoff J, et al. On the origin of obesity: identifying the biological, environmental and cultural drivers of genetic risk among human populations. Obes Rev. 2018;19(2):121–49.

104. Van Der Klaauw AA, Farooqi IS. The hunger genes: Pathways to obesity. Cell [Internet]. 2015;161(1):119–32. Available from:

http://dx.doi.org/10.1016/j.cell.2015.03.008

105. Reilly SM, Saltiel AR. Adapting to obesity with adipose tissue inflammation. Nat Rev Endocrinol [Internet]. 2017;13(11):633–43. Available from: http://dx.doi.org/10.1038/nrendo.2017.90

106. Hotamisligil GS. Inflammation and metabolic disorders. Nature. 2006;444(7121):860–7.

107. Lumeng CN, Saltiel AR. Inflammatory links between obesity and metabolic disease. J Clin Invest. 2011;121(6):2111–7.

108. Kotas ME, Medzhitov R. Homeostasis, inflammation, and disease susceptibility. Cell. 2015;160(5):816–27.

109. Longo M, Zatterale F, Naderi J, Parrillo L, Formisano P, Raciti GA, et al. Adipose tissue dysfunction as determinant of obesity-associated metabolic complications. Int J Mol Sci. 2019;20(9).

110. Pellegrinelli V, Carobbio S, Vidal-Puig A. Adipose tissue plasticity: how fat depots respond differently to pathophysiological cues. Diabetologia [Internet]. 2016;59(6):1075–88. Available from: http://dx.doi.org/10.1007/s00125-016-3933-4

111. Spalding KL, Arner E, Westermark PO, Bernard S, Buchholz BA, Bergmann O, et al. Dynamics of fat cell turnover in humans. Nature. 2008;453(7196):783–7.

112. Weyer C, Foley J.E, Borgadus C, Tataranni P.A, Pratley R.E. Enlarged subcutaneous adbominal adipocyte size, but not obesity itself, predicts Type II diabetes independent of insulin resistance. Diabetologia. 2000;43:1498–506.

113. Skurk T, Alberti-Huber C, Herder C, Hauner H. Relationship between adipocyte size and adipokine expression and secretion. J Clin Endocrinol Metab. 2007;92(3):1023–33.

114. Strissel KJ, Stancheva Z, Miyoshi H, Perfield JW, DeFuria J, Jick Z, et al. Adipocyte death, adipose tissue remodeling, and obesity complications. Diabetes. 2007;56(12):2910–8.

115. Roberts R, Hodson L, Dennis AL, Neville MJ, Humphreys SM, Harnden KE, et al. Markers of de novo lipogenesis in adipose tissue: Associations with small adipocytes and insulin sensitivity in humans. Diabetologia. 2009;52(5):882–90.

116. Wueest S, Rapold RA, Rytka JM, Schoenle EJ, Konrad D. Basal lipolysis, not the degree of insulin resistance, differentiates large from small isolated adipocytes in high-fat fed mice. Diabetologia. 2009;52(3):541–6.

117. Joe AWB, Lin Y, Even Y, Vogl AW, Rossi FMV. Depot-specific differences in adipogenic progenitor abundance and proliferative response to high-fat diet. Stem Cells. 2009;27(10):2563–70.

118. Tchoukalova YD, Koutsari C, Votruba SB, Tchkonia T, Giorgadze N, Thomou T, et al. Sex- and depot-dependent differences in adipogenesis in normal-weight humans. Obes (Silver Spring). 2010;18(10):1875–80.

119. Wilson, M.S. , Metink-Kane MM. Tracking adipogenesis during white adipose tissue development, expansion and regeneration. Nat Med [Internet]. 2013;19(10):1338–44. Available from: https://www.ncbi.nlm.nih.gov/pmc/articles/PMC3624763/pdf/nihms412728.pdf

120. Jeffery E, Church CD, Holtrup B, Colman L, Matthew S. Rapid depot-specific activation of adipocte precursor cells at the Onset of Obesity. Nat Cell Biol. 2015;17(4):376–85.

121. Kim SM, Lun M, Wang M, Senyo SE, Guillermier C, Patwari P, et al. Loss of White Adipose Hyperplastic Potential Is Associated with Enhanced Susceptibility to Insulin Resistance. Cell Metab. 2014;20(6):1049–58.

122. Guillermier C, Fazeli PK, Kim S, Lun M, Zuflacht JP, Milian J, et al. Imaging mass spectrometry demonstrates age-related decline in human adipose plasticity. JCI Insight. 2017;2(5):1–11.

123. Vishvanath L, Gupta RK. Contribution of adipogenesis to healthy adipose tissue expansion in obesity. J Clin Invest. 2019;129(10):4022–31.

124. Gustafson B, Hammarstedt A, Hedjazifar S, Hoffmann JM, Svensson PA, Grimsby J, et al. BMP4 and BMP antagonists regulate human white and beige adipogenesis. Diabetes. 2015;64(5):1670–81.

125. Hammarstedt A, Hedjazifar S, Jenndahl L, Gogg S, Gruñberg J, Gustafson B, et al. WISP2 regulates preadipocyte commitment and PPARγ activation by BMP4. Proc Natl Acad Sci U S A. 2013;110(7):2563–8.

126. Hammarstedt A, Gogg S, Hedjazifar S, Nerstedt A, Smith U. Impaired adipogenesis and dysfunctional adipose tissue in human hypertrophic obesity. Physiol Rev.

2018;98(4):1911–41.

127. Aprile M, Cataldi S, Ambrosio MR, D'Esposito V, Lim K, Dietrich A, et al. PPARγΔ5, a Naturally Occurring Dominant-Negative Splice Isoform, Impairs PPARγ Function and Adipocyte Differentiation. Cell Rep. 2018;25(6):1577–92.

128. Alessi M, Bastelica D, Morange P, Berthet B, Leduc I, Verdier M, et al. Plasminogen activator inhibitor 1, transforming growth factor-beta1, and BMI are closely associated in human adipose tissue during morbid obesity. Diabetes. 2000;49(August):1374–80.

129. van Beek L, van Klinken JB, Pronk ACM, van Dam AD, Dirven E, Rensen PCN, et al. The limited storage capacity of gonadal adipose tissue directs the development of metabolic disorders in male C57Bl/6J mice. Diabetologia. 2015;58(7):1601–9.

130. Saad MJA, Santos A, Prada PO. Linking gut microbiota and inflammation to obesity and insulin resistance. Physiology. 2016;31(4):283–93.

131. Nguyen MTA, Favelyukis S, Nguyen AK, Reichart D, Scott PA, Jenn A, et al. A subpopulation of macrophages infiltrates hypertrophic adipose tissue and is activated by free fatty acids via toll-like receptors 2 and 4 and JNK-dependent pathways. J Biol Chem [Internet]. 2007;282(48):35279–92. Available from: http://dx.doi.org/10.1074/jbc.M706762200

132. Pasarica M, Sereda OR, Redman LM, Albarado DC, Hymel DT, Roan LE, et al. Reduced adipose tissue oxygenation in human obesity evidence for rarefaction, macrophage chemotaxis, and inflammation without an angiogenic response. Diabetes. 2009;58(3):718–25.

133. Cao Y. Adipose tissue angiogenesis as a therapeutic target for obesity and metabolic diseases. Nat Rev Drug Discov [Internet]. 2010;9(2):107–15. Available from: http://dx.doi.org/10.1038/nrd3055

134. Hosogai N, Fukuhara A, Oshima K, Miyata Y, Tanaka S, Segawa K, et al. Adipose tissue hypoxia in obesity and its impact on adipocytokine dysregulation. Diabetes. 2007;56(4):901–11.

135. Trayhurn P. Hypoxia and adipose tissue function and dysfunction in obesity. Physiol Rev. 2013;93(1):1–21.

136. Rausch ME, Weisberg S, Vardhana P, Tortoriello D V. Obesity in C57BL/6J mice is characterized by adipose tissue hypoxia and cytotoxic T-cell infiltration. Int J Obes.

2008;32(3):451–63.

137. Lumeng CN, DeYoung SM, Bodzin JL, Saltiel AR. Increased inflammatory properties of adipose tissue macrophages recruited during diet-induced obesity. Diabetes. 2007;56(1):16–23.

138. Haase J, Weyer U, Immig K, Klöting N, Blüher M, Eilers J, et al. Local proliferation of macrophages in adipose tissue during obesity-induced inflammation. Diabetologia. 2014;57(3):562–71.

139. Odegaard JI, Ricardo-gonzalez RR, Goforth MH, Christine R, Subramanian V, Mukundan L, et al. Macrophage-specific PPARγ controls alternative activation and improves insulin resistance. Nature. 200AD;447(7148):1116–20.

140. Kang K, Reilly SM, Karabacak V, Gangl MR, Fitzgerald K, Hatano B, et al. Adipocyte-Derived Th2 Cytokines and Myeloid PPARδ Regulate Macrophage Polarization and Insulin Sensitivity. Cell Metab. 2008;7(6):485–95.

141. Fujisaka S, Usui I, Bukhari A, Ikutani M, Oya T, Kanatani Y, et al. Regulatory mechanisms for adipose tissue M1 and M2 macrophages in diet-induced obese mice. Diabetes. 2009;58(11):2574–82.

142. Wang L xun, Zhang S xi, Wu H juan, Rong X lu, Guo J. M2b macrophage polarization and its roles in diseases. J Leukoc Biol. 2019;106(2):345–58.

143. Li Y, Yun K, Mu R. A review on the biology and properties of adipose tissue macrophages involved in adipose tissue physiological and pathophysiological processes. Lipids Health Dis. 2020;19(1):1–9.

144. Olefsky JM, Glass CK. Macrophages, Inflammation, and Insulin Resistance. Annu Rev Physiol [Internet]. 2010 Mar 17 [cited 2019 Feb 13];72(1):219–46. Available from: http://www.annualreviews.org/doi/10.1146/annurev-physiol-021909-135846

145. Shi H, Kokoeva M V., Inouye K, Tzameli I, Yin H, Flier JS. TLR4 links innate immunity and fatty acid-induced insulin resistance. J Clin Invest. 2006;116(11):3015–25.

146. Himes RW, Smith CW. Tlr2 is critical for diet-induced metabolic syndrome in a murine model . FASEB J. 2010;24(3):731–9.

147. Zick Y. Ser / Thr Phosphorylation of IRS Proteins: A Molecular Basis for Insulin Resistance. Sci stke. 2005;(268):1–3.

148. Nakamura T, Furuhashi M, Li P, Cao H, Tuncman G, Sonenberg N, et al. Double-

stranded RNA-dependent protein kinase links pathogen sensing with stress and metabolic homeostasis. Cell [Internet]. 2010;140(3):338–48. Available from: https://www.ncbi.nlm.nih.gov/pmc/articles/PMC3624763/pdf/nihms412728.pdf

149. Xu X, Grijalva A, Skowronski A, Van Eijk M, Serlie MJ, Ferrante AW. Obesity activates a program of lysosomal-dependent lipid metabolism in adipose tissue macrophages independently of classic activation. Cell Metab. 2013;18(6):816–30.

150. Bray GA, Heisel WE, Afshin A, Jensen MD, Dietz WH, Long M, et al. The science of obesity management: An endocrine society scientific statement. Endocr Rev. 2018;39(2):79–132.

151. Gadde KM, Martin CK, Berthoud H, Steven B, Biomedical P, Rouge B. Obesity: Pathophysiology and Management. J Am Coll Cardiol. 2018;71(1):69–84.

152. Bray GA, Frühbeck G, Ryan DH, Wilding JPH. Management of obesity. Lancet. 2016;387(10031):1947–56.

153. Heymsfield SB, Wadden TA. Mechanisms, Pathophysiology, and Management of Obesity. N Engl J Med. 2017;376(3):254–66.

154. Magkos F, Hjorth MF, Astrup A. Diet and exercise in the prevention and treatment of type 2 diabetes mellitus. Nat Rev Endocrinol [Internet]. 2020;16(10):545–55. Available from: http://dx.doi.org/10.1038/s41574-020-0381-5

155. Speakman JR, Mitchell SE. Caloric restriction. Mol Aspects Med [Internet]. 2011;32(3):159–221. Available from: http://dx.doi.org/10.1016/j.mam.2011.07.001

156. McCracken AW, Adams G, Hartshorne L, Tatar M, Simons MJP. The hidden costs of dietary restriction: Implications for its evolutionary and mechanistic origins. Sci Adv. 2020;6(8):1–12.

157. Griel AE, Ruder EH, Kris-Etherton PM. The changing roles of dietary carbohydrates: From simple to complex. Arterioscler Thromb Vasc Biol. 2006;26(9):1958–65.

158. Astrup A, Magkos F, Bier DM, Brenna JT, de Oliveira Otto MC, Hill JO, et al. Saturated Fats and Health: A Reassessment and Proposal for Food-Based Recommendations: JACC State-of-the-Art Review. J Am Coll Cardiol. 2020;76(7):844–57.

159. Calder PC. Functional Roles of Fatty Acids and Their Effects on Human Health. J Parenter Enter Nutr. 2015;39:18S-32S.

160. Soriguer F, Rojo-Martínez G, Goday A, Bosch-Comas A, Bordiú E, Caballero-Díaz F, et al. Olive oil has a beneficial effect on impaired glucose regulation and other cardiometabolic risk factors. Di@bet.es study. Eur J Clin Nutr. 2013;67(9):911–6.

161. Hsu KJ, Liao C De, Tsai MW, Chen CN. Effects of exercise and nutritional intervention on body composition, metabolic health, and physical performance in adults with sarcopenic obesity: A meta-analysis. Nutrients. 2019;11(9).

162. Zouhal H, Ben Abderrahman A, Khodamoradi A, Saeidi A, Jayavel A, Hackney AC, et al. Effects of physical training on anthropometrics, physical and physiological capacities in individuals with obesity: A systematic review. Obes Rev. 2020;21(9).

163. Pontzer H. Constrained Total Energy Expenditure and the Evolutionary Biology of Energy Balance. Exerc Sport Sci Rev. 2015;43(3):110–6.

164. Severinsen MCK, Pedersen BK. Muscle–Organ Crosstalk: The Emerging Roles of Myokines. Endocr Rev. 2020;41(4):594–609.

165. Lair B, Laurens C, Van Den Bosch B, Moro C. Novel insights and mechanisms of lipotoxicity-driven insulin resistance. Int J Mol Sci. 2020;21(17):1–27.

166. Czech MP. Insulin action and resistance in obesity and type 2 diabetes. Nat Med. 2017;23(7):804–14.

167. Watt MJ, Miotto PM, De Nardo W, Montgomery MK. The Liver as an Endocrine Organ - Linking NAFLD and Insulin Resistance. Endocr Rev. 2019;40(5):1367–93.

168. Meex RCR, Watt MJ. Hepatokines: Linking nonalcoholic fatty liver disease and insulin resistance. Nat Rev Endocrinol [Internet]. 2017;13(9):509–20. Available from: http://dx.doi.org/10.1038/nrendo.2017.56

169. Estes C, Razavi H, Loomba R, Younossi Z, Sanyal AJ. Modeling the epidemic of nonalcoholic fatty liver disease demonstrates an exponential increase in burden of disease. Hepatology. 2018;67(1):123–33.

170. Younossi ZM, Koenig AB, Abdelatif D, Fazel Y, Henry L, Wymer M. Global epidemiology of nonalcoholic fatty liver disease—Meta-analytic assessment of prevalence, incidence, and outcomes. Hepatology. 2016;64(1):73–84.

171. Bugianesi E, Gastaldelli A, Vanni E, Gambino R, Cassader M, Baldi S, et al. Insulin resistance in non-diabetic patients with non-alcoholic fatty liver disease: Sites and mechanisms. Diabetologia. 2005;48(4):634–42.

172. Korenblat KM, Fabbrini E, Mohammed BS, Klein S. Liver, muscle, and adipose tissue insulin action is directly related to intrahepatic triglyceride content in obese subjects. Gastroenterology. 2008;134(5):1369–75.

173. Marchesini G, Brizi M, Bianchi G, Tomassetti S, Bugianesi E, Lenzi M, et al. Nonalcoholic fatty liver disease: a feature of the metabolic syndrome. Diabetes. 2001;50(8):1844–50.

174. Dongiovanni P, Stender S, Pietrelli A, Mancina RM, Cespiati A, Petta S, et al. Causal relationship of hepatic fat with liver damage and insulin resistance in nonalcoholic fatty liver. J Intern Med. 2018;283(4):356–70.

175. Manchanayake J, Chitturi S, Nolan C, Farrell GC. Postprandial hyperinsulinemia is universal in non-diabetic patients with nonalcoholic fatty liver disease. J Gastroenterol Hepatol. 2011;26(3):510–6.

176. McClain CJ, Barve S, Deaciuc I. Good fat/bad fat. Hepatology. 2007;45(6):1343–6.

177. Samuel VT, Liu ZX, Wang A, Beddow SA, Geisler JG, Kahn M, et al. Inhibition of protein kinase Cε prevents hepatic insulin resistance in nonalcoholic fatty liver disease. J Clin Invest. 2007;117(3):739–45.

178. Perry RJ, Samuel VT, Petersen KF, Shulman GI. The role of hepatic lipids in hepatic insulin resistance and type 2 diabetes. Gene Expr. 2014;510(7503):84–91.

179. Pagadala M, Kasumov T, McCullough AJ, Zein NN, Kirwan JP. Role of Ceramides in Nonalcoholic Fatty Liver Disease. Trends Endocrinol Metab. 2012;23(8):365–71.

180. Konstantynowicz-Nowicka K, Harasim E, Baranowski M, Chabowski A. New evidence for the role of ceramide in the development of hepatic insulin resistance. PLoS One. 2015;10(1):1–13.

181. Dresner A, Laurent D, Marcucci M, Griffin ME, Dufour S, Cline GW, et al. Effects of free fatty acids on glucose transport and IRS-1 – associated phosphatidylinositol 3-kinase activity. J Clin Invest. 1999;103(2):253–9.

182. Boden G, Chen X, Ruiz J. Mechanisms of fatty acid-induced inhibition of glucose uptake. J Clin Invest. 1994;93:2438–46.

183. Morales PE, Bucarey JL, Espinosa A. Muscle lipid metabolism: Role of lipid droplets and perilipins. J Diabetes Res. 2017;2017:1–10.

184. Itani SI, Ruderman NB, Schmieder F, Boden G. Lipid-induced insulin resistance in

human muscle is associated with changes in diacylglycerol, protein kinase C, and IkappaB-alpha. Diabetes [Internet]. 2002;51:2005–11. Available from: http://www.diabetes.org/diabetes/

185. Dubé JJ, Amati F, Stefanovic-Racic M, Toledo FGS, Sauers SE, Goodpaster BH. Exercise-induced alterations in intramyocellular lipids and insulin resistance: The athlete's paradox revisited. Am J Physiol - Endocrinol Metab. 2008;294(5):882–8.

186. Fahy E, Subramaniam S, Brown HA, Glass CK, Merrill AH, Murphy RC, et al. A comprehensive classification system for lipids. J Lipid Res. 2005;46(5):839–61.

187. Fahy E, Cotter D, Sud M, Subramaniam S. Lipid classification, structures and tools. Biochim Biophys Acta. 2011;1811(11):637–47.

188. Lydic TA, Goo Y-H. Lipidomics unveils the complexity of the lipidome in metabolic diseases. Lydic Goo Clin Trans Med [Internet]. 2018;7(4):1–13. Available from: https://doi.org/10.1186/s40169-018-0182-9

189. Wenk MR. The emerging field of lipidomics. Nat Rev Drug Discov. 2005;4(7):594–610.

190. Pradas I, Huynh K, Cabré R, Ayala V, Meikle PJ, Jové M, et al. Lipidomics reveals a tissue-specific fingerprint. Front Physiol. 2018;9:1–17.

191. Gonzalez-franquesa A, Gama-perez P, Kulis M, Szczepanowska K, Dahdah N, Moreno-gomez S, et al. Remission of obesity and insulin resistance is not sufficient to restore mitochondrial homeostasis in visceral adipose tissue. Redox Biol [Internet]. 2022; Available from: https://doi.org/10.1016/j.redox.2022.102353

192. Vinaixa M, Ángel Rodríguez M, Rull A, Beltrán R, Bladé C, Brezmes J, et al. Metabolomic assessment of the effect of dietary cholesterol in the progressive development of fatty liver disease. J Proteome Res. 2010;9(5):2527–38.

193. Teijeiro A, Garrido A, Ferre A, Perna C, Djouder N. Inhibition of the IL-17A axis in adipocytes suppresses diet-induced obesity and metabolic disorders in mice. Nat Metab [Internet]. 2021;3(4):496–512. Available from: http://dx.doi.org/10.1038/s42255-021-00371-1

194. Ma L, Ni Y, Wang Z, Tu W, Ni L, Zhuge F, et al. Spermidine improves gut barrier integrity and gut microbiota function in diet-induced obese mice. Gut Microbes [Internet]. 2020;12(1):1–19. Available from: https://doi.org/10.1080/19490976.2020.1832857

195. Xu L, Nagata N, Nagashimada M, Zhuge F, Ni Y, Chen G, et al. SGLT2 Inhibition by Empagliflozin Promotes Fat Utilization and Browning and Attenuates Inflammation and Insulin Resistance by Polarizing M2 Macrophages in Diet-induced Obese Mice. EBioMedicine [Internet]. 2017;20:137–49. Available from: http://dx.doi.org/10.1016/j.ebiom.2017.05.028

196. Acosta-Rodríguez VA, H.M. de Groot M, Rijo-Ferreira F, Green CB, Takahashi JS. Mice Under Caloric Restriction Self-Impose a Temporal Restriction of Food Intake as Revealed by an Automated Feeder System. Cell Metab. 2017;26(1):267–77.

197. Arble DM, Bass J, Laposky AD, Vitaterna MH, Turek FW. Circadian timing of food intake contributes to weight gain. Obesity. 2009;17(11):2100–2.

198. Shamsi NA, Salkeld MD, Rattanatray L, Voultsios A, Varcoe TJ, Boden MJ, et al. Metabolic consequences of timed feeding in mice. Physiol Behav [Internet]. 2014;128:188–201. Available from: http://dx.doi.org/10.1016/j.physbeh.2014.02.021

199. Chaix A, Deota S, Bhardwaj R, Lin T, Panda S. Sex- and age-dependent outcomes of 9-hour time-restricted feeding of a Western high-fat high-sucrose diet in C57BL/6J mice. Cell Rep. 2021;36(7):1–27.

200. Regmi P, Chaudhary R, Page AJ, Hutchison AT, Vincent AD, Liu B, et al. Early or delayed time-restricted feeding prevents metabolic impact of obesity in mice. J Endocrinol. 2021;248(1):75–86.

201. García-Gaytán AC, Miranda-Anaya M, Turrubiate I, López-De Portugal L, Bocanegra-Botello GN, López-Islas A, et al. Synchronization of the circadian clock by time-restricted feeding with progressive increasing calorie intake. Resemblances and differences regarding a sustained hypocaloric restriction. Sci Rep. 2020;10(1):1–17.

202. Jain M, Ngoy S, Sheth SA, Swanson RA, Rhee EP, Liao R, et al. A systematic survey of lipids across mouse tissues. Am J Physiol - Endocrinol Metab. 2014;306(8):854–68.

203. Hou B, Zhao Y, He P, Xu C, Ma P, Lam SM, et al. Targeted lipidomics and transcriptomics profiling reveal the heterogeneity of visceral and subcutaneous white adipose tissue. Life Sci. 2020 Mar 15;245:1–12.

204. Cortie CH, Hulbert AJ, Hancock SE, Mitchell TW, McAndrew D, Else PL. Of mice, pigs and humans: An analysis of mitochondrial phospholipids from mammals with very different maximal lifespans. Exp Gerontol [Internet]. 2015;70:135–43. Available

from: http://dx.doi.org/10.1016/j.exger.2015.08.011

205. Turner N, Kowalski GM, Leslie SJ, Risis S, Yang C, Lee-Young RS, et al. Distinct patterns of tissue-specific lipid accumulation during the induction of insulin resistance in mice by high-fat feeding. Diabetologia. 2013;56(7):1638–48.

206. Borg ML, Omran SF, Weir J, Meikle PJ, Watt MJ. Consumption of a high-fat diet, but not regular endurance exercise training, regulates hypothalamic lipid accumulation in mice. J Physiol. 2012 Sep;590(17):4377–89.

207. Lee JC, Park SM, Kim IY, Sung H, Seong JK, Moon MH. High-fat diet-induced lipidome perturbations in the cortex, hippocampus, hypothalamus, and olfactory bulb of mice. Biochim Biophys Acta - Mol Cell Biol Lipids. 2018 Sep 1;1863(9):980–90.

208. Mannock DA, Lewis RNAH, Mcmullen TPW, Mcelhaney RN. The effect of variations in phospholipid and sterol structure on the nature of lipid – sterol interactions in lipid bilayer model membranes. Chem Phys Lipids [Internet]. 2010;163(6):403–48. Available from: http://dx.doi.org/10.1016/j.chemphyslip.2010.03.011

209. Morgan AE, Auley MTM. Cholesterol homeostasis: An in silico investigation into how aging disrupts its key hepatic regulatory mechanisms. Biology (Basel). 2020;9(10):1–18.

210. Veen JN Van Der, Kennelly JP, Wan S, Vance JE, Vance DE, Jacobs RL. The critical role of phosphatidylcholine and phosphatidylethanolamine metabolism in health and disease. BBA - Biomembr [Internet]. 2017;1859(9):1558–72. Available from: http://dx.doi.org/10.1016/j.bbamem.2017.04.006

211. Griffin ME, Marcucci MJ, Cline GW, Bell K, Barucci N, Lee D, et al. Free Fatty Acid–Induced Insulin Resistance Is Associated With Activation of Protein Kinase C theta and Alterations in the Insulin Signaling Cascade. Diabetes. 1999;48(June):1270–4.

212. Yu C, Chen Y, Cline GW, Zhang D, Zong H, Wang Y, et al. Mechanism by Which Fatty Acids Inhibit Insulin Activation of Insulin Receptor Substrate-1 (IRS-1) -associated Phosphatidylinositol 3-Kinase Activity in Muscle. J Biol Chem [Internet]. 2002;277(52):50230–6. Available from: http://dx.doi.org/10.1074/jbc.M200958200

213. Goodpaster BH, He J, Watkins S, Kelley DE. Skeletal muscle lipid content and insulin resistance: Evidence for a paradox in endurance-trained athletes. J Clin Endocrinol Metab. 2001;86(12):5755–61.

214. Erion DM, Shulman GI. Diacylglycerol-mediated insulin resistance. Nat Med. 2013;16(4):400–2.

215. Dubé JJ, Amati F, Stefanovic-racic M, Toledo FGS, Sarah E, Goodpaster BH. Exercise-Induced alterations in intramyocellular lipids and insulin resistance: The athlete's paradox revisited. Am J Physiol Endocrinol Metab. 2013;294(5):1–15.

216. Turner N, Cooney GJ, Kraegen EW, Bruce CR. Fatty acid metabolism, energy expenditure and insulin resistance in muscle. Vol. 220, Journal of Endocrinology. 2014. p. 61–79.

217. Kim J, Hickner RC, Cortright RL, Dohm GL, Houmard JA, Hickner RC, et al. Lipid oxidation is reduced in obese human skeletal muscle. Am J Physiol Endocrinol Metab. 2000;279:1039–44.

218. Hulver MW, Berggren JR, Cortright RN, Dudek RW, Thompson RP, Pories WJ, et al. Skeletal muscle lipid metabolism with obesity. Am J Physiol Endocrinol Metab. 2003 Apr 1;284:741–7.

219. Kelley DE, He J, Menshikova E V, Ritov VB. Dysfunction of mitochondria in human skeletal muscle in type 2 diabetes. Diabetes. 2002;51:2944–50.

220. Holloway GP, Bonen A, Spriet LL. Regulation of skeletal muscle mitochondrial fatty acid metabolism in lean and obese individuals. Am J Clin Nutr. 2009;89:455–62.

221. Garcia-roves P, Huss JM, Han D, Hancock CR, Iglesias-gutierrez E, Chen M, et al. Raising plasma fatty acid concentration induces increased biogenesis of mitochondria in skeletal muscle. PNAS. 2007;104(25):10709–13.

222. Holmström MH, Iglesias-gutierrez E, Zierath JR, Garcia-roves PM. Tissue-specific control of mitochondrial respiration in obesity-related insulin resistance and diabetes. Am J Physiol Endocrinol Metab. 2012;302:731–9.

223. Turner N, Bruce CR, Beale SM, Hoehn KL, So T, Rolph MS, et al. Excess lipid availability increases mitochondrial fatty acid oxidative capacity in muscle. Evidence against a role for reduced fatty acid oxidation in lipid-induced insulin resistance. Diabetes. 2007;56(August):2085–92.

224. Bosma M. Lipid homeostasis in exercise. Drug Discov Today [Internet]. 2014;19(7):1019–23. Available from: http://dx.doi.org/10.1016/j.drudis.2014.03.007

225. Kiens B. Skeletal Muscle Lipid Metabolism in Exercise and Insulin Resistance. Physiol Rev. 2006;86:205–43.

226. Hargreaves M, Spriet LL. Exercise metabolism: Fuels for the fire. Cold Spring Harb Perspect Med. 2018;8:1–15.

227. Madsbad S. Dietary intervention increases n-3 long-chain polyunsaturated fatty acids in skeletal muscle membrane phospholipids of obese subjects . Implications for insulin sensitivity. Clin Endocrinol. 2006;64:169–78.

228. Turner N, Lee JS, Bruce CR, Mitchell TW, Else PL, Hulbert AJ, et al. Greater effect of diet than exercise training on the fatty acid profile of rat skeletal muscle. J Appl Physiol. 2021;974–80.

229. Ibrahim A, Natarajan S. Substituting dietary linoleic acid with a -linolenic acid improves insulin sensitivity in sucrose fed rats. BBA. 2005;1733:67–75.

230. Windt DJ Van Der, Sud V, Zhang H, Tsung A, Huang H, Nash B. The effects of physical exercise on fatty liver disease. Gene Expression. 2018;18:89–101.

231. Nguyen P, Leray V, Diez M, Serisier S, Bloc J Le, Siliart B, et al. Liver lipid metabolism. J Anim Physiol Anim Nutr. 2008;92:272–83.

232. Svegliati-baroni G, Pierantonelli I, Torquato P, Marinelli R, Ferreri C, Chatgilialoglu C, et al. Lipidomic biomarkers and mechanisms of lipotoxicity in non-alcoholic fatty liver disease. Free Radic Biol Med [Internet]. 2019;144(May):293–309. Available from: https://doi.org/10.1016/j.freeradbiomed.2019.05.029

233. Fuente FP, Quezada L, Sepúlveda C, Monsalves-alvarez M, Rodríguez JM, Sacristán C, et al. Exercise regulates lipid droplet dynamics in normal and fatty liver. BBA - Mol Cell Biol Lipids [Internet]. 2019;1864(12):1–10. Available from: https://doi.org/10.1016/j.bbalip.2019.158519

234. Trentzsch M, Nyamugenda E, Miles TK, Grif H, Russell S, Koss B, et al. Delivery of phosphatidylethanolamine blunts stress in hepatoma cells exposed to elevated palmitate by targeting the endoplasmic reticulum. Cell Death Discov. 2020;6(8):1–16.

235. Signaling I, Zorzano A, Sebastia D, Mun JP. Mitofusin 2 as a Driver That Controls Energy. ANTIOXIDANTS & REDOX SIGNALING. 2015;22(12):1020–31.

236. Golabi P, Locklear CT, Austin P, Afdhal S, Byrns M, Gerber L, et al. Effectiveness of

exercise in hepatic fat mobilization in non- alcoholic fatty liver disease: Systematic review. World J Gastroenterol. 2016;22(27):6318–27.

237. Grzybek M, Palladini A, Alexaki VI, Surma MA, Simons K. Comprehensive and quantitative analysis of white and brown adipose tissue by shotgun lipidomics. Mol Metab [Internet]. 2019;22(January):12–20. Available from: https://doi.org/10.1016/j.molmet.2019.01.009

238. Virtue S, Vidal-puig A. Adipose tissue expandability, lipotoxicity and the Metabolic Syndrome — An allostatic perspective. BBA - Mol Cell Biol Lipids [Internet]. 2010;1801(3):338–49. Available from: http://dx.doi.org/10.1016/j.bbalip.2009.12.006

239. Ferrara D, Montecucco F, Dallegri F, Carbone F. Impact of different ectopic fat depots on cardiovascular and metabolic diseases. J Cell Physiol. 2019;234:21630–41.

240. Rasouli N, Molavi B, Elbein SC, Kern PA. Ectopic fat accumulation and metabolic syndrome. Diabetes Obes Metab. 2007;9:1–10.

241. Caesar R, Manieri M, Kelder T, Boekschoten M, Evelo C, Kooistra T, et al. A combined transcriptomics and lipidomics analysis of subcutaneous , epididymal and mesenteric adipose tissue reveals marked functional differences. PLoS One. 2010;5(7).

242. Piché M, Poirier P. Ectopic fat and cardiac metabolism. Expert Rev Endocrinol Metab [Internet]. 2018;13(4):213–21. Available from: https://doi.org/10.1080/17446651.2018.1500894

243. Zabielski P, Ksi M. The impact of oMEGA-3 fatty acids supplementation on insulin resistance and content of adipocytokines and biologically active lipids in adipose tissue of high-fat diet fed rats. Nutrients. 2019;11(835):1–18.

244. Rocha-rodrigues S, Rodríguez A, Gonçalves IO, Moreira A, Maciel E, Santos S, et al. Impact of physical exercise on visceral adipose tissue fatty acid pro fi le and inflammation in response to a high-fat diet regimen. Int J Biochem Cell Biol [Internet]. 2017;87(April):114–24. Available from: http://dx.doi.org/10.1016/j.biocel.2017.04.008

245. Parlee SD, Lentz SI, Mori H, MacDougald OA. Quantifying size and number of adipocytes in adipose tissue. Methods Enzymol. 2014;537:93–122.

246. Cottam DR, Mattar SG, Barinas-Mitchell E, Eid G, Kuller L, Kelley DE, et al. The chronic inflammatory hypothesis for the morbidity associated with morbid obesity: Implications and effect of weight loss. Obes Surg. 2004;14(5):589–600.

247. Burhans MS, Hagman DK, Kuzma JN, Schmidt KA, Kratz M, Program P, et al. Contribution of adipose tissue inflammation to the development of type 2 diabetes HHS Public Access. Physiol Behav. 2019;9(1):1–58.

248. Magkos F, Fraterrigo G, Yoshino J, Luecking C, Kirbach K, Kelly SC, et al. Effects of moderate and subsequent progressive weight loss on metabolic function and adipose tissue biology in humans with obesity. Cell Metab. 2016;23(4):591–601.

249. Capel F, Klimčáková E, Viguerie N, Roussel B, Vítková M, Kováčiková M, et al. Macrophages and adipocytes in human obesity: Adipose tissue gene expression and insulin sensitivity during calorie restriction and weight stabilization. Diabetes. 2009;58(7):1558–67.

250. Kováčiková M, Sengenes C, Kováčová Z, Šiklová-Vítková M, Klimčáková E, Polák J, et al. Dietary intervention-induced weight loss decreases macrophage content in adipose tissue of obese women. Int J Obes. 2011;35(1):91–8.

251. Srámková V, Rossmeislová L, Krauzová E, Kračmerová J, Koc M, Langin D, et al. Comparison of early (2 Days) and Later (28 Days) response of adipose tissue to very low-calorie diet in obese women. J Clin Endocrinol Metab. 2016;101(12):5021–9.

252. Schmitz J, Evers N, Awazawa M, Nicholls HT, Brönneke HS, Dietrich A, et al. Obesogenic memory can confer long-term increases in adipose tissue but not liver inflammation and insulin resistance after weight loss. Mol Metab [Internet]. 2016;5(5):328–39. Available from: http://dx.doi.org/10.1016/j.molmet.2015.12.001

253. Horiguchi M, Hata S, Tsurudome Y, Ushijima K. Characterizing the degeneration of nuclear membrane and mitochondria of adipose-derived mesenchymal stem cells from patients with type II diabetes. J Cell Mol Med. 2021;25(9):4298–306.

254. Choi JW, Jo A, Kim M, Park HS, Chung SS, Kang S, et al. BNIP3 is essential for mitochondrial bioenergetics during adipocyte remodelling in mice. Diabetologia. 2016;59(3):571–81.

255. Michalek RD, Gerriets VA, Jacobs SR, Macintyre AN, MacIver NJ, Mason EF, et al.

Cutting Edge: Distinct Glycolytic and Lipid Oxidative Metabolic Programs Are Essential for Effector and Regulatory CD4+ T Cell Subsets. J Immunol. 2011;186(6):3299–303.

256. Chen YC, Wu YT, Wei YH. Depletion of mitoferrins leads to mitochondrial dysfunction and impairment of adipogenic differentiation in 3T3-L1 preadipocytes. Free Radic Res. 2015;49(11):1285–95.

257. Kladnická I, Čedíková M, Kripnerová M, Dvořáková J, Kohoutová M, Tůma Z, et al. Mitochondrial respiration of adipocytes differentiating from human mesenchymal stem cells derived from adipose tissue. Physiol Res. 2019;68:S287–96.

258. Hofmann AD, Beyer M, Krause-Buchholz U, Wobus M, Bornhäuser M, Rödel G. Oxphos supercomplexes as a hallmark of the mitochondrial phenotype of adipogenic differentiated human MSCS. PLoS One. 2012;7(4).

259. Zhang Y, Marsboom G, Toth PT, Rehman J. Mitochondrial Respiration Regulates Adipogenic Differentiation of Human Mesenchymal Stem Cells. PLoS One. 2013;8(10).

260. Joffin N, Paschoal VA, Gliniak CM, Crewe C, Szweda LI, Zhang Q, et al. Mitochondrial metabolism is a key regulator of the fibro- inflammatory and adipogenic stromal subpopulations in white adipose tissue. Cell Stem Cell. 2021;28(4):702–17.

261. Hepler C, Shan B, Zhang Q, Henry GH, Shao M, Vishvanath L, et al. Identification of functionally distinct fibro-inflammatory and adipogenic stromal subpopulations in visceral adipose tissue of adult mice. Elife. 2018;7:1–36.

262. Vishvanath L, MacPherson KA, Hepler C, Wang QA, Shao M, Spurgin SB, et al. Pdgfrβ+ Mural Preadipocytes Contribute to Adipocyte Hyperplasia Induced by High-Fat Diet Feeding and Prolonged Cold Exposure in Adult Mice. Cell Metab. 2016;23(2):350–9.

263. Gupta RK, Mepani RJ, Kleiner S, Lo JC, Khandekar MJ, Frontini A, et al. Zfp423 expression identifies committed preadipocytes and localizes to adipose endothelial and perivascular cells. Cell Metab. 2012;15(2):230–9.

264. Shan B, Shao M, Zhang Q, Hepler C, Paschoal VA, Barnes SD, et al. Perivascular Mesenchymal Cells Control Adipose Tissue Macrophage Accrual in Obesity. Nat Metab. 2020;2(11):1332–49.

265. Caslin HL, Bhanot M, Bolus WR, Hasty AH. Adipose tissue macrophages: Unique

polarization and bioenergetics in obesity. Immunol Rev. 2020;295(1):101–13.

266. Russo L, Lumeng CN. Properties and functions of adipose tissue macrophages in obesity. Immunology. 2018;155(4):407–17.

267. Amano SU, Cohen JL, Vangala P, Tencerova M, Sarah M, Yawe JC, et al. Local proliferation of macrophages contributes to obesity- associated adipose tissue inflammation. Cell Metab. 2014;19(1):162–71.

268. Zamarron BF, Mergian TA, Cho KW, Martinez-Santibanez G, Luan D, Singer K, et al. Macrophage proliferation sustains adipose tissue inflammation in formerly obese mice. Diabetes. 2017;66(2):392–406.

269. Muir LA, Kiridena S, Griffin C, DelProposto JB, Geletka L, Martinez-Santibañez, et al. Rapid adipose tissue expansion triggers unique proliferation and lipid accumulation profiles in adipose tissue macrophages. J Leukoc Biol. 2018;103(4):615–28.

270. Orlicky DJ, Libby AE, Bales ES, McMahan RH, Monks J, La Rosa FG, et al. Perilipin-2 promotes obesity and progressive fatty liver disease in mice through mechanistically distinct hepatocyte and extra-hepatocyte actions. J Physiol. 2019;597(6):1565–84.

271. O'Neill LAJ, Kishton RJ, Rathmell J. A guide to immunometabolism for immunologists. Nat Rev Immunol. 2016;16(9):553–65.

272. Liu PS, Wang H, Li X, Chao T, Teav T, Christen S, et al. a-Ketoglutarate Orchestrates Macrophage Activation Through Metabolic and Epigenetic Reprogramming. Nat Immunol. 2017;18(9):985–94.

273. Jha AK, Huang SCC, Sergushichev A, Lampropoulou V, Ivanova Y, Loginicheva E, et al. Network integration of parallel metabolic and transcriptional data reveals metabolic modules that regulate macrophage polarization. Immunity [Internet]. 2015;42(3):419–30. Available from: http://dx.doi.org/10.1016/j.immuni.2015.02.005

274. Boutens L, Hooiveld GJ, Dhingra S, Cramer RA, Netea MG, Stienstra R. Unique metabolic activation of adipose tissue macrophages in obesity promotes inflammatory responses. Diabetologia. 2018;61(4):942–53.

275. Kadl A, Meher AK, Sharma PR, Lee MY, Doran AC, Johnstone SR, et al. Identification of a novel macrophage phenotype that develops in response to atherogenic

phospholipids via Nrf2. Circ Res. 2010;107(6):737–46.

276. Kosteli A, Sugaru E, Haemmerle G, Martin JF, Lei J, Zechner R, et al. Weight loss and lipolysis promote a dynamic immune response in murine adipose tissue. J Clin Invest. 2010;120(10):3466–79.

277. Weinstock A, Brown EJ, Garabedian ML, Pena S, Sharma M, Lafaille J, et al. Single-Cell RNA Sequencing of Visceral Adipose Tissue Leukocytes Reveals that Caloric Restriction Following Obesity Promotes the Accumulation of a Distinct Macrophage Population with Features of Phagocytic Cells. Immunometabolism. 2019;1:1–26.

278. Burl RB, Ramseyer VD, Rondini EA, Pique-regi R, Lee YH, Granneman JG. Deconstructing adipogenesis induced by β3-adrenergic receptor activation with single-cell expression profiling. Cell Metab. 2019;28(2):300–9.

279. Carobbio S, Pellegrinelli V, Vedal-Puig A. Adipose Tissue Function and Expandability as Determinants of Lipotoxicity and the Metabolic Syndrome. Adv Exp Med Biol. 2017;960:161–96.

280. Lee YJ, Ko EH, Kim JE, Kim E, Lee H, Choi H, et al. Nuclear receptor PPARγ-regulated monoacylglycerol O-acyltransferase 1 (MGAT1) expression is responsible for the lipid accumulation in diet-induced hepatic steatosis. Proc Natl Acad Sci U S A. 2012;109(34):13656–61.

281. Datta R, Podolsky MJ, Atabai K. Fat fibrosis: friend or foe? JCI insight. 2018;3(19):1–16.

282. Sun K, Tordjman J, Clément K, Scherer PE. Fibrosis and adipose tissue dysfunction. Cell Metab. 2013;18(4):470–7.

283. Song B, Zhang H, Zhang S. Toll-like receptor 2 mediates deposition of collagen i in adipose tissue of high fat diet-induced obese mice. Mol Med Rep. 2018;17(4):5958–63.

284. Chen H jian, Yan X yue, Sun A, Zhang L, Zhang J, Yan Y e. High-Fat-Diet-Induced Extracellular Matrix Deposition Regulates Integrin—FAK Signals in Adipose Tissue to Promote Obesity. Mol Nutr Food Res. 2022;66(7):1–12.

285. Henegar C, Tordjman J, Achard V, Lacasa D, Cremer I, Guerre-Millo M, et al. Adipose tissue transcriptomic signature highlights the pathological relevance of extracellular matrix in human obesity. Genome Biol. 2008;9(1):1–32.

286. Vila IK, Badin PM, Marques MA, Monbrun L, Lefort C, Mir L, et al. Immune cell toll-like receptor 4 mediates the development of obesity- and endotoxemia-associated adipose tissue fibrosis. Cell Rep. 2014;7(4):1116–29.

287. Yamashita Y, Nakada S, Yoshihara T, Nara T, Furuya N, Miida T, et al. Perlecan, a heparan sulfate proteoglycan, regulates systemic metabolism with dynamic changes in adipose tissue and skeletal muscle. Sci Rep. 2018;8(1):1–14.

288. Wolff G, Taranko AE, Meln I, Weinmann J, Sijmonsma T, Lerch S, et al. Diet-dependent function of the extracellular matrix proteoglycan Lumican in obesity and glucose homeostasis. Mol Metab [Internet]. 2019;19(October 2018):97–106. Available from: https://doi.org/10.1016/j.molmet.2018.10.007